RODRIGO VIEIRA LEITE

FUEL CHARACTERIZATION USING REMOTE SENSING IN SUPPORT OF LARGE-SCALE WILDFIRE MANAGEMENT IN THE CERRADO BIOME

Thesis submitted to the Forest Science Graduate Program of the Universidade Federal de Viçosa in partial fulfillment of the requirements for the degree of *Doctor Scientiae*.

Adviser: Cibele Hummel do Amaral

VIÇOSA - MINAS GERAIS
2022

Ficha catalográfica elaborada pela Biblioteca Central da Universidade Federal de Viçosa - Campus Viçosa

T
L533f
2022

Leite, Rodrigo Vieira, 1992-
Fuel characterization using remote sensing in support of large-scale wildfire management in the Cerrado biome / Rodrigo Vieira Leite. – Viçosa, MG, 2022.
1 tese eletrônica (106 f.): il.

Texto em inglês.
Orientador: Cibele Hummel do Amaral.
Tese (doutorado) - Universidade Federal de Viçosa, Departamento de Engenharia Florestal, 2022.
Inclui bibliografia.
DOI: https://doi.org/10.47328/ufvbbt.2022.798
Modo de acesso: World Wide Web.

1. Incêndios florestais - Prevenção e controle. 2. Incêndios florestais - Sensoriamento remoto. 3. Aprendizado do computador. 4. Cerrados. I. Amaral, Cibele Hummel do, 1985-. II. Universidade Federal de Viçosa. Departamento de Engenharia Florestal. Programa de Pós-Graduação em Ciência Florestal. III. Título.

GDFC adapt. CDD 634.94322

Bibliotecário(a) responsável: Euzébio Luiz Pinto CRB-6/3317

RODRIGO VIEIRA LEITE

FUEL CHARACTERIZATION USING REMOTE SENSING IN SUPPORT OF LARGE-SCALE WILDFIRE MANAGEMENT IN THE CERRADO BIOME

Thesis submitted to the Forest Science Graduate Program of the Universidade Federal de Viçosa in partial fulfillment of the requirements for the degree of *Doctor Scientiae*.

APPROVED: December 21, 2022.

Assent:

gov.br Documento assinado digitalmente
RODRIGO VIEIRA LEITE
Data: 03/01/2023 09:41:48-0300
Verifique em https://verificador.iti.br

Rodrigo Vieira Leite
Author

gov.br Documento assinado digitalmente
CIBELE HUMMEL DO AMARAL
Data: 02/01/2023 22:11:48-0300
Verifique em https://verificador.iti.br

Cibele Hummel do Amaral
Adviser

AGRADECIMENTOS

A Deus, por estar comigo em todos os momentos, me conduzir, proteger, me dar força para superar as dificuldades, mostrar os caminhos nas horas incertas, e me dar saúde e paz para trabalhar.

Ao meu pai, Domingos Luiz Leite, e minha mãe, Leoneza Helena Vieira Leite, pelo apoio incondicional e por estarem sempre ao meu lado. Obrigado, mãe e pai, por todas as orações, por todo carinho, e grandes exemplos que vocês são para mim.

À minha companheira Patricia, pelo carinho, amor, cuidado e apoio incondicional.

À minha irmã Fernanda e cunhado Daniel pelo apoio, e presença na minha vida sempre compartilhando todos os momentos.

A toda minha família que está sempre torcendo por mim e me apoiando. Em especial ao meu tio Hélio, pelos conselhos, conversas, ensinamentos, e apoio de sempre.

À Universidade Federal de Viçosa e ao Departamento de Engenharia Florestal, pelo suporte e oportunidades.

À professora Cibele Hummel do Amaral, pela orientação, ensinamentos, apoio e pelo exemplo de pessoa e profissional me acompanhando e ajudando desde o início do mestrado. Também ao professor Carlos Alberto Silva, pela coorientação, conselhos, oportunidades, incentivo e suporte durante todo o processo.

Aos colegas e funcionarios do programa de pós-graduação em Ciência Florestal que estiveram junto comigo durante esses anos em especial os membros do laboratório SIGMA (UFV) e Forest Bioimetrics and Remote Sensing da Universidade da Florida.

A todos que torceram por mim e que de forma direta ou indireta contribuíram para a realização deste trabalho.

O presente trabalho foi realizado com apoio da Coordenação de Aperfeiçoamento de Pessoal de Nível Superior – Brasil (CAPES) – Código de Financiamento 001

Obrigado!

AGRADECIMENTOS

A Deus, por estar comigo em todos os momentos, me conduzir, proteger, me dar força para superar as dificuldades, mostrar os caminhos nas horas incertas, e me dar saúde e paz para trabalhar.

Ao meu pai, Domingos Luiz Leite, e minha mãe, Leoneza Helena Vieira Leite, pelo apoio incondicional e por estarem sempre ao meu lado. Obrigado, mãe e pai, por todas as orações, por todo carinho, e grandes exemplos que vocês são para mim.

À minha companheira Patricia, pelo carinho, amor, cuidado e apoio incondicional.

À minha irmã Fernanda e cunhado Daniel pelo apoio, e presença na minha vida sempre compartilhando todos os momentos.

A toda minha família que está sempre torcendo por mim e me apoiando. Em especial ao meu tio Hélio, pelos conselhos, conversas, ensinamentos, e apoio de sempre.

À Universidade Federal de Viçosa e ao Departamento de Engenharia Florestal, pelo suporte e oportunidades.

À professora Cibele Hummel do Amaral, pela orientação, ensinamentos, apoio e pelo exemplo de pessoa e profissional me acompanhando e ajudando desde o início do mestrado. Também ao professor Carlos Alberto Silva, pela coorientação, conselhos, oportunidades, incentivo e suporte durante todo o processo.

Aos colegas e funcionarios do programa de pós-graduação em Ciência Florestal que estiveram junto comigo durante esses anos em especial os membros do laboratório SIGMA (UFV) e Forest Bioimetrics and Remote Sensing da Universidade da Florida.

A todos que torceram por mim e que de forma direta ou indireta contribuíram para a realização deste trabalho.

O presente trabalho foi realizado com apoio da Coordenação de Aperfeiçoamento de Pessoal de Nível Superior – Brasil (CAPES) – Código de Financiamento 001

Obrigado!

There's an ancient parable about a farmer who lost his horse. And neighbors came over to say, "Oh, that's too bad", and the farmer said,

- "Good or bad, hard to say."

Days later, the horse returns and brings with it seven wild horses. And neighbors come over to say, "Oh, that's so good!" And the farmer just shrugs and says,

- "Good or bad, hard to say."

The next day, the farmer's son rides one of the wild horses, is thrown off and breaks his leg. And the neighbors say, "Oh, that's terrible luck." And the farmer says,

- "Good or bad, hard to say."

Eventually, officers come knocking on people's doors, looking for men to draft for an army, and they see the farmer's son and his leg, and they pass him by. And neighbors say, "Ooh, that's great luck!" And the farmer says,

- "Good or bad, hard to say."

(*Heather Lanier - "Good" and "Bad" are Incomplete Stories We Tell Ourselves at TED Conference*)

RESUMO

LEITE, Rodrigo Vieira. Universidade Federal de Viçosa, dezembro de 2022. **Caracterização de material combustível por sensoriamento remoto como suporte ao manejo de incêndios florestais em larga escala no bioma Cerrado**. Orientador: Cibele Hummel do Amaral.

O Cerrado é a savana tropical com maior biodiversidade do mundo, caracterizada por uma variedade de estruturas de vegetação incluindo formações campestres e florestais. No entanto, a estabilidade do Cerrado tem sido ameaçada por mudanças antrópicas no regime natural de fogo. A gestão do material combustível da vegetação é uma das opções mais importantes que temos para reduzir os impactos negativos dos incêndios florestais na sociedade e no ambiente e amplificar os positivos na flora dependente do fogo. Grandes áreas como o Cerrado geralmente requerem sensores remotos para caracterizar combustíveis, especialmente aqueles a bordo de plataformas orbitais. Embora os sensores em plataformas orbitais já existam há mais de 50 anos, novas oportunidades surgem com sensores lançados recentemente com características inéditas. No entanto, as propriedades do material combustível do Cerrado e seu potencial para serem caracterizadas com a nova geração de sensores ainda são pouco estudadas e, nesta tese, são apresentadas abordagens de sensoriamento remoto como mais um passo para ampliar a caracterização e monitoramento do material combustível no Cerrado. Esta dissertação está dividida em três capítulos, onde: i) o teor de umidade do combustível é predito usando espectroscopia foliar e algoritmos de aprendizado de máquina, ii) a carga de combustível é predita para toda a extensão do Cerrado usando dados lidar coletados a partir de aeronave não ocupada, aprendizado de máquina e dados do sensor espacial GEDI, recentemente lançado, e iii) uma revisão é apresentada sobre os novos sensores remotos espaciais com potencial para serem usados na caracterização das principais variáveis relacionadas ao material combustível para manejo integrado do fogo. Os resultados mostraram a aplicabilidade de dados de espectroscopia e lidar, aliados ao uso de modelos de aprendizado de máquina, na recuperação de características do combustível importantes para o manejo do fogo. Com o aumento da disponibilidade de dados de sensores com novas tecnologias e capacidades, que permitem a escalada de informação coletada em campo, sugere-se que estamos diante de uma nova era para o mapeamento e monitoramento de material combustível, o que é essencial para o desenvolvimento de programas de manejo integrado do fogo visando a preservação do e bioma Cerrado e outros ecossistemas semelhantes em todo o mundo.

Palavras-chave: Risco de incêndio; Combustível vegetal; Espectroscopia, Lidar, GEDI, Aprendizado de máquina, Sensores satelitários

ABSTRACT

LEITE, Rodrigo Vieira, Universidade Federal de Viçosa, December, 2022. **Fuel characterization using remote sensing in support of large-scale wildfire management in the Cerrado biome**. Adviser: Cibele Hummel do Amaral.

Cerrado is the most biodiverse tropical savanna in the world characterized by a range of vegetation structures from grasslands to forests. However, Cerrado's stability has been threatened by anthropogenic changes in the fire regime. Managing fuels is one of the most important options we have for reducing wildfire's negative impacts on society and the environment and amplifying positive ones on fire-dependent flora. Large areas such as Cerrado often require remote sensors to characterize fuels, especially those on-board space-based platforms. Even though spaceborne sensors have been around for over 50 years, new opportunities arise with recently launched sensors with unprecedented characteristics. Yet, Cerrado fuel properties and their potential to be characterized with the new generation of sensors are still little studied. In this thesis proximal and near-surface approaches as a step forward to scale-up Cerrado fuel properties are presented. The thesis is divided into three chapters, where: i) fuel moisture content is predicted using leaf spectroscopy and machine learning algorithms, ii) fuel load is predicted for the whole Cerrado extent using lidar data collected from unoccupied aerial vehicles and the recently launched GEDI spaceborne lidar sensor and iii) a review of the novel spaceborne remote sensors with potential to be used for fuel characterization and the main fuel-related variables for integrated fire management is presented. The results showed the applicability of spectroscopy and lidar data together with machine learning to retrieve important fuel characteristics for fire management. With the increasing availability of data from sensors with new technologies and capabilities, which allow the upscaling of information collected in the field, it is suggested that we are facing a new era for the mapping and monitoring of fuels, which is essential for the development of integrated fire management programs aiming at preserving the Cerrado biome and similar ecosystems worldwide.

Keywords: Fire risk, Vegetation fuel, Spectroscopy, Lidar, GEDI, Machine learning, Satellite-borne sensors

SUMÁRIO

General introduction

Cerrado is a neotropical savanna biome classified as one of the world's biodiversity hotspots and home to more than 10,000 plant species that are mostly endemic. (Strassburg et al. 2017). Cerrado's ecological stability is threatened by fire regime alterations associated with anthropic activities (Durigan and Ratter, 2016, Gomes et al. 2018). Cerrado vegetation types range from grasslands to forests that can present different sensitivity to fire occurrence and intensity. For example, fire occurrence in sensitive vegetation (i.e., not adapted to fire) can lead to tree mortality, reduction of forested areas, and threaten nearby communities. On the other hand, completely suppressing fire in areas where the vegetation is adapted to it might be harmful to ecosystems functional diversity stability (Rosan et al. 2019, Durigan 2020). Understanding the variables affecting fire in Cerrado is therefore essential for managing fire and preserving this biome (Rodrigues and Fidelis 2022).

Fire management practices often focus on managing fuels since other parameters related to fire are harder or not possible to directly control (e.g., ignition source, weather, wind, topography). The fuel load, structure, physical and chemical properties affect fire ignition probability, spreading rate, fire emissions, and the potential fire severity and extent (Chuvieco et al. 2020, Stavros et al. 2018; Fig. 1). With the information on fuel amount, type, condition, and distribution, it is possible to prescribe low-severity burns, model fire behavior and predict fire risk (Gale et al. 2021).

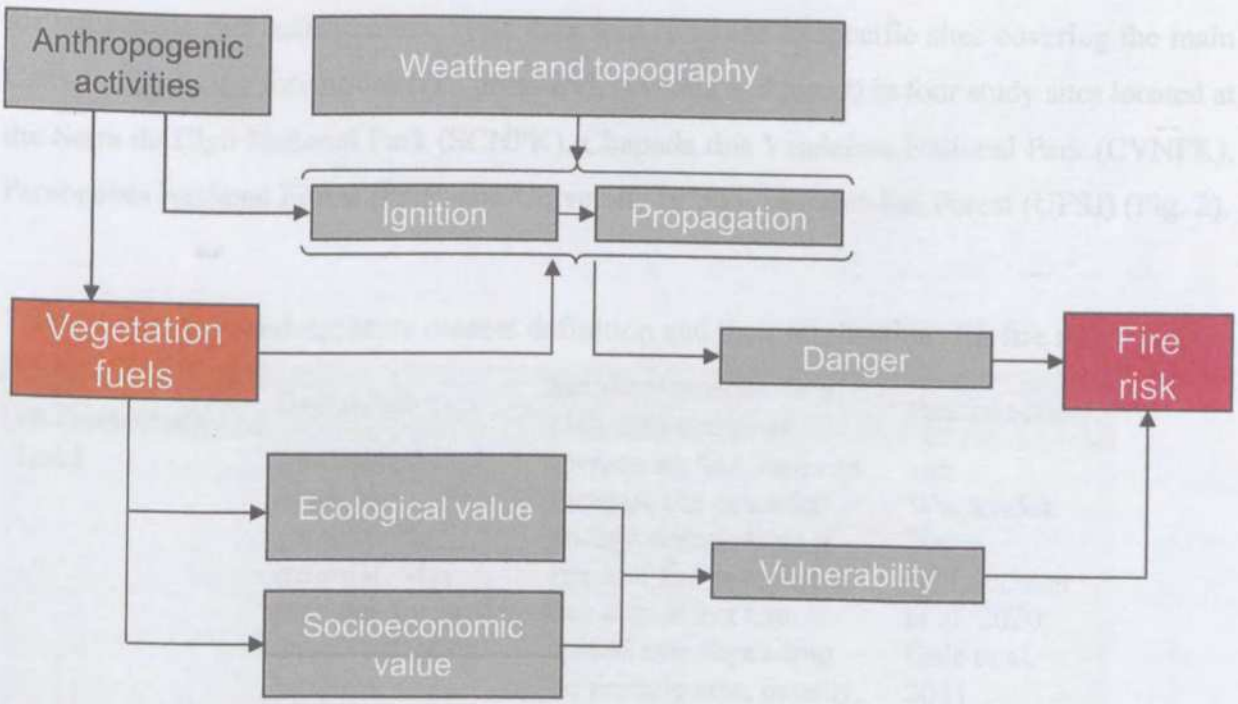

Fig. 1. Fire risk framework adapted from Chuvieco et al. 2014

Although the number of studies to characterize fuels has increased in the last decade, reproducible approaches to characterize fuels in large areas such as the Cerrado are still being developed (Pettinari e Chuvieco 2020). It is very common to use spaceborne remote sensing for large-area vegetation assessment due to the worldwide data availability. The science related to the use of these sensors for Earth observation is over 50 years old (Tatem et al 2009, Ustin et al. 2021). However, even greater advances are expected in the coming decades due to the planning and launching of new space missions with unprecedented characteristics. These sensors can assist with fuel monitoring and support integrated fire management practices in Cerrado.

The objective of this dissertation was to propose and test frameworks for fuel characterization that can be potentially applicable to large-scale fire management. The focus was on two of the most important fuel characteristics related to fire risk that can be managed for efficient wildfire management, namely, fuel load and moisture content (Table 1). In the first chapter, fuel moisture content (FMC) was predicted using leaf-level visible to short-wave infrared (400-2,500 nm) spectroscopy measurements and machine learning. In the second chapter, a framework using UAV-borne and spaceborne lidar sensors to predict fuel load for the entire Cerrado extent was developed. Finally, an overview of the main fuel-related variables and the novel spaceborne remote sensors with potential to be used for fuel characterization was presented in the third chapter, looking forward to the application of the developed frameworks for large scale fuel management. Field data was collected in specific sites covering the main Cerrado vegetation formations (i.e., grassland, savanna and forest) in four study sites located at the Serra do Cipó National Park (SCNPK), Chapada dos Veadeiros National Park (CVNPK), Paraopebas National Forest (PNF) and University of São João Del-Rei Forest (UFSJ) (Fig. 2).

Table 1. Fuel load and moisture content definition and their implications for fire management.

Fuel characteristic	Definition	Implications for fire risk management	References
Load	Amount of available combustible material. May includes live and dead vegetation biomass	Increasing fuel load can increase the potential energy release from a fire and fire severity. It can also affect fire spread rate depending on particle size, density, moisture and ratio between live and dead vegetation.	van Wagtendok 2006; McLauchlan et al. 2020; Gale et al. 2021

Moisture content	Ratio between vegetation's water and total dry mass	Affects fuel ignition probability and spread rate. Drier vegetation ignites more easily and makes fire spread faster since water works as a heat sink. Dead fuel moisture is usually related to weather. Live vegetation moisture is also affected by weather, plant phenology, species adaption strategies and water availability in the soil	Yebra et al. 2013; Pettinari and Chuvieco et al. 2020

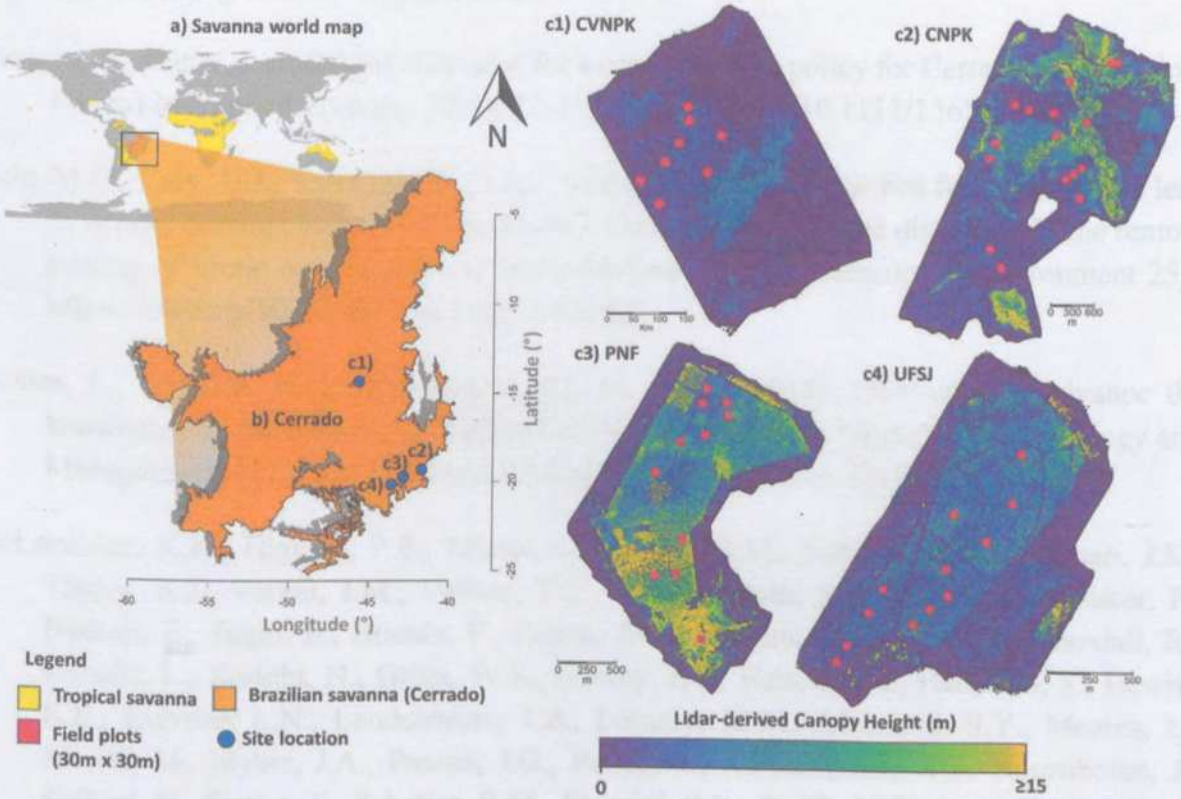

Fig. 2. Spatial location of the Brazilian savanna (Cerrado) (a, b) and study sites for data collection, namely, Chapada dos Veadeiros National Park (CVNPK, c1), Serra do Cipó National Park (SCNPK, c2) Paraopeba National Forest (PNF, c3) and University of São João Del-Rei's Forest (UFSJ, c4). Fig.c1 to c4 show a canopy height model for the sites derived from a UAV-lidar 3D point cloud.

References

Chuvieco, E., Aguado, I., Jurdao, S., Pettinari, M.L., Yebra, M., Salas, J., Hantson, S., De La Riva, J., Ibarra, P., Rodrigues, M., Echeverría, M., Azqueta, D., Román, M. V., Bastarrika, A., Martínez, S., Recondo, C., Zapico, E., Martínez-Vega, F.J., 2014. Integrating geospatial information into fire risk assessment. International Journal of Wildland Fire 23, 606–619. https://doi.org/10.1071/WF12052

Chuvieco, E., Aguado, I., Salas, J., García, M., Yebra, M., Oliva, P., 2020. Satellite Remote Sensing Contributions to Wildland Fire Science and Management. Current Forestry Reports 6, 81–96. https://doi.org/10.1007/s40725-020-00116-5

Durigan, G., Pilon, N. A., Abreu, R. C., Hoffmann, W. A., Martins, M., Fiorillo, B. F., Vasconcelos, H. L. (2020). No net loss of species diversity after prescribed fires in the Brazilian Savanna. Frontiers in Forests and Global Change, 3, 13. https://doi.org/10.3389/ffgc.2020.00013

Durigan, G., Ratter, J. A. (2016). The need for a consistent fire policy for Cerrado conservation. Journal of Applied Ecology, 53(1), 11-15. https://doi.org/10.1111/1365-2664.12559

Gale, M.G., Cary, G.J., Van Dijk, A.I.J.M., Yebra, M., 2021. Forest fire fuel through the lens of remote sensing: Review of approaches, challenges and future directions in the remote sensing of biotic determinants of fire behaviour. Remote Sensing of Environment 255. https://doi.org/10.1016/j.rse.2020.112282

Gomes, L., Miranda, H. S., Bustamante, M. M. da C. (2018). How can we advance the knowledge on the behavior and effects of fire in the Cerrado biome?. Forest Ecology and Management, 417, 281–290. https://doi.org/10.1016/j.foreco.2018.02.032

McLauchlan, K.K., Higuera, P.E., Miesel, J., Rogers, B.M., Schweitzer, J., Shuman, J.K., Tepley, A.J., Varner, J.M., Veblen, T.T., Adalsteinsson, S.A., Balch, J.K., Baker, P., Batllori, E., Bigio, E., Brando, P., Cattau, M., Chipman, M.L., Coen, J., Crandall, R., Daniels, L., Enright, N., Gross, W.S., Harvey, B.J., Hatten, J.A., Hermann, S., Hewitt, R.E., Kobziar, L.N., Landesmann, J.B., Loranty, M.M., Maezumi, S.Y., Mearns, L., Moritz, M., Myers, J.A., Pausas, J.G., Pellegrini, A.F.A., Platt, W.J., Roozeboom, J., Safford, H., Santos, F., Scheller, R.M., Sherriff, R.L., Smith, K.G., Smith, M.D., Watts, A.C., 2020. Fire as a fundamental ecological process: Research advances and frontiers. Journal of Ecology 108, 2047–2069. https://doi.org/10.1111/1365-2745.13403

Pettinari, M.L., Chuvieco, E., 2020. Fire Danger Observed from Space. Surveys in Geophysics 41, 1437–1459. https://doi.org/10.1007/s10712-020-09610-8

Rodrigues, C. A. & Fidelis, A. Should we burn the Cerrado? Effects of fire frequency on open savanna plant communities. J Vegetation Science 33, (2022).

Rodrigues, C. A. & Fidelis, A. Should we burn the Cerrado? Effects of fire frequency on open savanna plant communities. J Vegetation Science 33, (2022).

Rosan, T. M., Aragão, L. E., Oliveras, I., Phillips, O. L., Malhi, Y., Gloor, E., & Wagner, F. H. (2019). Extensive 21st-century woody encroachment in South America's savanna. Geophysical Research Letters, 46(12), 6594-6603.

Stavros, E.N., Coen, J., Peterson, B., Singh, H., Kennedy, K., Ramirez, C., Schimel, D., 2018. Use of imaging spectroscopy and LIDAR to characterize fuels for fire behavior prediction. Remote Sensing Applications: Society and Environment 11, 41–50. https://doi.org/10.1016/j.rsase.2018.04.010

Strassburg, B. B., Brooks, T., Feltran-Barbieri, R., Iribarrem, A., Crouzeilles, R., Loyola, R., ... & Balmford, A. (2017). Moment of truth for the Cerrado hotspot. Nature Ecology & Evolution, 1(4), 1-3. https://doi.org/10.1038/s41559-017-0099

Tatem, A.J., Goetz, S.J., Hay, S.I., 2009. UKPMC Funders Group Fifty Years of Earth Observation Satellites : Earth 96, 1–7. https://doi.org/10.1511/2008.74.390.Fifty

Ustin, S.L., Middleton, E.M., 2021. Current and near-term advances in Earth observation for ecological applications. Ecological Processes 10, 1–57. https://doi.org/10.1186/s13717-020-00255-4

Van Wagtendonk, J. W., 2006. Fire as a physical process. Fire in California's ecosystems, 38-57.

Yebra, M. et al. A global review of remote sensing of live fuel moisture content for fire danger assessment: Moving towards operational products. Remote Sensing of Environment 136, 455–468 (2013)

Chapter 1: Fuel moisture content prediction in the Brazilian tropical savanna using leaf spectroscopy and machine learning approaches

ABSTRACT

LEITE, Rodrigo Vieira, Universidade Federal de Viçosa, December, 2022. **Fuel moisture content prediction in the Brazilian tropical savanna using leaf spectroscopy and machine learning approaches**. Adviser: Cibele Hummel do Amaral.

Fuel moisture content (FMC) is one of the most important variables that should be considered in wildfire management. Large-area assessments are usually required for fire-prone ecosystems such as the Brazilian tropical savanna (Cerrado) – the most biodiverse savanna in the world. Spectroscopy is a non-destructive remote sensing method that may allow effective FMC monitoring for such spatial scale, especially with the increasing availability of spaceborne imaging spectroscopy sensors. Developing approaches to support FMC prediction using spectroscopy are necessary to support fire management in Cerrado and similar ecosystems worldwide. In this study, we used leaf spectroscopy and machine learning methods to predict FMC for a range of vegetation fuel classes (surface, ladder, and canopy fuels) in Cerrado. Leaf samples of 541 individuals were collected in the three main Cerrado formations (grassland, savanna, and forest) to measure leaf spectral response (400-2500 nm). Vegetation indices related to several leaf traits were calculated and used as inputs to train a Random Forest (RF), Artificial Neural Network (ANN) and Support Vector Machine (SV) algorithms to predict FMC for surface, ladder and canopy fuels separately or in a single model. Overall, the methods predicted FMC with RMSE of about 20%. Only slight differences were observed using separate or a single model for all fuel classes to predict FMC. It was observed that vegetation indices that use bands related to leaf traits such as dry mass and pigments were as important as those related to water content. In addition, the findings support the use of wavelengths in the SWIR region to predict FMC highlighting the importance of imaging spectroscopy sensors that cover this region.

1. Introduction

Global warming is a global concern for its impact on Earth's ecosystem functionality and stability. One of the main consequences is related to the rising trend of fire-prone weather conditions (i.e., hot, dry, and windy events) (Seneviratne et al. 2021). Extreme events such as heat waves and large-scale wildfires are becoming more frequent contributing to carbon emissions and threatening human health (Fidelis et al. 2019, Lizundia-Loiola et al. 2019, Adams et al. 2020). Those effects are observed even in fire-adapted vegetation ecosystems such as the Brazilian tropical savanna (Cerrado) where temperature increase might be in the order of 2–4°C and relative humidity decrease of ~15% (Hofmann et al. 2020). Efficient fire management has been necessary to maintain the appropriate fire regimes in Cerrado and other fire-prone ecosystems due to the current climate change scenarios and the anthropic-related landscape changes (Rodrigues and Fidelis 2022).

Fire management practices usually require the characterization of fuels – defined as the organic vegetation matter available for burning. Fuel characteristics will impact the fire ignition probability, spread rate, and total emissions (Stavros et al., 2018, Ogle et al., 2019, Gomes et al., 2020). The availability of fuels to be burned is highly dependent on the fuel moisture content (FMC) as drier vegetation is more easily ignited and facilitates fire spread. The FMC in non-photosynthetic active vegetation – e.g., dead woody debris and litter – has relatively higher sensitivity to weather changes (e.g., rain, and relative humidity) than photosynthetic active vegetation, and, therefore, be potentially retrieved by relating FMC to weather-related variables. On the other hand, FMC for live vegetation can be more difficult to obtain as it will also depend on factors such as the vegetation's adaptative traits and soil water availability. Those traits can have a wide range in structurally complex ecosystems such as Cerrado, with species of different growth forms (herbaceous vs. arboreous) (Streher et al. 2020). Effective FMC monitoring requires approaches capable of capturing these variations for large area extents.

The characterization of FMC using passive remote sensors is a non-destructive technique that allows timely larger area assessment, especially using space-borne remote sensors (Szpakowski et al. 2019, Chuvieco et al. 2020). Large-scale FMC monitoring is possible using coarse-resolution passive sensors such as MODIS (Yebra et al. 2018, Zhu et al. 2021). Nonetheless, image spectrometers with higher spectral and spatial resolution are part of the present and future of spaceborne remote sensors (Ustin et al. 2021) with the recent launch of spectrometers with about 10-nm spectral resolution and 30-m spatial resolution DESIS (Alonso et al. 2019, Krutz et al. 2019), PRISMA (Cogliati et al. 2021), HISUI (Matsunaga et al. 2020),

and ENMAP (Guanter et al. 2015). In addition, new missions, which are in preparatory phases such as SBG-NASA (Cawse-Nicholson et al. 2021) and CHIME-ESA (Nieke et al. 2018), bring perspectives for a new era of high-temporal-resolution imaging spectroscopy at a global scale. The use of these sensors can potentially improve the characterization of FMC at large scales but frameworks that incorporate narrow-band spectroscopic measurements to estimate FMC are still needed, especially for species in fire-prone ecosystems.

Water content affects the leaf's spectral response especially in water absorption features in the near-infrared (NIR, ~ 800-1,300 nm) and short-wave infrared (SWIR, ~ 1,300-2,500 nm) regions centered at around 970, 1200, 1450, and 1940 nm (Knipling 1970, Danson and Bowyer 2004, Yebra 2013). Nevertheless, changes in leaf moisture might affect other plants' properties which are related to their reflectance. As an example, drier plants might experience photosynthetic activity reduction and pigment degradation, which can be captured by reflectance changes in the visible (VIS, 400-700 nm) and the red-edge (~ 700-800 nm) spectral regions (Streher et al. 2020). Besides that, species might have their own spectral signature as a result of the combination of their specific leaf characteristics (e.g., anatomy and structural chemical constituents). Understanding all those variables that impact FMC prediction using spectroscopy still needs to be fully understood in tropical savanna ecosystems.

Assessing the methods and variables related to FMC prediction using spectroscopy is necessary to develop efficient approaches for FMC monitoring and fire management in large scales. In this study we assessed the spectral variability of several vegetation species of different growth forms (i.e., herbs, shrubs, and trees) from the Cerrado biome – one of the most biodiverse endangered tropical savannas in the world (Myers et al. 2000, Strassburg et al. 2017). The main objective was to i) define the best empirical approach to predict FMC of Cerrado species from different vegetation layers using machine learning and leaf spectroscopy ii) identify the most important spectral regions and vegetation indices to predict FMC.

2. Material and Methods

2.1. Study area

The study sites were selected to cover the three major Cerrado vegetation formations (i.e., grassland, savanna, and forest) (Fig. 1). Grasslands vegetation types can be characterized by the presence of grass species only (e.g. "Campo limpo"), grass species with scattered shrubs (e.g., "Campo sujo" and "Campo rupestre"). The savanna formation in Cerrado is composed by contorted short trees that does not yield a closed canopy and shrubs on top of a herbaceous layer

(e.g., "Cerrado sensu stricto"). Forest formations are those dominated by trees (e.g., "Cerradão", in addition to the extra-Cerrado forest formations as Riparian and Gallery forests) (Ribeiro and Walter, 1998). The sites were located in the Serra do Cipó National Park (SCNPK), Chapada dos Veadeiros National Park (CVNPK), Paraopebas National Forest (PNF) and University of São João Del-Reis Forest (UFSJ) (Fig. 1).

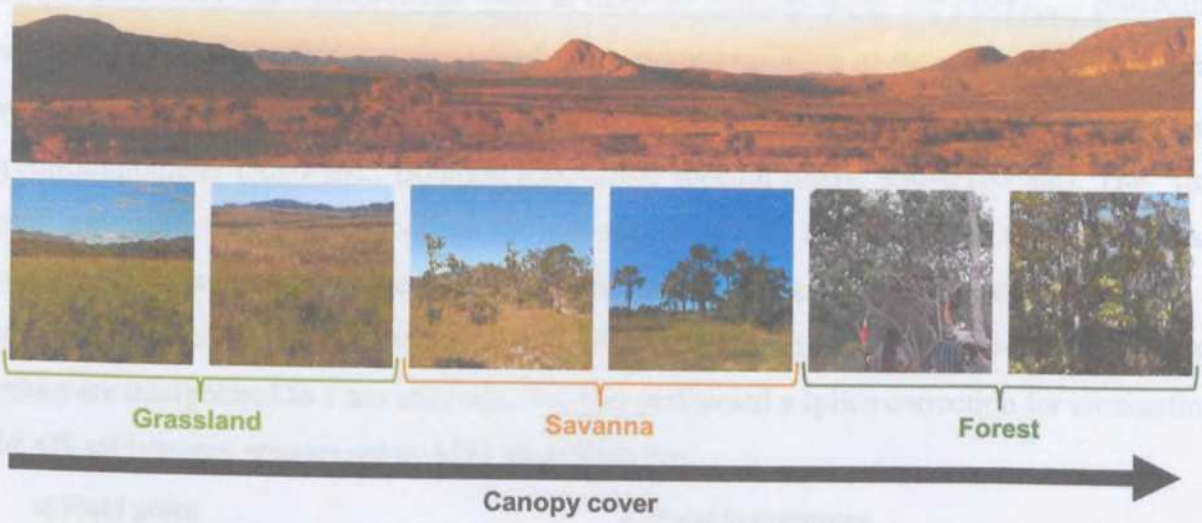

Fig. 1. Cerrado is a tropical savanna located in Brazil characterized by a wide range of vegetation types within three main formations: grassland, savanna and forest.

2.2 Field data collection, FMC calculation and spectroscopic measurements

Between June and July 2019, 50 square plots of 30 x 30 m (900 m^2) were established at the study sites. Three fuel classes were defined for the samples collection based on their vertical layer occupancy as surface ($Surface_{fuels}$), ladder ($Ladder_{fuels}$) and canopy fuels ($Canopy_{fuels}$): $Surface_{fuels}$ represent non-woody grasses, herbs and forbs at the sample plots; $Ladder_{fuels}$ were shrubs and trees with diameter at breast height (dbh, 1.3 m) < 10 cm; $Canopy_{fuels}$ are trees in the plots with $dbh \geq 10$ cm (Fig. 2).

Samples of the dominant species of each fuel class ($Surface_{fuels}$, $Ladder_{fuels}$ and $Canopy_{fuels}$) in each plot were collected. For $Canopy_{fuels}$ a whole representative branch with more than 5 leaves were collected and immediately stored in a black plastic bag. For $Surface_{fuels}$, clipped leaves were sealed in a plastic bag and immediately stored in an ice chest. The same procedure used for $Canopy_{fuels}$ was used for $Ladder_{fuels}$ with lignified stems whereas the $Surface_{fuels}$ procedure was used for $Ladder_{fuels}$ with non-lignified stems. A

sample was only collected if it was exposed to direct sunlight. A total of 512 individuals were collected being 342 $Canopy_{fuels}$, 101 $Ladder_{fuels}$ and 69 $Surface_{fuels}$ - from 73 species (171 individuals still unidentified).

The samples were transported to the closest facility where the spectral measurements were done aiming to preserve their physiological and biochemical properties. The time between sample collection and measurement were at most 40 minutes using $Surface_{fuels}$ procedure and 3 hours using $Canopy_{fuels}$ procedure. The spectral response of the samples was acquired by measuring the adaxial surfaces of the sampled leaves using FieldSpec 3 Hi-Res spectroradiometer (ASD Inc., Boulder, CO, USA; spectral range: 350–2500 nm). The "leaf clip" assembly was used to collect the spectra. It allows the collection of standardized, orthogonal measurements while excluding atmospheric influence in the spectra. FieldSpec 3 sampling interval is 1.4 nm between 350–1000 nm and 2 nm between 1000–2500 nm, these values are interpolated to 1 nm intervals. We also performed a splice correction for eliminating the off-set between sensors using ASD ViewSpec Pro.

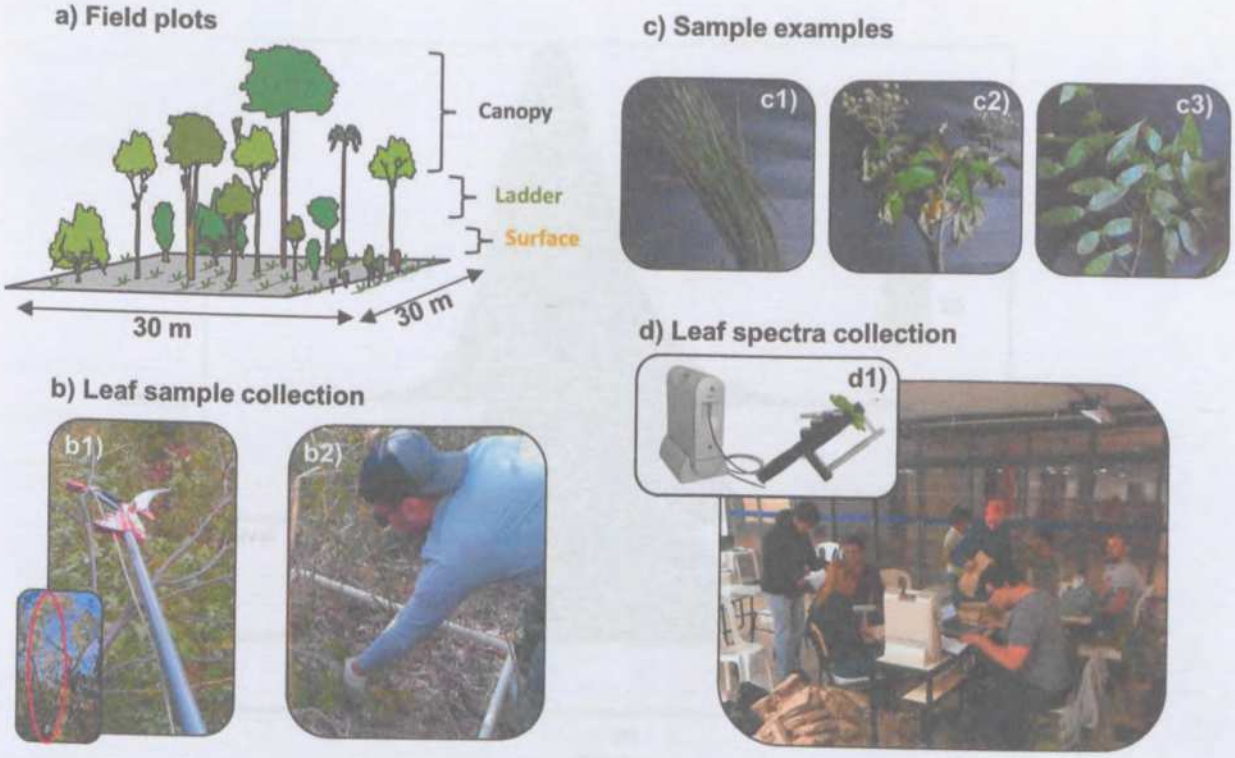

Fig. 2. Field data collection representation: a) field plot size and vertical layers from where samples were collected; b) branches and leaves collection with clipper (b1) and manually (b2); c) examples of leaves sample of surface (c1), ladder (c2) and canopy (c3) fuels; d) spectroscopy measurements using ASD FieldSpec with "leaf clip" assemble (d1).

To calculate the fuel moisture content (FMC), approximately 100 g of each sample was immediately placed in a paper bag and weighed with a 10 g precision scale to obtain the fresh weight (FW). These samples were oven dried at 65°C until a constant weight was reached in the laboratory. The dried samples were weighed to obtain the dry weight (DW). The fresh and dry weight of the samples were used to calculate FMC (Eq. 1) (Ustin et al. 2012). FMC values were classified into 5 classes defined as FMC30-40, FMC40-50, FMC50-60, FMC60-70 and FMC70-80 for FMC values ranging from 30 to 40, 40 to 50, 50 to 60, 60 to 70, and 70 to 80, respectively – the thresholds were based on the FMC distribution (Fig. 3).

$$FMC = (FW - DW)/DW, \quad \text{(eq.1)}$$

where: *FMC* is the fuel moisture content, *FW* is the sample's fresh weight (g) measured in the field and *DW* is its oven-dried weight (g).

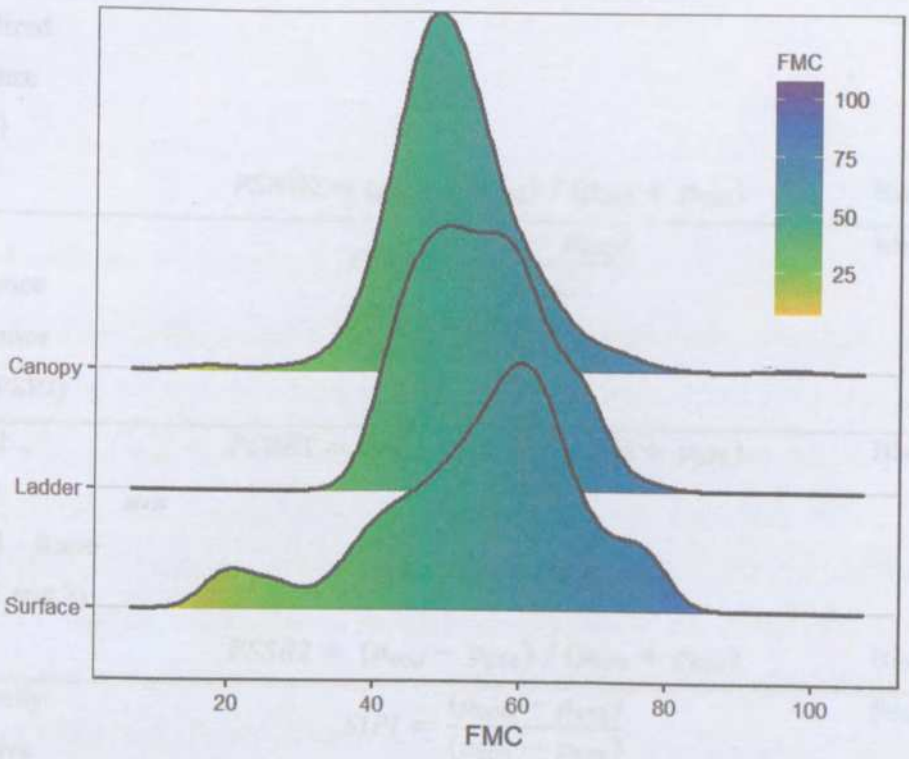

Fig. 3. Distribution of field fuel moisture content (FMC) measurements for Surface, Ladder and Canopy fuels.

2.3. Vegetation indices for FMC modeling

We computed several vegetation indices that relate to plant water content, pigments, and structure (Roberts et al. 2011, Table 1) to be used as predictors in a model to estimate FMC.

We computed indices that are exclusive for narrow-band spectrometers and also indices that have equivalent in broad-band sensors.

Table 1. Description and equation of vegetation indices used as predictors to predict fuel moisture content

Index	Equation	Reference
Normalized Difference Water Index (NDWI)	$NDWI = (\rho_{857} - \rho_{1241}) / (\rho_{857} + \rho_{1241})$	Gao 1996
Water Band Index (WBI)	$WBI = \rho_{900} - \rho_{970}$	Penuelas et al. 1997
Cellulose Absorption Index (CAI)	$CAI = 100x[0.5x(\rho_{2031} + \rho_{2211}) - \rho_{2101}]$	Daughtry 2001
Pigment Sensitive Normalized Difference (PSND)	$PSND1 = (\rho_{800} - \rho_{675}) / (\rho_{800} + \rho_{675})$	Blackburn et al. 1998b
	$PSND2 = (\rho_{800} - \rho_{650}) / (\rho_{800} + \rho_{650})$	Blackburn et al. 1998b
Plant Senescence Reflectance Index (PSRI)	$PSRI = \frac{(\rho_{680} - \rho_{500})}{(\rho_{750})}$	Merzlyak et al. 1999
Pigment Specific Spectral Ratio (PSRR1 and 2)	$PSRR1 = (\rho_{800} - \rho_{675}) / (\rho_{800} + \rho_{675})$	Blackburn 1998a
	$PSSR2 = (\rho_{800} - \rho_{650}) / (\rho_{800} + \rho_{650})$	Blackburn 1998a
Structurally Insensitive Pigment Index (SIPI)	$SIPI = \frac{(\rho_{800} - \rho_{445})}{(\rho_{800} - \rho_{680})}$	Penuelas et al. 1995
Chlorophyll Absorption	$CARI = (\rho_{700} - \rho_{670}) - 0.2\,x\,(\rho_{700} - \rho_{550})$	Kim 1994

Reflectance Index (CARI)		
Modified CARI (MCARI)	$MCARI = [(\rho_{700} - \rho_{670}) - 0.2\,x\,(\rho_{700} - \rho_{550})]x\,(\rho_{700} - \rho_{670})$	Daughtry et al. 2000
Carotenoid Reflectance Index (CRI)	$CRI1 = (1/\rho_{500}) - (1/\rho_{550})$	Gitelson 2002
	$CRI2 = (1/\rho_{500}) - (1/\rho_{700})$	Gitelson 2002
Normalized Difference Lignin Index (NDLI)	$NDLI = \frac{[log(1/\rho_{1754}) - log(1/\rho_{1680})]}{log(1/\rho_{1754}) + log(1/\rho_{1680})}$	Serrano et al. 2002
	$NDLI3 = log\ log\ (1/\rho_{1510})$	
Photochemical Reflectance Index (PRI)	$PRI = (\rho_{530} - \rho_{570}) / (\rho_{530} + \rho_{570})$	Gamon et al 1997
Red-edge Vegetation (RVSI)	$RVSI = (\rho_{714} - \rho_{752}) / (2 - \rho_{733})$	Merton & Huntington 1999

2.4. Fuel load and moisture content modeling

The FMC was modeled separately for each fuel class, therefore, resulting in three models with the vegetation indices as predictors and the FMC of $Surface_{fuels}$, $Ladder_{fuels}$, and $Canopy_{fuels}$ and as response variables. There algorithms were used as potential modeling approaches: Random Forest (RF) (Breiman et al., 1984, Breiman, 1996), Artificial Neural network (ANN) (Lippmann, 1987, Jain et al., 1996) and Support Vector Machine (SVM) (Boser et al., 1992, Vapnik, 1988). Those methods are flexible to the different data distributions, are relatively easier to interpret, and have been extensively used for empirical modeling of vegetation traits (e.g., Raczko Zagajewski 2017, Leite et al. 2020, Souza et al. 2019).

The RF algorithm was built setting the number of trees as 500 and tuning the number of predictors at each split (m_{try}). The ANN was trained tuning the number of units (nodes) in the single hidden layer that was defined. A SVM with the Radial Basis Function Kernel were tuned varying the parameter "Cost" (C) for the SVM algorithm. All algorithms were trained using

functions from the caret package (Kuhn 2020) loaded with the dependencies nnet (Venables and Ripley, 2002), randomForest (Liaw and Wiener, 2002) and kernlab (Karatzoglou et al. 2004) for ANN, RF and SVM, respectively.

The algorithms were trained using a 5-fold cross-validation selecting the best tuning parameters based on the lowest root mean square error (RMSE). The 5-fold cross-validation separate the dataset into 5 groups of similar size. One group is held out of the training process and is used for validation. The process is repeated so all the groups are left out of the training process. The statistic performance metrics are calculated for each of the iterations and the mean value of the iterations represents the final algorithm performance. This is an alternative approach when the dataset does not allow removing a single validation set for either being too small or not being representative sample of the population.

The performance of all algorithms was assessed using the coefficient of correlation (r) between the predicted and observed values, absolute and relative (%) root square mean error (RMSE) and mean difference (MD) (Eq. 8 to 11). In addition, feature importance was calculated for each of the trained algorithms.

$$RMSE\ (Mg\ /\ ha) = \sqrt{\frac{\sum_{i=1}^{n}\ (\hat{Y}_i - Y_i)^2}{n}}, \quad \text{(eq. 8)}$$

$$RMSE\ (\%) = \frac{RMSE}{\underline{Y}}\ x\ 100, \quad \text{(eq. 9)}$$

$$MD\ (Mg\ /\ ha) = \frac{\sum_{i=1}^{n}\ (\hat{Y}_i - Y_i)}{n}, \quad \text{(eq. 10)}$$

$$MD\ (\%) = \frac{MD}{\underline{Y}}\ x100, \quad \text{(eq. 11)}$$

where: $\hat{Y}_i$ is the estimated FMC, Y_i is the observed FMC; n is the number of samples.

3. Results

Lower FMC classes (e.g., FMC30-40) had lower absorbance in wavelengths related to water absorption in the shortwave infrared region (SWIR) (e.g., around 1400 nm and 1900 nm, Fig. 4) when analyzing fuel classes together. Meanwhile, higher FMC classes (e.g., FMC70-80) had higher absorbance in the same regions. In the near-infrared (NIR) region of the spectra near to 1200 it was also possible observe a pattern of higher absorption in higher fuel classes, even though the highest FMC class (i.e., FMC70-80) had a relatively lower absorption

compared to the second highest class (i.e., FMC60-70). Nonetheless, FMC70-80 had the highest reflectance in the red-edge region (~700-800 nm). The difference between high and low FMC classes was not as clear in the visible range (VIS) (~400-700 nm).

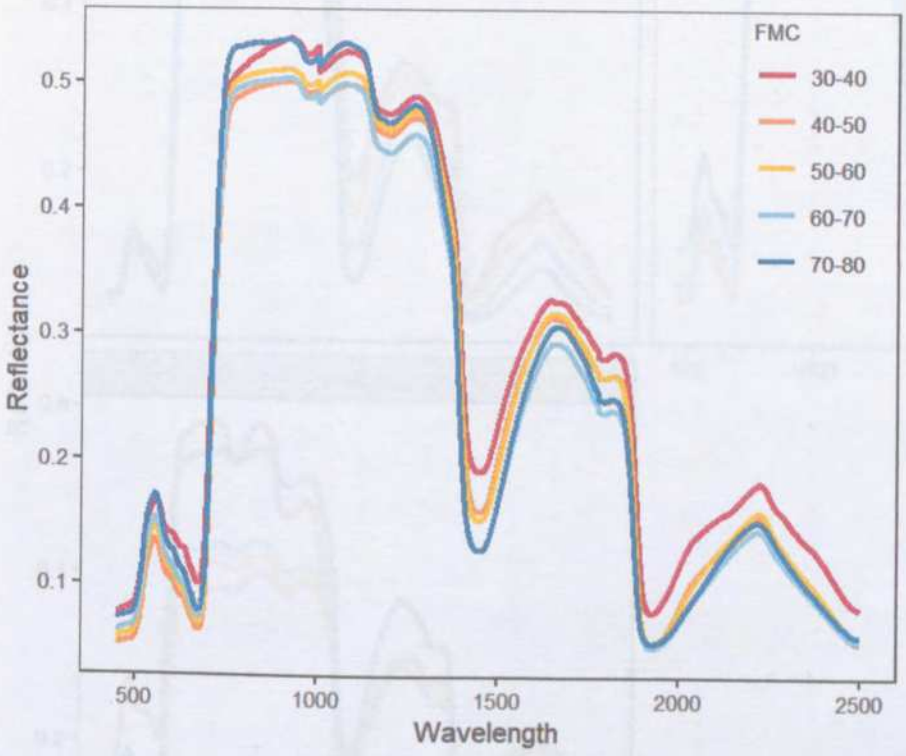

Fig. 4. Mean leaf reflectance of Cerrado species by fuel moisture content (FMC) classes 30-40 (n=18), 40-50 (n=206), 50-60 (n = 183), 60-70 (n = 79) and 70-80 (n = 15).

Most of the patterns held true when analyzing $Surface_{fuels}$, $Ladder_{fuels}$ and $Canopy_{fuels}$, separetly (Fig. 5). In general, FMC30-40 still had higher reflectance values in water content-related absorption features of the spectra (e.g. around 1400 and 1900 nm). In addition, biochemical features in the SWIR region, e.g., lignin, cellulose, and hemicellulose, which are present from ~ 1,600 to 2,400 nm and that usually are obscured by the water content in fresh leaves, are visible in the spectra of FMC classes < 50%.

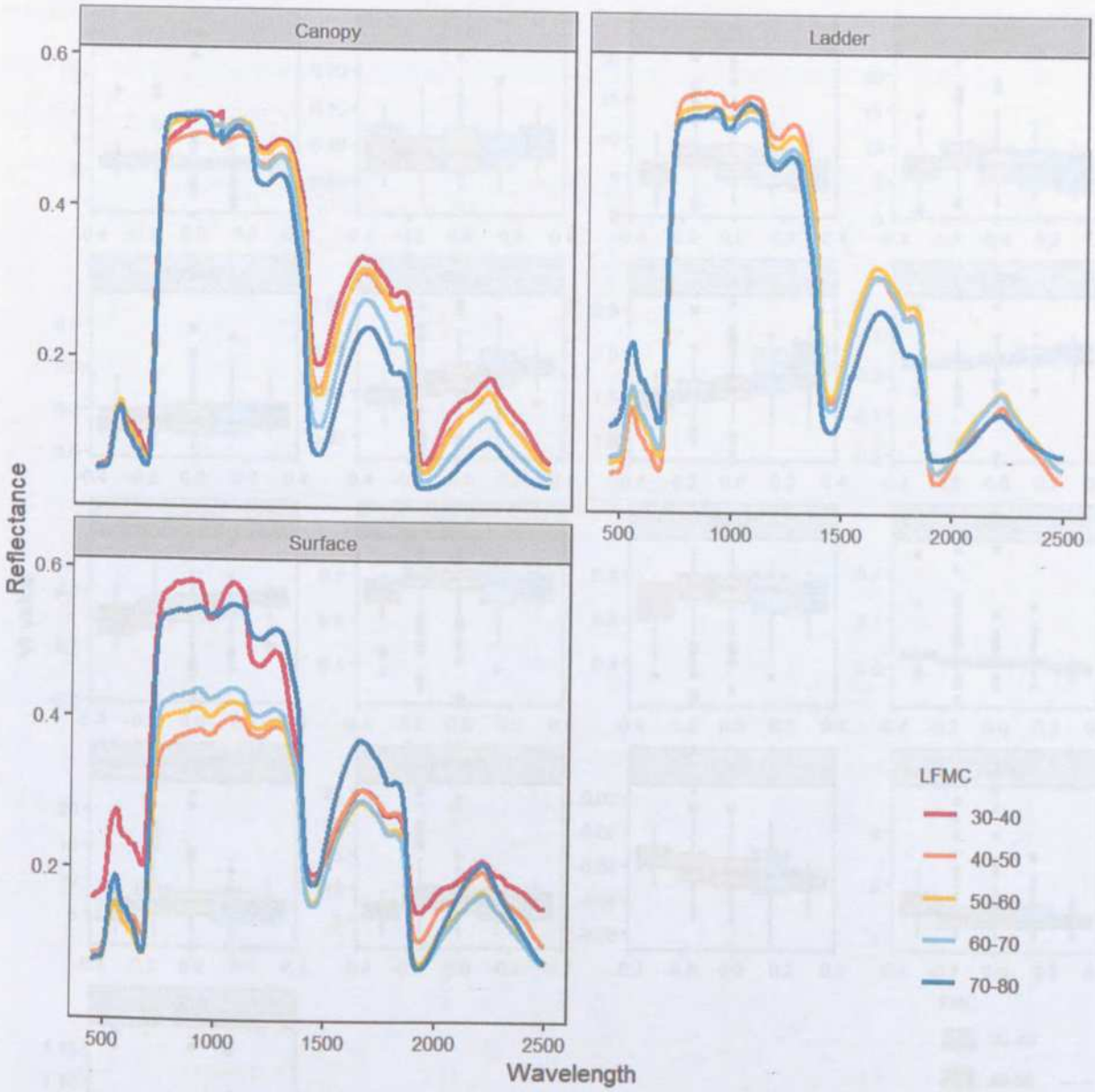

Fig. 5. Leaf reflectance of fuel moisture content (FMC) classes 30-40, 40-50, 50-60, 60-70 and 70-80. surface ($Surface_{fuels}$), ladder ($Ladder_{fuels}$) and canopy fuels ($Canopy_{fuels}$)

The vegetation indices using bands in the water absorption features of the spectra (e.g., WBI and NDWI) had a directly relationship with the FMC, i.e., the index value increase as FMC content increased (Fig. 6). Furthermore, WBI and NDWI seemed to have a shorter interquartile range than most of the other vegetation indices. It was also possible to observe a pattern of increasing values for NDLI and NDLI3 – which are also associated to water content – with the increase of FMC. On the other hand, an inverse relationship was observed with CAI – a cellulose, dry matter index – PSRI and RVSI. No clear linear relationship was observed for the other indices. In general, the intermediate classes (e.g., FMC50-60) presented had a higher number of outliers than the other classes.

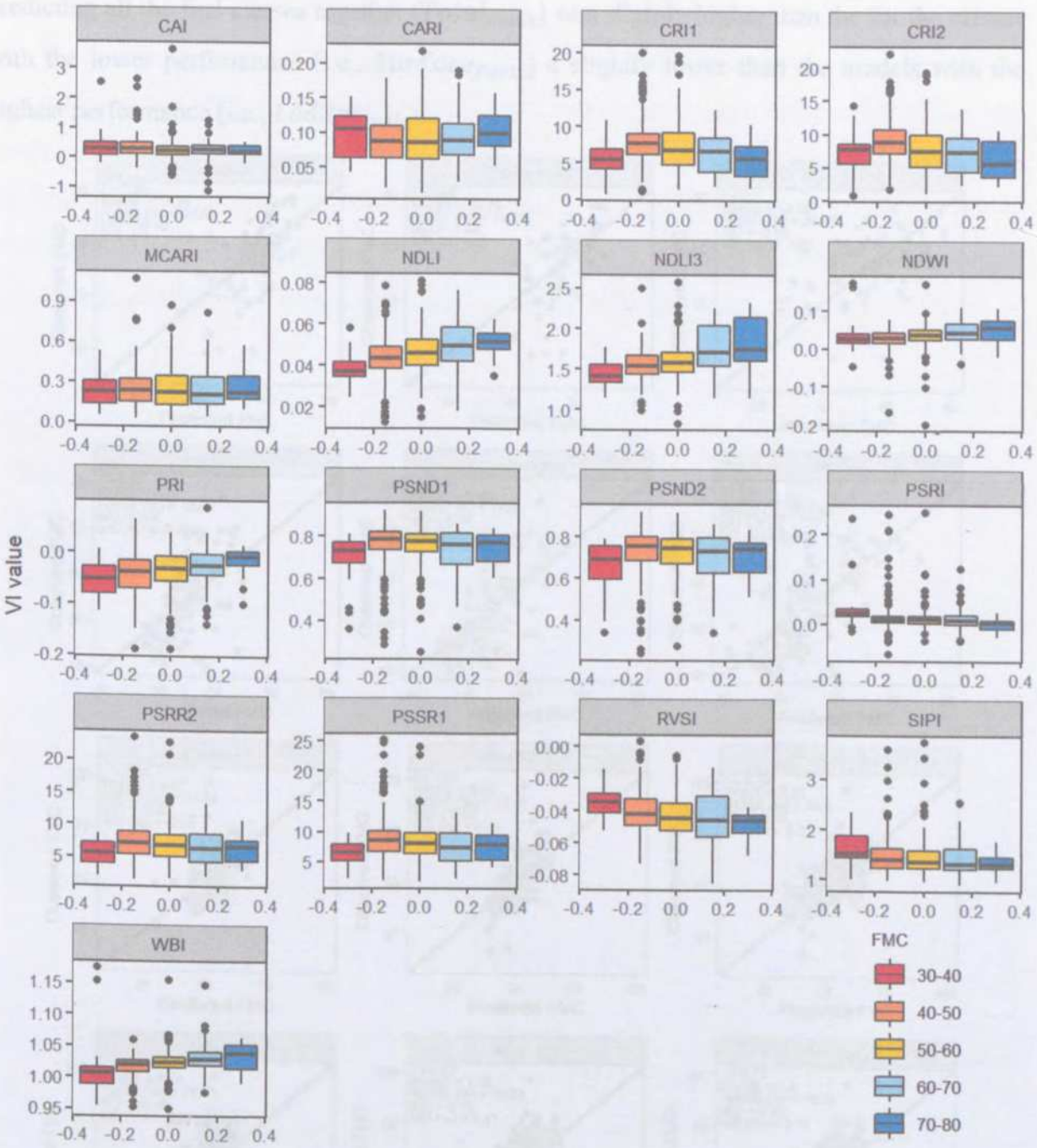

Fig. 6. Vegetation indices calculated for fuel moisture content (FMC) classes 30-40, 40-50, 50-60, 60-70 and 70-80.

Overall, the models had a relatively high precision for FMC prediction using all the prediction algorithms – most with RMSE% < 20% (Fig. 7). The lowest RMSE% was achieved for Ladder fuels using SVM (r = 0.64, RMSE = 11.91, MD = 0.24). In fact, the SVM method had a slightly better performance for all fuel classes FMC prediction. Conversely, the ANN method had the lowest performance compared to the other methods. The highest difference between methods occurred for the prediction of $Surface_{fuels}$ where the RMSE% using ANN was of ~25%. The lowest performances were observed for $Surface_{fuels}$. The precision for

predicting all the fuel classes together ($Total_{fuels}$) was slightly higher than the for the classes with the lower performance (i.e., $Surface_{fuels}$) a slightly lower than the models with the highest performance (i.e., $Ladder_{fuels}$).

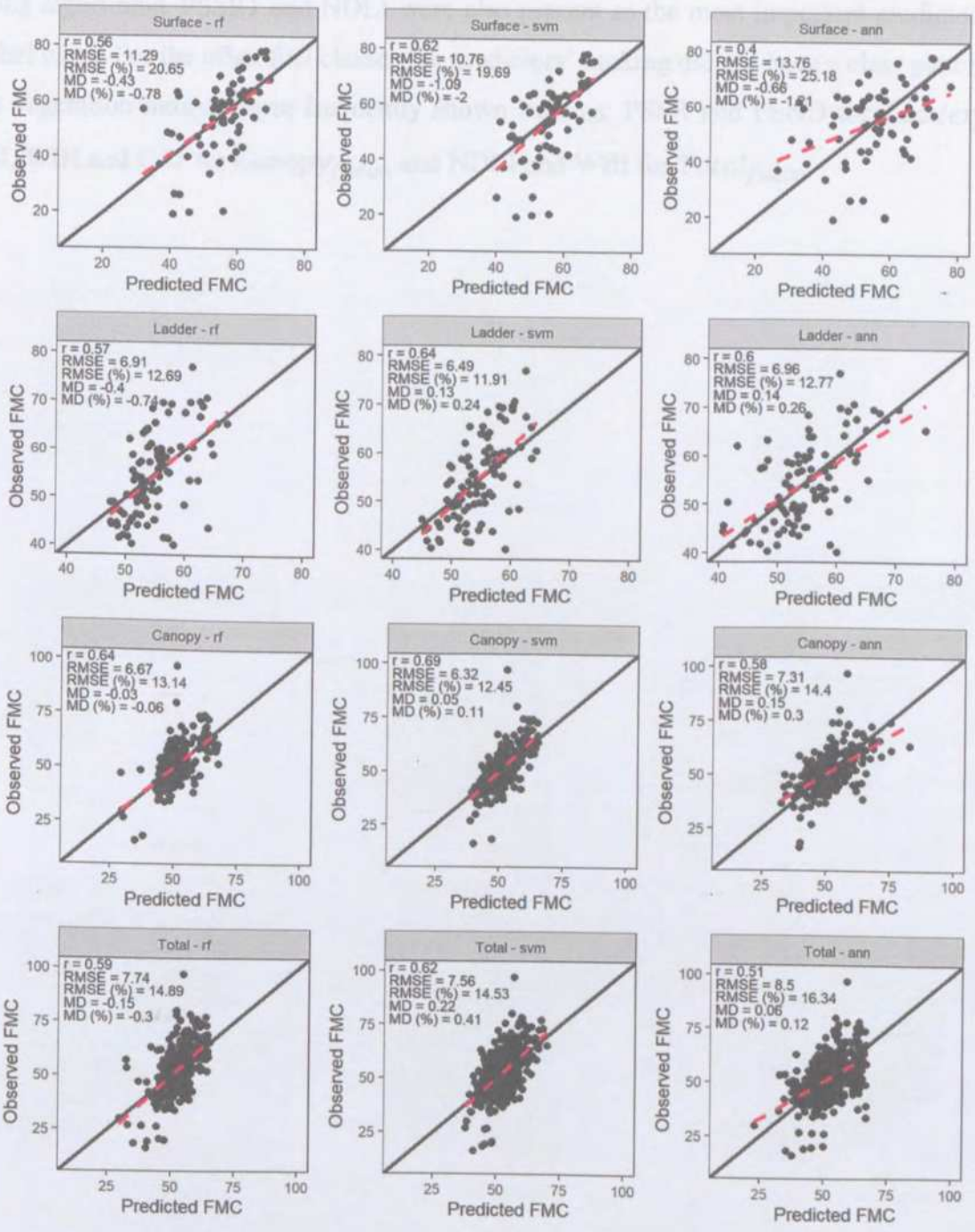

Fig. 7. Validation results for estimating FMC for surface ($Surface_{fuels}$), shrub and small trees ($Ladder_{fuels}$) and canopy fuels ($Canopy_{fuels}$) using Random Forest (RF), Support Vector Machine (SVM) and single layer Artificial Neural Network (ANN) algorithms as modeling approaches and vegetation indices as predictors. r = coefficient of correlation; RMSE = root mean square error; and MD = mean difference.

The most important predictors of FMC (i.e., vegetation indices) were slightly different for the fuel classes (Fig. 8). For $Surface_{fuels}$, CAI was the most important predictor for all the training algorithms. PSSR1 and NDLI were also present as the most important predictors for this fuel class. For the other fuel classes the predictors' ranking did not have a clear pattern but some vegetation indices more frequently shown such as: PSSR and PSND for $Ladder_{fuels}$; NDLI, WBI and CAI for $Canopy_{fuels}$, and NDLI and WBI for $Total_{fuels}$.

Fig. 8. Importance of vegetation indices used as inputs into Random Forest (rf), Support Vector Machine (svm) and Artificial Neural Network (ann) models to estimate fuel moisture content (FMC) for herbaceous fuels ($Surface_{fuels}$), shrubs and small trees ($Ladder_{fuels}$),woody fuels ($Canopy_{fuels}$), and total fuels ($Total_{fuels}$). The vegetation indices acronyms and equations are described in Table 1.

4. Discussion

Fuel moisture content (FMC) is one of the most important variables for effectively managing fire (Yebra et al. 2018, Szpakowski et al. 2019, Chuvieco et al. 2020). The results demonstrated the predictive capacity of using leaf spectroscopy to model FMC by using three machine learning algorithms and vegetation indices. The prediction could be done for each fuel class separately or in a single model despite the differences in leaf characteristics across growth forms. Furthermore, to account for the variability in FMC, vegetation indices that are associated with different leaf chemical and structural characteristics were important, besides the ones associated with water content.

The FMC predictions were performed for species of different growth forms (e.g., herbaceous, shrubby and arboreous) in Cerrado. They represent a range of leaf physical, structural and chemical properties that directly affect light interactions with the leaves in conjunction with FMC. For example, reflectance in water-related regions of the spectra might be less sensitive to water content variation in species with thicker leaves (Ustin et al. 2012, Sims and Gamon 2002, Gitelson et al. 2003). In addition, absorption features in the SWIR region that are related to lignin and cellulose can be masked in the presence of water (Buitagro et al. 2018) and when there are variations in both FMC and dry matter (Danson and Bowyer 2004). Some of the models in this study, especially for $Surface_{fuels}$, seemed to be more related to structural leaf components that are related leaf dry matter content rather than directly from light interaction with water. Part of this variability was captured for example with CAI as the most important vegetation index to predict $Surface_{fuels}$ (Nagler et al. 2000). $Surface_{fuels}$ also had the driest samples for our study, which might suggest the importance of those non-water related features for low FMC. This is also justified since reductions in water content will have impacts on plant physiology and pigments (Bowier and Danson 2004) and supports that the most correlated wavelengths (or vegetation indices) with FMC may depend on the range of FMC (Danson and Bowyer 2004).

In this study a single model for all fuel classes had similar performance to models per class. This implies that FMC variations could be captured in a single model, even though the leaf trait characteristics could be very distinct between the fuel classes - e.g., thick sclerophyllous leaves for woody plants and thin leaves in herbaceous species (Rossatto et al. 2015). Part of the unexplained variance could be related to species-specific characteristics that were not

accounted for such as leaf mass per area and leaf dry matter content that could vary even within the defined fuel classes (Streher et al. 2020). Furthermore, it is important to consider that the observations used in to train the machine learning algorithms came from 50 plots located in different study sites in Cerrado. During the data partition conducted in the training process the information regarding plot was not considered which can lead to training and validation datasets with the presence of observations from the same plot. The spatial autocorrelation that exists between the observations in a plot might be captured by machine learning algorithms which can lead to model performance improvements (Salazar et al. 2022). Further research should consider splitting the data for training and validation taking into account the plot information, i.e., keep in a same group (training or validation) all the observations from a given plot.

The definition of the vegetation indices and spectral bands for FMC prediction have implications for large-scale FMC monitoring in tropical savanna ecosystems such as Cerrado. Several spaceborne missions have been recently launched with sensors that accounts for the range of spectral regions that are necessary to compute the vegetation indices shown in this study, such as DESIS, PRISMA, HISUI, and ENMAP (Alonso et al. 2019, Krutz et al. 2019, Cogliati et al. 2021, Matsunaga et al. 2020, Guanter et al. 2015). It is important to highlight that for image spectroscopy a mixture of fuel classes with a range FMC may exist at a projected pixel (of about 30-m resolution) on the surface and their mixture could determine the overall reflectance of the pixel to predict FMC. In addition, limitations for FMC prediction can arise when the SWIR region is not covered (e.g., DESIS), even though there are indirect relationships of leaf water content reduction with variations in reflectance in the visible and NIR range (Streher et al. 2020, Bowyer and Danson 2004). Even though there are other robust methods to explore the estimation of FMC from spectroscopic measurements such as Partial Least Square Regression (PLSR) (Qi et al. 2014, Streher et al. 2020), Spectral Mixture Analysis (SMA) (Roberts et al. 2006) and PROSPECT (Marino et al. 2020) the use of vegetation indices appears as a potential method to scale-up fuel information. They represent an easy and meaningful method of dimensionality reduction / data mining and are not as influenced by sensor-specific noise as other methods which uses the entire spectrum. Coupled with the powerful of machine learning algorithms, our approach and findings are a step towards efficient FMC monitoring for large scale fire management.

5. Conclusions

In this study, leaf spectroscopy was used to predict fuel moisture content of different vegetation layers ($Surface_{fuels}$, $Ladder_{fuels}$and $Canopy_{fuels}$) of the Brazilian tropical

Savanna (Cerrado). Machine learning algorithms were used with vegetation indices related to leaf traits as inputs in models to predict FMC. The results support the expected benefits of using narrow-band passive sensors for retrieving FMC. In addition, it was observed that wavelengths from regions related to pigments and structural constituents are important to retrieve FMC, besides the bands directly related to water content. Next steps include i) decoupling species traits (e.g., morphology and chemical constituents) from FMC prediction and ii) using imaging spectroscopy sensors to assess FMC prediction in a mixture of fuel classes and a range of FMC values. The results can support the use of the current and new generation of imaging spectroscopy spaceborne sensors that can potentially be used to improve large-scale fire management in Cerrado and other fire-prone ecosystems

References

Adams, M.A., Shadmanroodposhti, M., Neumann, M., 2020. Causes and consequences of Eastern Australia's 2019–20 season of mega-fires: A broader perspective. Global Change Biology 26, 3756–3758. https://doi.org/10.1111/gcb.15125

Alonso, K., Bachmann, M., Burch, K., Carmona, E., Cerra, D., de los Reyes, R., Dietrich, D., Heiden, U., Hölderlin, A., Ickes, J., Knodt, U., Krutz, D., Lester, H., Müller, R., Pagnutti, M., Reinartz, P., Richter, R., Ryan, R., Sebastian, I., Tegler, M., 2019. Data products, quality and validation of the DLR earth sensing imaging spectrometer (DESIS). Sensors (Switzerland) 19, 1–44. https://doi.org/10.3390/s19204471

Breiman, L. (1996). Some properties of splitting criteria. Machine Learning, 24(1), 41-47. https://doi.org/10.1023/A:1018094028462

Breiman, L., 2001. Random forests. Machine Learning 2001. 45(1): 5–32.

Breiman, L., Friedman, J., Stone, C. J., & Olshen, R. A. (1984). Classification and regression trees. CRC press.

Cawse-Nicholson, K. et al. NASA's surface biology and geology designated observable: A perspective on surface imaging algorithms. Remote Sensing of Environment 257, 112349 (2021).

Chuvieco, E., Aguado, I., Salas, J., García, M., Yebra, M., Oliva, P. (2020). Satellite remote sensing contributions to wildland fire science and management. Current Forestry Reports, 6(2), 81-96. https://doi.org/10.1007/s40725-020-00116-5

Cogliati, S., Sarti, F., Chiarantini, L., Cosi, M., Lorusso, R., Lopinto, E., Miglietta, F., Genesio, L., Guanter, L., Damm, A., Pérez-López, S., Scheffler, D., Tagliabue, G., Panigada, C., Rascher, U., Dowling, T.P.F., Giardino, C., Colombo, R., 2021. The PRISMA imaging

spectroscopy mission: overview and first performance analysis. Remote Sensing of Environment 262. https://doi.org/10.1016/j.rse.2021.112499

Danson, F. M. & Bowyer, P. Estimating live fuel moisture content from remotely sensed reflectance. Remote Sensing of Environment 92, 309–321 (2004).

Fidelis, A., Alvarado, S., Barradas, A., Pivello, V., 2018. The Year 2017: Megafires and Management in the Cerrado. Fire 1, 49. https://doi.org/10.3390/fire1030049

Gomes, L., Miranda, H. S., Silvério, D. V., Bustamante, M. M. C. (2020). Effects and behaviour of experimental fires in grasslands, savannas, and forests of the Brazilian Cerrado. Forest Ecology and Management, 458, 117804,. https://doi.org/10.1016/j.foreco.2019.117804

Guanter, L. et al. The EnMAP Spaceborne Imaging Spectroscopy Mission for Earth Observation. Remote Sensing 7, 8830–8857 (2015).

Hoffmann, W. A., Jaconis, S. Y., McKinley, K. L., Geiger, E. L., Gotsch, S. G., & Franco, A. C. (2012). Fuels or microclimate? Understanding the drivers of fire feedbacks at savanna–forest boundaries. Austral Ecology, 37(6), 634-643. https://doi.org/10.1111/j.1442-9993.2011.02324.x

Jain, A. K., Mao, J., Mohiuddin, K. M., 1996. Artificial neural networks: A tutorial. Computer, 29(3), 31-44. doi:10.1109/2.485891

Karatzoglou, A., Smola, A., Hornik, K., Zeileis, A., 2004. kernlab - An S4 Package for Kernel Methods in R. Journal Of Statistical Software 11, 1–20

Knipling, E.B., 1970. Physical and physiological basis for the reflectance of visible and near-infrared radiation from vegetation. Remote Sensing of Environment 1, 155–159. https://doi.org/10.1016/S0034-4257(70)80021-9

Knipling, E.B., 1970. Physical and physiological basis for the reflectance of visible and near-infrared radiation from vegetation. Remote Sensing of Environment 1, 155–159. https://doi.org/10.1016/S0034-4257(70)80021-9

Krutz, D., Müller, R., Knodt, U., Günther, B., Walter, I., Sebastian, I., Säuberlich, T., Reulke, R., Carmona, E., Eckardt, A., Venus, H., Fischer, C., Zender, B., Arloth, S., Lieder, M., Neidhardt, M., Grote, U., Schrandt, F., Gelmi, S., Wojtkowiak, A., 2019. The instrument design of the DLR earth sensing imaging spectrometer (DESIS). Sensors (Switzerland) 19, 1–16. https://doi.org/10.3390/s19071622

Leite, R. V. et al. Estimating Stem Volume in Eucalyptus Plantations Using Airborne LiDAR: A Comparison of Area- and Individual Tree-Based Approaches. Remote Sensing 12, 1513 (2020).

Liaw, A., Wiener, M., 2002. Classification and Regression by randomForest. R News 2, 18–22.

Lippmann, R. P., 1987. An introduction to computing with neural nets. IEEE Assp magazine, 4(2), 4-22.

Lizundia-Loiola, J., Pettinari, M.L., Chuvieco, E., 2020. Temporal anomalies in burned area trends: Satellite estimations of the amazonian 2019 fire crisis. Remote Sensing 12. https://doi.org/10.3390/RS12010151

Myers, N., Mittermeier, R. A., Mittermeier, C. G., Da Fonseca, G. A., & Kent, J. (2000). Biodiversity hotspots for conservation priorities. Nature, 403(6772), 853-858. https://doi.org/10.1117/12.2029119

Nieke, J. & Rast, M. Towards the Copernicus Hyperspectral Imaging Mission For The Environment (CHIME). in IGARSS 2018 - 2018 IEEE International Geoscience and Remote Sensing Symposium 157–159 (IEEE, 2018). doi:10.1109/IGARSS.2018.8518384.

Ogle, S. M., Kurz, W. A., Green, C., Brandon, A., Baldock, J., Domke, G., Herold, M., Bernoux, M., ... & Waterworth, R. M. (2019). Chapter 2: Generic Methodologies Applicable To Multiple Land-Use Categories. 2019 Refinement to the 2006 IPCC Guidelines for National Greenhouse Gas Inventories 1–59.

R Core Team. (2020). R: A Language and Environment for Statistical Computing. R Foundation for Statistical Computing. Vienna, Austria. https://www.R-project.org/. (accessed 13 March 2021)

Raczko, E. & Zagajewski, B. Comparison of support vector machine, random forest and neural network classifiers for tree species classification on airborne hyperspectral APEX images. European Journal of Remote Sensing 50, 144–154 (2017).

Ribeiro, J. F. & Walter, B. M. T. Fitofisionomias do Bioma Cerrado. in SANO, S. M.; ALMEIDA, S. P. de (Ed.). Cerrado: ambiente e flora. Planaltina: EMBRAPA-CPAC 89-166. (1998).

Roberts, D. A., Dennison, P. E., Peterson, S., Sweeney, S. & Rechel, J. Evaluation of Airborne Visible/Infrared Imaging Spectrometer (AVIRIS) and Moderate Resolution Imaging Spectrometer (MODIS) measures of live fuel moisture and fuel condition in a shrubland ecosystem in southern California: AVIRIS AND MODIS LIVE FUEL MOISTURE. J. Geophys. Res. 111, (2006).

Roberts, D.A., Dennison, P.E., Gardner, M.E., Hetzel, Y., Ustin, S.L., Lee, C.T. (2003). Evaluation of the potential of Hyperion for fire danger assessment by comparison to the airborne visible/infrared imaging spectrometer. IEEE Transactions on Geoscience and Remote Sensing 41, 1297–1310. https://doi.org/10.1109/TGRS.2003.812904

Rodrigues, C. A. & Fidelis, A. Should we burn the Cerrado? Effects of fire frequency on open savanna plant communities. J Vegetation Science 33, (2022).

Rossatto, D. R., Kolb, R. M. & Franco, A. C. Leaf anatomy is associated with the type of growth form in Neotropical savanna plants. Botany 93, 507–518 (2015).

Salazar, J. J., Garland, L., Ochoa, J. & Pyrcz, M. J. Fair train-test split in machine learning: Mitigating spatial autocorrelation for improved prediction accuracy. Journal of Petroleum Science and Engineering 209, 109885 (2022).

Sims, D. A. & Gamon, J. A. Relationships between leaf pigment content and spectral reflectance across a wide range of species, leaf structures and developmental stages. Remote Sensing of Environment 81, 337–354 (2002).

Souza, G. S. A. de et al. Multi-sensor prediction of Eucalyptus stand volume: A support vector approach. ISPRS Journal of Photogrammetry and Remote Sensing 156, 135–146 (2019).

Stavros, E. N., Coen, J., Peterson, B., Singh, H., Kennedy, K., Ramirez, C., Schimel, D. (2018). Use of imaging spectroscopy and LIDAR to characterize fuels for fire behavior prediction. Remote Sensing Applications: Society and Environment, 11, 41–50. https://doi.org/10.1016/j.rsase.2018.04.010

Strassburg, B. B., Brooks, T., Feltran-Barbieri, R., Iribarrem, A., Crouzeilles, R., Loyola, R., ... & Balmford, A. (2017). Moment of truth for the Cerrado hotspot. Nature Ecology & Evolution, 1(4), 1-3. https://doi.org/10.1038/s41559-017-0099

Streher, A. S., Torres, R. da S., Morellato, L. P. C. & Silva, T. S. F. Accuracy and limitations for spectroscopic prediction of leaf traits in seasonally dry tropical environments. Remote Sensing of Environment 244, 111828 (2020).

Szpakowski, D. M., Jensen, J. L. (2019). A review of the applications of remote sensing in fire ecology. Remote Sensing, 11(22), 2638. https://doi.org/10.3390/rs11222638

Tatem, A.J., Goetz, S.J., Hay, S.I., 2009. UKPMC Funders Group Fifty Years of Earth Observation Satellites : Earth 96, 1–7. https://doi.org/10.1511/2008.74.390.Fifty

Turner, M. G., Gardner, R. H., & O'neill, R. V. (1995). Ecological dynamics at broad scales. BioScience, 45, S29-S35.

Ustin, S. L., Riaño, D. & Hunt, E. R. Estimating canopy water content from spectroscopy. Israel Journal of Plant Sciences 60, 9–23 (2012).

Ustin, S.L., Middleton, E.M., 2021. Current and near-term advances in Earth observation for ecological applications. Ecological Processes 10, 1–57. https://doi.org/10.1186/s13717-020-00255-4

Vapnik, V. N., 1998. Statistical learning theory. Wiley Interscience.

Venables, W. N. & Ripley, B. D. (2002) Modern Applied Statistics with S.

Yebra, M., Quan, X., Riaño, D., Rozas Larraondo, P., van Dijk, A.I.J.M., Cary, G.J., 2018. A fuel moisture content and flammability monitoring methodology for continental Australia based on optical remote sensing. Remote Sensing of Environment 212, 260–272. https://doi.org/10.1016/j.rse.2018.04.053

Zhu, L., Webb, G.I., Yebra, M., Scortechini, G., Miller, L., Petitjean, F., 2021. Live fuel moisture content estimation from MODIS: A deep learning approach. ISPRS Journal of Photogrammetry and Remote Sensing 179, 81–91. https://doi.org/10.1016/j.isprsjprs.2021.07.010

Chapter 2: Large scale multi-layer fuel load characterization in tropical savanna using GEDI spaceborne lidar data

ABSTRACT

LEITE, Rodrigo Vieira, Universidade Federal de Viçosa, December, 2022. **Large scale multi-layer fuel load characterization in tropical savanna using GEDI spaceborne lidar data**. Adviser: Cibele Hummel do Amaral.

Quantifying fuel load over large areas is essential to support integrated fire management initiatives in fire-prone regions to preserve carbon stock, biodiversity and ecosystem functioning. It also allows a better understanding of global climate regulation as a potential carbon sink or source. Large area assessments usually require data from spaceborne remote sensors, but most of them cannot measure the vertical variability of vegetation structure, which is required for accurately measuring fuel loads and defining management interventions. The recently launched NASA's Global Ecosystem Dynamics Investigation (GEDI) full-waveform lidar sensor holds potential to meet this demand. However, its capability for estimating fuel load has yet not been evaluated. In this study, we developed a novel framework and tested machine learning models for predicting multi-layer fuel load in the Brazilian tropical savanna (i.e., Cerrado biome) using GEDI data. First, lidar data were collected using an unnamed aerial vehicle (UAV). The flights were conducted, over selected sample plots in distinct Cerrado vegetation formations (i.e., grassland, savanna, forest) where field measurements were conducted to determine the load of surface, herbaceous, shrubs and small trees, woody fuels and the total fuel load. Subsequently, GEDI-like full-waveforms were simulated from the high-density UAV-lidar 3-D point clouds from which vegetation structure metrics were calculated and correlated to field-derived fuel load components using Random Forest models. From these models, we generate fuel load maps for the entire Cerrado using all on-orbit available GEDI data. Overall, the models had better performance for woody fuels and total fuel loads ($r = 0.93$ and 0.84, respectively). For components at the lower stratum, models had moderate to low performance (r between 0.38 and 0.55) but still showed reliable results. The presented framework can be extended to other fire-prone regions where accurate measurements of fuel components are needed. We hope this study will contribute to the expansion of spaceborne lidar applications for integrated fire management activities and supporting carbon monitoring initiatives in tropical savannas worldwide.

1. Introduction

Climate change mitigation and biodiversity conservation efforts across the world require an understanding of wildfire dynamics (Bowman et al., 2013, Lehmann et al. 2014). Tropical Savanna ecosystems are generally fire-adapted (Simon et al., 2009, Hoffmann et al., 2012, Durigan & Ratter, 2016), but human activities have affected fire regimes and landscape characteristics (Hantson et al., 2015, Andela et al., 2017, Andela et al., 2018, Rosan et al. 2019, Durigan et al. 2020). Fire dynamics in tropical savannas depend, among other factors, on the vegetation structure and accumulated fuel loads (combustible contents) (Sandberg et al., 2001, Chuvieco et al., 2003, Keane et al., 2013). Fuel load structure continuity, condition (live or dead) and moisture are important variables for modeling fire behavior (Stavros et al., 2018, Gomes et al., 2020a), assessing its severity (Hu et al. 2019, Klauberg et al., 2019), calculating greenhouse gas emissions (GHG) (Ogle et al., 2019, Gomes et al., 2020a) and improving landscape management and conservation strategies to promote a pyro-diverse ecosystem (Schmidt et al., 2018, Franke et al., 2018). These applications demand measurements of all fuel components as they interact with fire differently. That includes necromass (e.g., duff, litter, downed wood debris) and different plant types (e.g., grasses, herbs, forbs, shrubs, trees).

Remote sensing technologies are commonly used to examine fuel load distribution and spatial variability over large areas. In this regard, lidar (light detection and ranging) sensors are preferred as they can directly detect different vegetation strata with high accuracy (Erdody et al., 2010, Gajardo et al., 2014, Szpakowski and Jensen 2019, Chuvieco et al., 2020). Generally, the approach for local scale fuel mapping relies on discrete-return or full-waveform lidar sensors in aircraft or unnamed aerial vehicle (UAV) platforms to collect lidar data and calculate lidar-derived metrics that will subsequently serve as predictor variables in statistical models (Hermosilla et al., 2014, Hudak et al., 2016a, Bright et al., 2017, Stefanidou et al., 2020). Nonetheless, when there are limited resources for airborne and UAV-lidar surveys, or it is necessary to upscale analyses to a regional/global level, images acquired by satellite systems operating in either optical or microwave domain are then required (Wulder et al., 2012, Garcia et al., 2017, Franke et al., 2018). The Geoscience Laser Altimeter System (GLAS, onboard ICESat-1 – Zwally et al., 2002) was the first spaceborne lidar sensor to collect sample data globally, and it was operational between 2003 and 2009. Although its main objective was to measure ice-sheet changes, GLAS was also used for forest and fuel-related studies (Lefsky et al., 2006, Duncanson et al., 2010, Ashworth et al., 2010, García et al., 2012, Peterson et al.,

2013, Ferreira et al. 2011). Its successor mission launched in 2018, ICESat-2, is a photon-counting lidar system that also provides valuable 3-D sample data globally that can be similarly used for biomass estimation (Narine et al., 2020). Yet, neither of these missions' characteristics were optimized for collecting data over the global range of forest canopy structures which limits opportunities to use these data to examine some important biomes at regional scale.

A new promising near-global dataset for fuel load estimation comes from the Global Ecosystem Dynamics Investigation (GEDI) sensor, with unprecedented high resolution lidar data samples collected between ~52° north and south latitudes, available since April 2019 (Dubayah et al., 2020a). As the first of its kind, GEDI was specifically designed to measure forest structure. The sensor is characterized as a large-footprint (diameter of ~25 m) full-waveform lidar with penetration capability in forests with up to ~99% canopy cover (Hancock et al., 2019, Duncanson et al., 2020). GEDI's penetration capabilities in dense vegetation is what mainly differentiates it from the previous spaceborne lidar sensors designed for ice sheet measurements. Furthermore, the footprints are separated at 60 m along track and 600 m across track - an improvement to GLAS' 70 m footprint separated ~170 m along track (Zwally et al. 2002). The improved technical specification makes GEDI more suitable than any previous spaceborne sensor to measure forest structure at regional and global scales.

The GEDI mission plan includes the delivery of a global aboveground dry biomass (AGB) product at a spatial resolution of 1-km (Dubayah et al. 2020a) that is suitable for global biomass mapping requirements (Hall et al., 2011). These AGB estimates are expected to be the global benchmark of forest AGB, essential for measuring the world's carbon stocks. Furthermore, recent studies used GEDI waveform metrics for developing models to estimate forest height (Potapov et al., 2021, Rishmawi et al., 2021), biomass (Saarela et al., 2018, Silva et al., 2021, Duncanson et al., 2020, Rishmawi et al., 2021), and canopy structure diversity (Marselis et al., 2018, Schneider et al., 2020, Rishmawi et al., 2021). However, to date, no published study on estimation of fuel loads from GEDI data is available and the GEDI AGB products may be of limited use for fire-related applications because calibration data to derive information on important layers may be lacking – such as from duff, litter, down woody debris, grasses, forbs and shrubs. In addition, these lower fuel strata layers that are crucial for fire behavior and emissions are commonly not considered in previous studies using spaceborne lidar sensors (Lefsky et al. 2005, Garcia et al. 2012, Peterson et al. 2013). Therefore, it is necessary to develop models using GEDI-derived metrics that consider all fuel load components for

effectively meeting integrated fire management criteria and for improving carbon budget estimates.

Confirming GEDI's capability to predict fuel loads in savannas will open a range of new opportunities to improve fire management planning and decisions at regional and global scales. Furthermore, the possibility of having this information from space also opens the range of GEDI applications to map fuel loads during the mission life-span and for upcoming lidar satellite missions (e.g., Multi-footprint Observation Lidar and Imager - MOLI (Murooka et al., 2013, Kimura et al., 2017, Asai et al., 2018). The applications of such technological advances include mapping fire risk, carbon emissions and estimate fire behavior and fuel load dynamics for larger areas such as countries or entire biomes, thus contributing to mitigate the impacts of climate change in these regions. The overall aim of this study was to assess the capability of GEDI for estimating large-scale multi-layer fuel loads in the Brazilian tropical savanna (Cerrado). Herein, we developed a framework to i) calibrate and validate Random Forest (RF) models for predicting different fuel layers (ground, surface, shrubs, trees and total fuel load) at the plot level across the complex gradient of Cerrado formations (i.e., grassland, savanna and forest) in Brazil from field and simulated GEDI data; and ii) characterize large-scale, multi-layer fuel loads across the entire Cerrado (i.e. 1.9 million km²) by applying the calibrated RF models to on-orbit GEDI data collected over its whole extent, and then aggregating the footprint level fuel load estimates to 1-km-resolution grid across the biome.

2. Material and Methods

2.1. Study area

The Brazilian Cerrado is the most biodiverse savanna in the world and considered as a top global hotspot for conservation priorities (Myers et al. 2000). It has been rapidly converted to crop and pasturelands and less than half of its original vegetation cover remains (Strassburg et al. 2017). This native vegetation, however, has been severely impacted by human-mediated shifts in fire regimes and widespread invasion of fire-prone African fodder grasses (Durigan and Ratter, 2016). Our study sites are located in the Serra do Cipó National Park (SCNPK), Chapada dos Veadeiros National Park (CVNPK), Paraopebas National Forest (PNF) and University of São João Del-Reis Forest (UFSJ) (Fig. 1). Site locations were chosen to span a range of vegetation structures within the Cerrado biome, covering the three major formations (i.e., grassland, savanna, and forest). In Cerrado, grasslands are characterized by the presence of grass species alone (vegetation type locally known as "Campo limpo"), with scattered shrubs

("Campo sujo" and "Campo rupestre"), or dominated by grasses and shrubs with scattered trees ("Cerrado ralo"). The savanna formation is mostly dominated by contorted short trees with scattered shrubs and grasses (e.g., "Cerrado sensu stricto"). Forests are tree-dominated formations (e.g., "Cerradão", in addition to the extra-Cerrado forest formations as Riparian and Gallery forests).

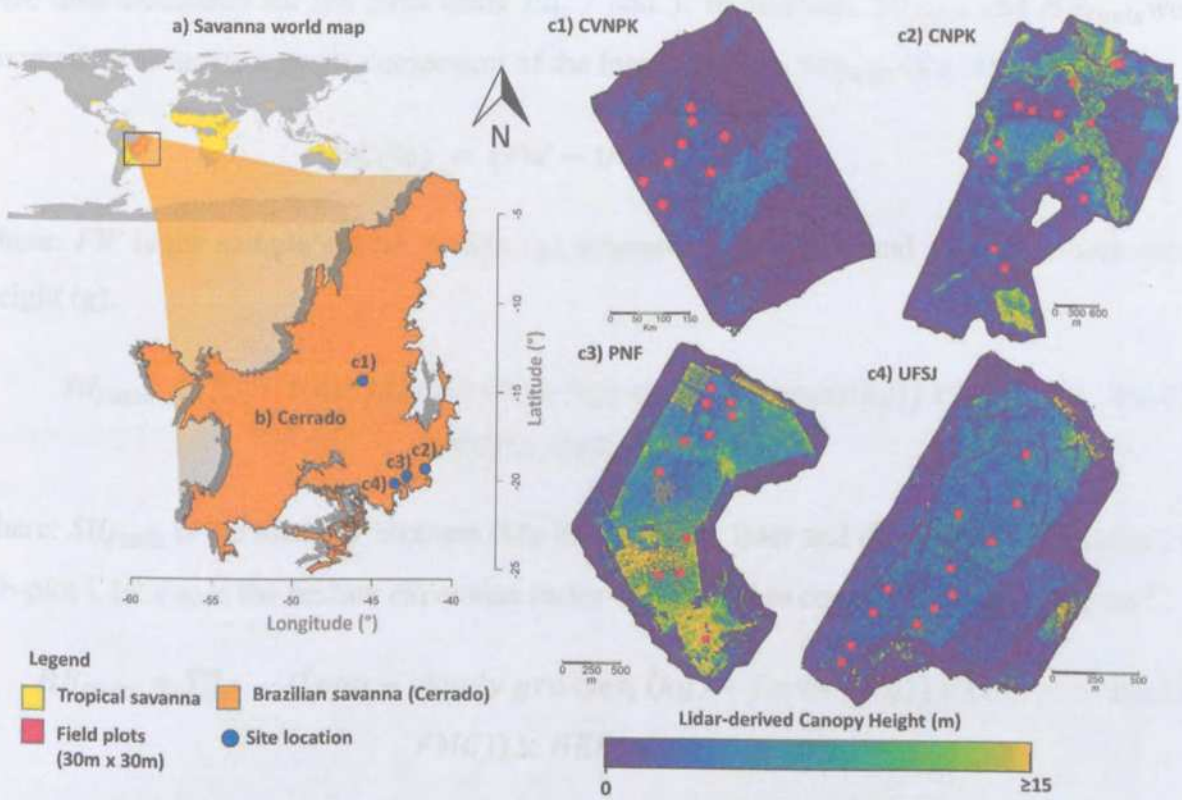

Fig. 1. Spatial location of the Brazilian savanna (Cerrado) (a, b) and study sites where UAV-lidar and field data were collected, namely, Chapada dos Veadeiros National Park (CVNPK, c1), Serra do Cipó National Park (SCNPK, c2) Paraopeba National Forest (PNF, c3) and University of São João Del-Rei's Forest (UFSJ, c4). Fig.c1-c4 show the UAV-lidar coverage and canopy height model derived from the 3D point cloud.

2.2 Fuel load measurements

We established sample plots in different Cerrado vegetation formations (i.e., grassland, savanna, and forest) between June and July 2019. First, 50 square plots of 30 x 30 m (900 m^2) were set across the study sites (Fig. 2a). Each plot corner was geolocated using a Differential Global Navigation Satellite System (Fig. 2c). Subsequently, four 1 x 1 m (1 m^2) and two 1 x 5 m (5 m^2) subplots were set within each plot to measure surface and shrubs/small trees fuel components, respectively (Fig. 2b, 2d). In the field, all duff, litter and downed woody debris

(surface fuels; SU_{fuels}) were separated from non-woody grasses, herbs and forbs (herbaceous fuels; HB_{fuels}). They were immediately weighed with a 10 g precision scale. Three 500 g samples were taken to be weighed on a laboratory scale (precision of 1 mg) and oven dried at 65°C until a constant weight was reached. The fresh and dry weight of the samples were used to calculate fuel moisture content (FMC, Eq. 1). The total dry biomass of SU_{fuels} and HB_{fuels} were then calculated for the plots using Eq. 2 and 3. In addition, SU_{fuels} and HB_{fuels} were summed up to create a single component of the lowest stratum SH_{fuels} (Eq. 4).

$$FMC(\%) = (FW - DW)/DW, \quad \text{(eq.1)}$$

where: FW is the sample's fresh weight (g) measured in the field and DW is its oven-dried weight (g).

$$SU_{fuels} = \sum_{i=1}^{n} \left((duff_i(kg) + litter_i(kg) + downed\ wood_i(kg)\right) x\ (1 - FMC))\ x\ HEF_{SU}, \quad \text{(eq.2)}$$

where: SU_{fuels} is the total dry biomass (Mg ha^{-1}) of duff, litter and downed wood collected in sub-plot i. HEF_{SU} is the hectare expansion factor of 2.5 used to convert from kg to Mg ha^{-1}.

$$HB_{fuels} = \sum_{i=1}^{n} \left((non - woody\ grasses_i\ (kg) + forbs\ _i(kg)\right) x\ (1 - FMC))\ x\ HEF_{SU}, \quad \text{(eq.3)}$$

where: HB_{fuels} is the total dry biomass (Mg ha^{-1}) in plot i of non-woody grasses and forbs collected in subplot j.

$$SH_{fuels} = SU_{fuels} + HB_{fuels}, \quad \text{(eq.4)}$$

where: SH_{fuels} is the total dry biomass (Mg ha^{-1}) of the lowest vegetation stratum.

Similarly, all the shrubs and trees with diameter at breast height (dbh, 1.3 m) < 10 cm were harvested and immediately weighed with a 10 g precision scale. Three 500 g samples of stems, branches and leaves were taken to be weighed in a laboratory scale (precision 1 mg) and oven dried at 65°C until constant weight was reached. The total dry biomass of this component was then calculated using Eq. 5.

$$SS_{fuels} = \sum_{i=1}^{n} \left((shrubs_i\ (kg) + small\ trees_i\ (kg)\right) x\ (1 - FMC))\ x\ HEF_{SS} \quad \text{(eq.5)}$$

where: SS_{fuels} is the total dry biomass (Mg ha^{-1}) of shrubs and small trees (dbh < 10 cm). HEFss = 2.5.

Finally, all the trees in the plots with $dbh \geq 10$ cm were measured for total height (ht) and dbh using a digital clinometer and diameter tape, respectively. We used those measurements to estimate the dry aboveground biomass of trees (WD_{fuels}) using Eq. 6 (Chave et al., 2014).

$$WD_{fuels} = \sum_{j=1}^{n} \quad 0.0673\ x\ (\rho\ x\ dbh_j^{\ 2}\ x\ ht_j)^{0.976}\ x\ HEF_{wd}, \qquad \text{(eq.6)}$$

where: WD_{fuels} is the total dry aboveground biomass of trees (Mg ha^{-1}); dbh_j and ht_j are the dbh (cm) and ht (m) per tree j; ρ is the wood density (g cm^{-3}) derived from Zanne et al. (2009). HEFwd = 0.011. The total fuel load (TF_{fuels}) was calculated by summing all the components (Eq. 7). Table 1 summarizes fuel load component values in the sample plots by each Cerrado formation and a description of the data collection authorization process is in the supplementary material.

$$TF_{fuels} = SU_{fuels} + HB_{fuels} + SS_{fuels} + WD_{fuels} \qquad \text{(eq.7)}$$

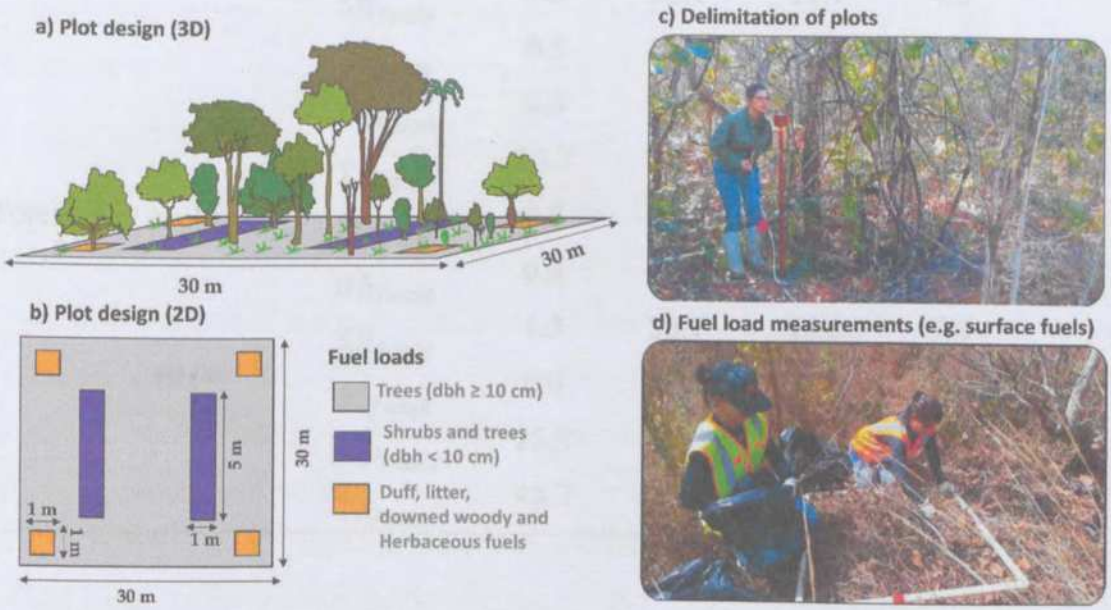

Fig. 2. Summary of field data survey where different plot sizes were designed for collecting tree, shrub, and surface fuels (a, b). Subfigures c) and d) depict plot sampling configuration and surface fuel collection, respectively.

Table 1. Summary of field measurements of surface fuels (SU_{fuels}), herbaceous (HB_{fuels}), surface and herbaceous fuels (SH_{fuels}), shrubs (SS_{fuels}, dbh < 10 cm), woody fuels (WD_{fuels}, dbh ≥ 10 cm) and total fuel load (TF_{fuels}) over the different Cerrado formations (i.e., grassland, savanna and forests).

Cerrado formation	Number of plots	Fuel component	Fuel load (Mg ha^{-1})			
			min	max	mean	sd
Grassland	5	SU_{fuels}	2.7	10.3	5.1	3.1
		HB_{fuels}	3.7	19.9	10.6	6.8
		SH_{fuels}	6.6	25.6	15.7	8.5
		SS_{fuels}	0.1	4.5	1.4	1.8
		WD_{fuels}	0.0	0.6	0.1	0.3
		TF_{fuels}	11.7	25.9	17.2	7.3
Savanna	30	SU_{fuels}	2.0	22.4	8.0	4.1
		HB_{fuels}	0.6	7.7	3.7	1.9
		SH_{fuels}	3.8	26.1	11.7	4.5
		SS_{fuels}	0.5	39.7	10.1	9.2
		WD_{fuels}	0.0	55.6	18.6	17.1
		TF_{fuels}	13.3	100.2	40.4	23.5
Forest	15	SU_{fuels}	0.8	30.1	13.9	7.3
		HB_{fuels}	0.4	6.7	1.3	1.6
		SH_{fuels}	1.3	30.7	15.3	7.8
		SS_{fuels}	0.0	36.8	11.9	13.1
		WD_{fuels}	25.9	138.1	77.1	39.2
		TF_{fuels}	43.7	187.9	104.2	42.4

2.3. UAV-lidar data acquisition and processing

The UAV-lidar 3-D point clouds were acquired with the GatorEye Gen 1 UAV system (Broadbent et al., 2021) in July 2019. The GatorEye platform was a DJI M600 Pro hexacopter that integrated a Velodyne VLP-32c dual-return laser scanner lidar with an Inertial Measurement Unit (Fig. 3), and it was coupled with a dual-return lidar sensor with 32 separate

lasers, each having a 360° vertical field of view (FOV). The sensor emitted around 600,000 pulses per second with a theoretical return number of 1.2 million returns per second and in parallel, a Global Navigation Satellite System (GNSS) receiver collected static geolocation data to calculate a post-processing kinematic (PPK) flight trajectory. Herein, UAV-lidar 3D point cloud data pre-processing included: i) implementing the GatorEye Multi-scalar Post-Processing Workflow (Broadbent et al., 2021), ii) aligning the flight lines, iii) classifying ground, iv) creating a digital terrain model, v) normalizing point cloud height and vi) clipping the point clouds within the field plots for GEDI data simulation (Section 2.4).

Fig. 3. GatorEye UAV-lidar (Gen 1) system. a) DJI M600 Pro hexacopter, with Phoenix Scout Ultra, hyperspectral, and visual sensors; b) three GNSS antennas for navigation, and one for sensor trajectory (positioned in the middle); c) Velodyne Ultra Puck lidar system.

2.4. GEDI data

2.4.1. GEDI full-waveform simulation

We simulated GEDI data from the UAV-lidar 3D point cloud for calibrating fuel load models to avoid the geolocation errors of GEDI (~10-20 m) and due to the fact that GEDI orbits are likely not to overlay our field plots. The GEDI pre-launch plan included the development of a GEDI simulator that is able to reproduce the on-orbit GEDI data characteristics for the calibration of aboveground biomass models (Hancock et al., 2019). The simulation includes transforming discrete-return lidar point clouds into full-waveform signals (Blair and Hofton 1999) in GEDI-sized footprints and with the expected GEDI instrument noise added. The waveform signal-to-noise ratio (SNR) on the on-orbit GEDI data depends on characteristics such as laser type (power or coverage), acquisition time (day or night), canopy cover and atmospheric conditions (Hancock et al., 2019, Dubayah et al., 2020a, Ducanson et al., 2020). The simulator ensures consistency across point cloud flight characteristics especially for high-density lidar point clouds, as used as input in this study, that allow consistently transferring models to the on-orbit GEDI data. Complete description and validation of the GEDI simulator

are described in detail in Hancock et al., 2019. GEDI-like waveforms were simulated from the high-density UAV-lidar point clouds clipped to the study sample plots using the *gediWFSimulator* tool in the rGEDI package (Silva et al., 2020) in R (R Core Team 2020). Realistic noise was added considering a beam sensitivity of 0.98 (i.e., the canopy cover at which ground is detected 90% of the time with 5% probability of a false positive Hancock et al. (2019)) by using a link margin of 4.956 at 95% of canopy cover that relates to noise of the power beam collecting data at night (Boucher et al., 2020). For ground detection and metrics calculation, the waveforms were denoised and smoothed by setting the noise threshold as the mean plus 3 standard deviations and smoothing width (applied after denoising) equal to 0.5 m (Qi et al., 2019, Silva et al., 2021).

2.4.2. GEDI-derived vegetation structure metrics

We calculated the following metrics from the simulated GEDI full-waveforms (Table 2): RH (relative height) at the 98th height percentile (RH98, in m), canopy cover fraction (CCF, in %), plant area index (PAI, in m^2 m^{-2}), and Foliage Height Diversity (FHD, unitless). These metrics were selected to match to the GEDI Level 2A and 2B products and facilitate model interpretability. RH98 represents the height below which 98% of the returned laser energy is registered. It was selected to represent the top of the canopy, avoiding the noise of using the last return elevation value (Silva et al. 2018). The CCF is related to the percent of the ground covered by the vertical projection of canopy material calculated from the Gaussian fitted ground signal. PAI is the projected area of plant elements per unit ground surface, which relates to the canopy cover and plant occupation of the vertical space. The FHD is an index for expressing canopy structure complexity and vertical distribution (MacArthur and Horn 1969). It is calculated by summing the product between the proportion of vertical PAI profiles and its logarithm in a selected horizontal layer (Tang and Armston, 2019). The theoretical basis and full description of cover and vertical profile GEDI metrics are detailed in the algorithm theoretical basis document (Tang and Armston, 2019). The metrics were calculated using the *gediWFMetrics* function in rGEDI (Silva et al., 2020) (Fig. 4).

Table 2. GEDI waveform metrics used as predictors to estimate fuel load components

Acronym	Description
RH98	Relative height at the 98th height percentile (m)
PAI	Plant Area Index (m^2 m^{-2})
CCF	Canopy cover fraction (%)
FHD	Foliage Height Diversity (unitless)

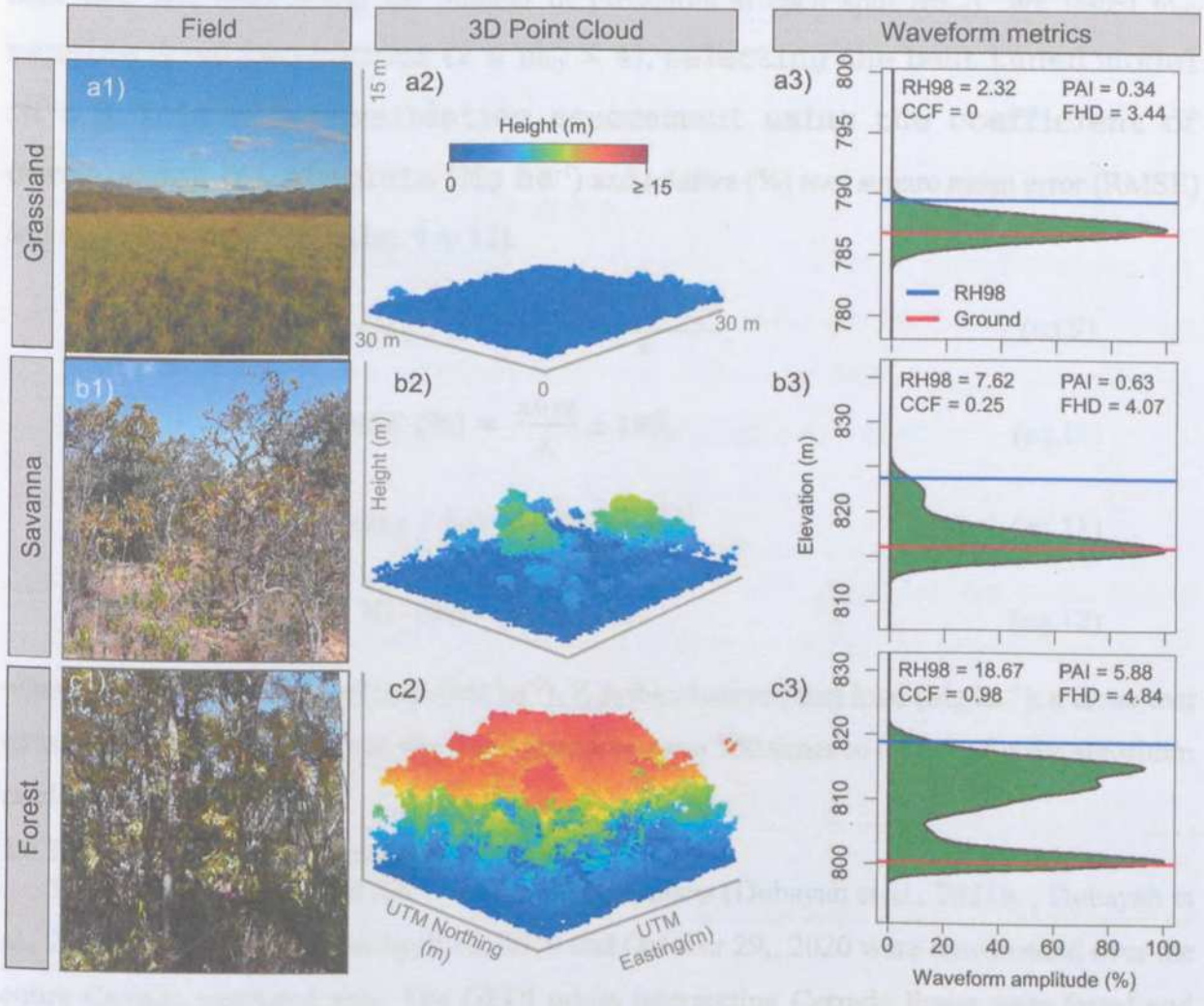

Fig. 4. Cerrado formations (a1, b1, and c1) and respective 3D point clouds from a UAV lidar survey (a2, b2, and c2) and metrics from the simulated waveforms (a3, b3, and c3).

2.5 Fuel load modeling development

Principal Component Analysis (PCA) was applied using the R package FactoMineR (Lê et al., 2008) for characterizing fuel load and GEDI metrics across field plots and vegetation formations. An explorative analysis of the derived PC scores was conducted in the first two components to analyze the relationships between field and GEDI variables.

Fuel loads were modeled separately, yielding five models with the GEDI metrics as

predictors and SU_{fuels}, HB_{fuels}, SH_{fuels}, SS_{fuels}, WD_{fuels} and TF_{fuels} as response variables. We used the random forest (RF) algorithm implemented through the Caret R package (Kuhn 2020) as our modeling approach. RF builds regression tree ensembles from bootstrapping the data, and the final prediction is the average ensemble outcome (Breiman et al., 1984, Breiman 1996). This method was selected for being flexible to the different data distributions present in our dataset due to the various vegetation structures in the Cerrado formations. Each RF was built with 500 trees tuning the number of predictors at each split (m_{try}). We tested m_{try} ranging from two to four ($2 \leq m_{try} \leq 4$), selecting the best tuned model in a 5-fold cross-validation assessment using the coefficient of correlation (r), absolute (Mg ha^{-1}) and relative (%) root square mean error (RMSE) and mean difference (MD) (Eq. 9 to 12).

$$RMSE\ (Mg\ /\ ha) = \sqrt{\frac{\sum_{i=1}^{n}\ (\hat{Y}_i - Y_i)^2}{n}}, \quad \text{(eq.9)}$$

$$RMSE\ (\%) = \frac{RMSE}{\underline{Y}}\ x\ 100, \quad \text{(eq.10)}$$

$$MD\ (Mg\ /\ ha) = \frac{\sum_{i=1}^{n}\ (\hat{Y}_i - Y_i)}{n}, \quad \text{(eq.11)}$$

$$MD\ (\%) = \frac{MD}{\underline{Y}}\ x100, \quad \text{(eq.12)}$$

where: $\hat{Y}_i$ is the estimated fuel load (Mg ha^{-1}), Y_i is the observed fuel load (Mg ha^{-1}); n is number of samples. For each fuel layer, the tuned model was run 500 times to account for the algorithm randomness.

2.6 Fuel loads characterization in Cerrado

The GEDI Level 2A and 2B version 2 data products (Dubayah et al., 2021b, , Dubayah et al., 2021c) collected between April 18, 2019 and October 29,, 2020 were downloaded over the entire Cerrado vegetated area. The GEDI orbits intersecting Cerrado limits were found and downloaded using the *gedifinder* and *gediDownload* functions in rGEDI package (Silva et al., 2020). The footprints were masked to the Cerrado vegetated area based on the land cover classification from Mapbiomas for the same year of the data collection (Souza et al. 2020). The GEDI footprint-level metrics (Table 2) were extracted using the *getLevel2AM* and *getLevel2B* functions and filtered using the quality flag (quality_flag = 1). This flag indicates usable data by summarizing individual quality assessment parameters based on waveform shot energy, sensitivity (< 0.9 over land), amplitude, and real-time surface tracking quality (Hofton and Blair 2019, Beck et al., 2020).

The fuel load models developed in item 2.5 were applied to the GEDI footprints (diameter of ~25 m) collected across the Cerrado biome extent. Fuel load maps of each component were created by taking the average of the footprint-level estimates at 1-km² grid cells for mapping purposes and compatibility with planned gridded GEDI products (Dubayah et al., 2020a) and requirements for global biomass maps (Hall et al., 2011).

We calculated the uncertainty of fuel load predictions in each cell by accounting for the footprints' variability within the cell, uncertainty associated with the RF algorithm, and RF lack of fit. To show this we start by assuming that the fuel load estimate at footprint i with model m is given:

$$RF_{im} = \theta_i + e_{im}, \quad \text{(eq.13)}$$

where θ_i is the overall mean prediction for footprint i and e_{im} is an error term. We assume that the expected value and variance of this error are $E[e_{im}] = 0$ and $Var[e_{im}] = \tau_i^2$, respectively. The parameter τ_i^2 captures the within-footprint variability associated with the randomness of the RF algorithm. We also assume that the RF mean prediction $\theta_i$is given by:

$$\theta_i = \mu_i + \epsilon_i \quad \text{(eq.14)}$$

where μ_i is the true biomass of footprint i and $\epsilon_i$is another error term. This error term accounts for the fact that mean RF prediction is not identical to the true biomass. We assume that $E[\epsilon_i] = 0$ and $Var[\epsilon_i] = \psi^2$, where ψ^2 quantifies the uncertainty associated with the lack of fit of the RF model. These equations imply that:

$$RF_{im} = \mu_i + \epsilon_i + e_{im}. \quad \text{(eq.15)}$$

The fuel load prediction at footprint i is then given by the average of the RF models applied to footprint i:

$$\underline{RF_i} = \frac{\sum_m RF_{im}}{M} = \frac{M\mu_i}{M} + \frac{M\epsilon_i}{M} + \frac{\sum_m e_{im}}{M} = \mu_i + \epsilon_i + \frac{\sum_m e_{im}}{M} \quad \text{(eq.16)}$$

where $\underline{RF_i}$ is the mean fuel load estimate at footprint i and M is the number of RF models that were fit. Assuming no correlation between lack of model fit (ϵ_i) and differences between RF models (e_{im}), this implies that:

$$Var\left(\underline{RF_i}|\mu_i\right) = \psi^2 + \frac{\tau_i^2}{M} \quad \text{(eq.17)}$$

Recall that we took the average of all GEDI footprint-level fuel load predictions within a 1-

km2 cell. Assuming no spatial correlation in the mean fuel load in each footprint and model lack of fit, we have that the uncertainty associated with each cell is:

$$Var(\underline{RF_k}) = Var\left(\frac{\sum_i \underline{RF_{ik}}}{n_k}\right) = Var\left(\frac{\sum_i \mu_{ik}}{n_k} + \frac{\sum_i \epsilon_{ik}}{n_k} + \frac{\sum_i \frac{\sum_m e_{imk}}{M}}{n_k}\right) \quad \text{(eq.18)}$$

where n_k is the number of GEDI footprints within the 1-km2 cell (k).

If we assume that the uncertainty associated with model lack of fit (ψ^2) does not vary from footprint to footprint, then:

$$= Var\left(\frac{\sum_i \mu_{ik}}{n_k}\right) + Var\left(\frac{\sum_i \epsilon_{ik}}{n_k}\right) + Var\left(\frac{\sum_i \frac{\sum_m e_{imk}}{M}}{n_k}\right) \quad \text{(eq.19)}$$

$$= Var\left(\frac{\sum_i \mu_{ik}}{n_k}\right) + \frac{n_k\psi^2}{n_k^2} + \frac{1}{n_k^2}\left(\sum_i \frac{M\tau_{ik}^2}{M^2}\right) \quad \text{(eq.20)}$$

$$= Var\left(\frac{\sum_i \mu_{ik}}{n_k}\right) + \frac{\psi^2}{n_k} + \frac{\sum_i \tau_{ik}^2}{n_k^2 M} \quad \text{(eq.21)}$$

Finally, if we assume that $E[\mu_{ik}] = m_k$ and $Var[\mu_{ik}] = \delta_k^2$, then the overall uncertainty at each cell (k) is given by:

$$= \frac{\delta_k^2}{n_k} + \frac{\psi^2}{n_k} + \frac{\sum_i \tau_{ik}^2}{n_k^2 M} \quad \text{(eq.22)}$$

This expression shows that the variance for each cell k can be partitioned into the variability of biomass within each cell k (captured by δ_k^2), model lack of fit (captured by ψ^2) and RF uncertainty (captured by τ_{ik}^2). Notice that, as the number of GEDI footprints within cell k increases (i.e., n_k increases), then overall uncertainty decreases. Furthermore, increasing the number of RF models (i.e., M) only decreases the last uncertainty piece.

For each cell, we estimated δ_k^2 and $\hat{\tau}_{ik}^2$ with the following equations:

$$\hat{\delta}_k^2 = \frac{\sum_i \left(\underline{RF_{ik}} - \underline{RF_k}\right)^2}{n_k - 1} \quad \text{(eq.23)}$$

$$\hat{\tau}_{ik}^2 = \frac{\sum_m \left(RF_{ikm} - \underline{RF_{ik}}\right)^2}{M - 1} \quad \text{(eq.24)}$$

where $\underline{RF_{ik}}$ is the mean fuel load prediction of footprint i in cell k, $\underline{RF_k}$ is the mean fuel load prediction in cell k, $\underline{RF_{ikm}}$ is the fuel load prediction of footprint i in cell k using RF model m. The uncertainty is presented in absolute values by taking the square-root of the summed

variance parameters. A workflow summarizing the full methodology applied in this study is provided in Fig. 5.

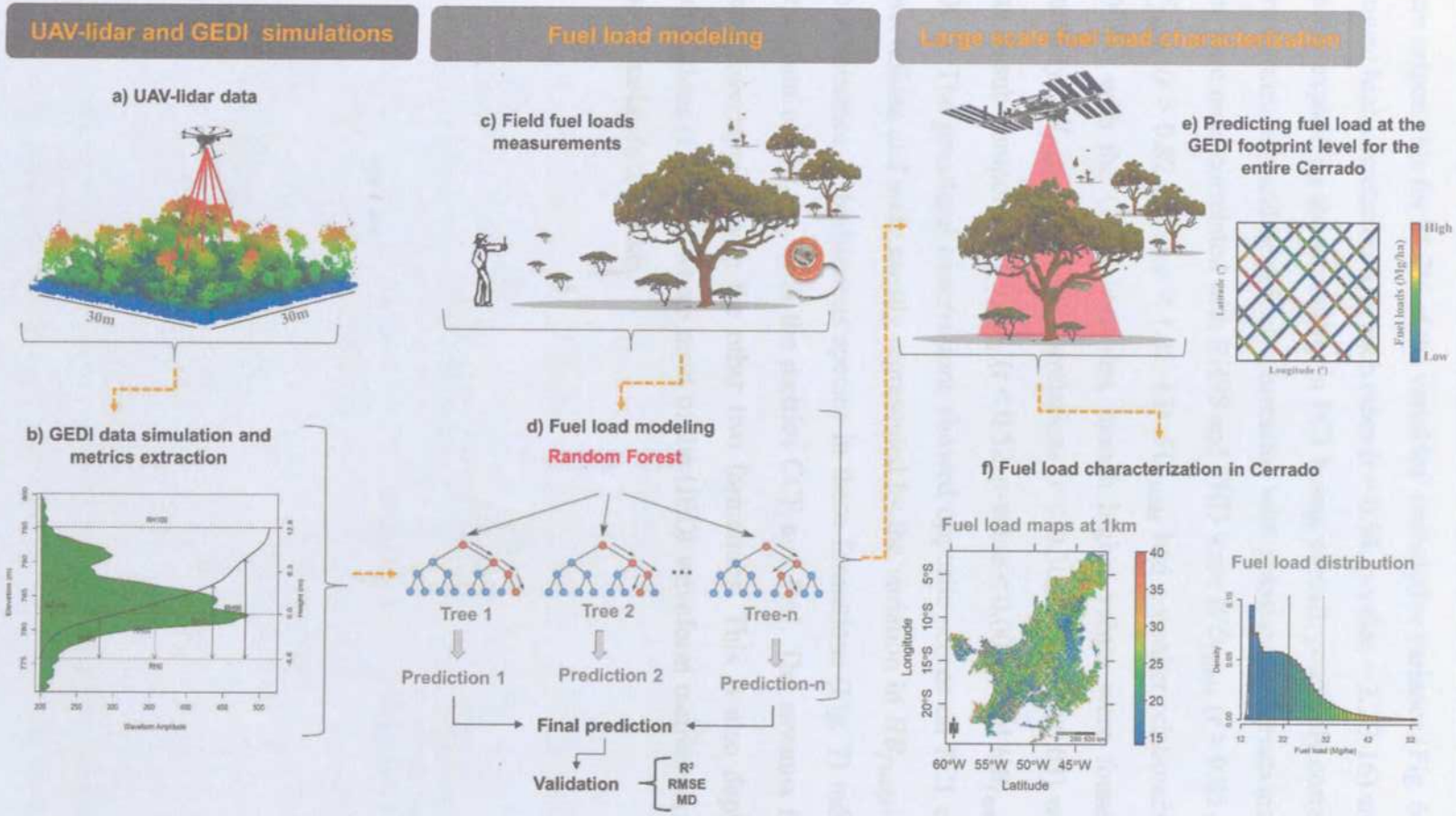

Fig. 5. Workflow to estimate fuel load components in Cerrado using GEDI data. High density UAV-lidar point clouds were collected (a) from which GEDI-like waveforms were simulated (b). The models were created using fuel load measurements from the field (c) as response variables in a random forest (RF) model and GEDI waveform metrics as predictors (d). The RF models were applied to the 25-m GEDI footprints in Cerrado opposite and averaged into 1-km grid cells (f).

3. Results

3.1. Exploratory analysis of GEDI metrics and fuel components in the Cerrado formations

The PCA biplot shows distinct scores for the Cerrado formations and these first two PCs were responsible for 75.7% of the variables' cumulative variance (Fig. 6a). The RH98 and FHD showed high correlation with each other (r = 0.94, p-value = 2.2E-16) and were the two metrics mainly explaining the variability in PC1 being, overall, positively correlated to samples in the forest formation and negatively correlated with grassland observations. The fuel components that were most correlated with RH98 and FHD were WD_{fuels} (r > 0.85 p-value < 2.2E-15) and TF_{fuels} (r > 0.82, p-value < 1.3E-13). SU_{fuels} had a weaker relationship (r < 0.51, p-value < 0.0008) with the GEDI variables, though higher values were found in forests (Fig. 6b). Similarly, SH_{fuels} had lower correlations (r < |0.30|, p-value < 0.03) with the GEDI variables than its sub-components SU_{fuels} (r < 0.52, p-value < 0.0008) and HB_{fuels} (r < |0.59|, p-value < 0.002). The grassland observations showed opposite scores on PC1 compared to the forest observations and were mostly represented by the variation in HB_{fuels}; this is consistent with the dominance of herbaceous species in these formations (Fig. 7) indicated by the negative correlation of HB_{fuels} with the metrics CCF and PAI. The savanna formation lies near the center, overlapping with the other two formations. This is also depicted in the variables' distributions (Fig. 6b), where most of the GEDI waveform metrics showed increasing values from grasslands to forests.

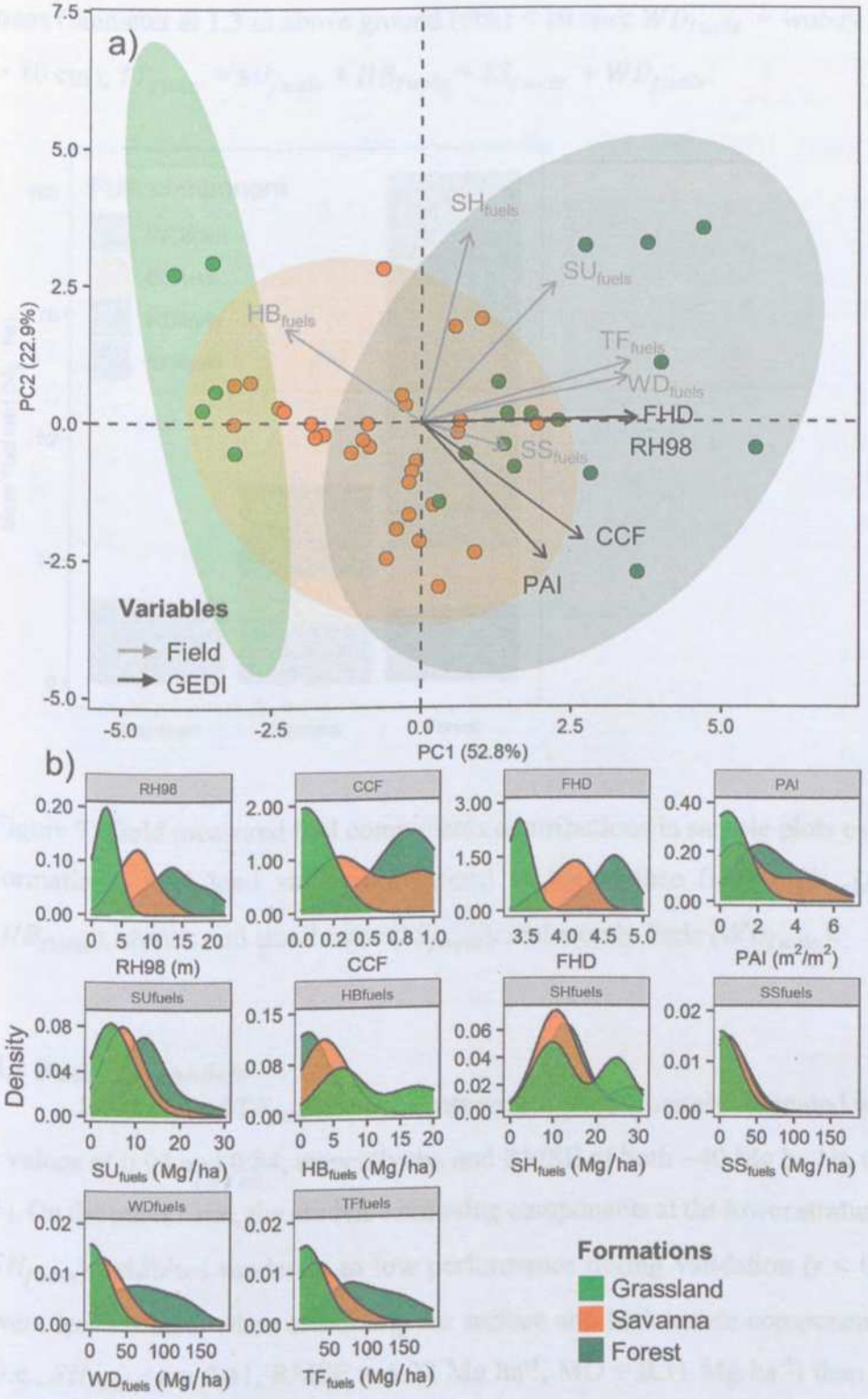

Fig. 6. Biplot of the first two axes of a principal component analysis of simulated GEDI waveforms metrics and field fuel load measurements (a) and their respective density plots (b). RH98 = Relative height at the 98 th height percentile; CCF = canopy cover fraction; FHD = Foliage Height Diversity; PAI = Plant Area Index; SU_{fuels} = surface fuels (duff, litter, downed wood); HB_{fuels} = Herbaceous fuels; $SH_{fuels} = SU_{fuels} + HB_{fuels}$; SS_{fuels} = shrubs and small

trees (diameter at 1.3 m above ground (dbh) < 10 cm); WD_{fuels} = woody fuels (trees with dbh > 10 cm); $TF_{fuels} = SU_{fuels} + HB_{fuels} + SS_{fuels} + WD_{fuels}$.

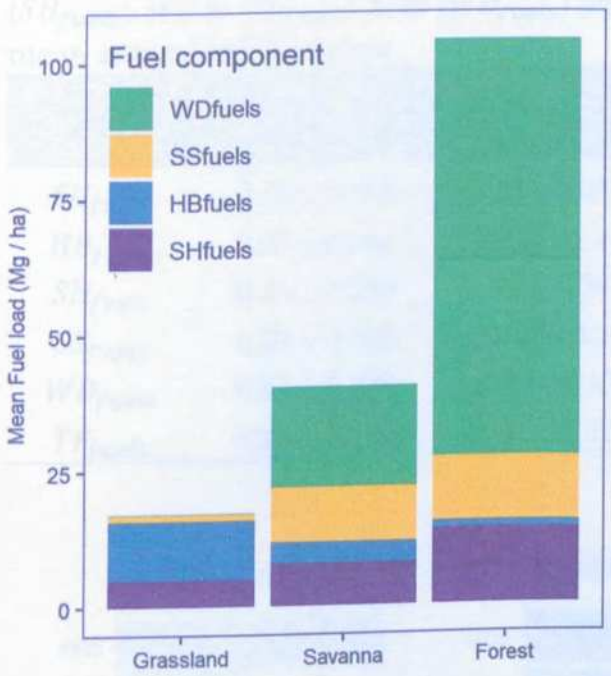

Figure 7. Field measured fuel components contributions in sample plots over different Cerrado formations. Fuel load values correspond to the surface fuels (SU_{fuels}), herbaceous fuels (HB_{fuels}), shrubs and small trees (SS_{fuels}), and woody fuels (WD_{fuels}).

3.2 Fuel load models

WD_{fuels} and TF_{fuels} components were more accurately estimated with models, yielding r values of 0.93 and 0.84, respectively, and RMSE of both ~40 Mg ha^{-1} in the validation (Table 3). On the other hand, the models estimating components at the lower stratum (SU_{fuels}, HB_{fuels}, SH_{fuels}) exhibited moderate to low performance during validation (r < 0.67). The estimates were less accurate when estimating the surface and herbaceous components in a single model (i.e., SH_{fuels}; r = 0.41, RMSE = 6.22 Mg ha^{-1}, MD = 0.31 Mg ha^{-1}) than in separate models; i.e., for HB_{fuels} (r = 0.67, RMSE = 2.81 Mg ha^{-1}, MD = 0.12 Mg ha^{-1}) and for SU_{fuels} (r = 0.55, RMSE = 5.22 Mg ha^{-1}, MD = 0.13 Mg ha^{-1}). The most important variables in the models varied for the fuel components (Fig. 8). Nonetheless, RH98 was one of the most important variables in all models except for HB_{fuels}.

Table 3. Cross-validation performance assessment in 500 iterations of models used to estimate surface fuels (SU_{fuels}), herbaceous fuel (HB_{fuels}), surface and herbaceous fuels (SH_{fuels}), shrub (SS_{fuels}), tree (WD_{fuels}) and total fuel load (TF_{fuels}). Values represent mean ± standard deviation.

Fuel	R	RMSE		MD	
		(Mg ha^{-1})	%	(Mg ha^{-1})	%
SU_{fuels}	0.55 ± 0.265	5.22 ± 0.21	55.51 ± 2.79	0.13 ± 0.18	4.61 ± 2.92
HB_{fuels}	0.67 ± 0.261	2.81 ± 0.2	78.6 ± 6.38	0.12 ± 0.14	10.01 ± 5.46
SH_{fuels}	0.41 ± 0.253	6.22 ± 0.34	47.49 ± 2.89	0.31 ± 0.28	4.04 ± 2.57
SS_{fuels}	0.38 ± 0.249	10.55 ± 0.5	113.32 ± 11.09	0.35 ± 0.35	16.01 ± 10.87
WD_{fuels}	0.93 ± 0.170	13.07 ± 0.67	40.6 ± 3.64	-0.32 ± 0.67	1.51 ± 2.83
TF_{fuels}	0.84 ± 0.228	23.01 ± 1.13	40.78 ± 2.4	0.22 ± 0.94	2.09 ± 2.12

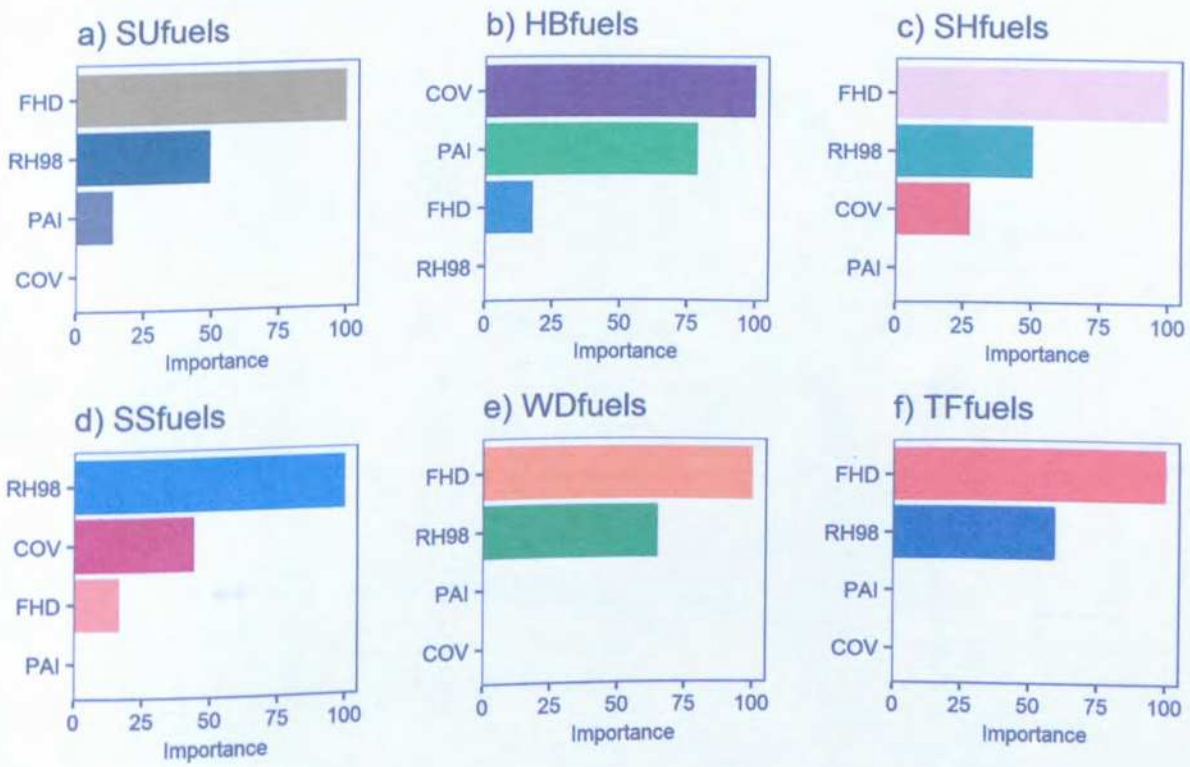

Fig. 8. Importance of lidar metrics used as inputs into Random Forest models to estimate surface fuels (SU_{fuels}), herbaceous fuels (HB_{fuels}), surface and herbaceous fuels (SH_{fuels}), shrubs and small trees (SS_{fuels}) , woody fuels (WD_{fuels}) and total fuel load (TF_{fuels}). The variables tested as input were Relative height at the 98th height percentile (RH98), Plant Area Index (PAI), Canopy cover fraction (CCF) and Foliage Height Diversity (FHD)

3.3 Fuel loads characterization across the Cerrado biome

Fuel load estimates were obtained from the application of the models to the on-orbit GEDI data. The estimates were obtained for the entire Cerrado biome in the 25 m-radii GEDI footprints. In a Cerrado subset (Fig. 9), gradients of fuel load associated with topography were observed in the different formations. For instance, there was a pattern of higher WD_{fuels} and TF_{fuels} estimates in forests (Fig. 9 e2 and f2) than in the other formations (Fig. 9 a2 - d2). On the other hand, HB_{fuels} estimates were significantly higher in grasslands (Fig. 9 a2), mainly when compared to forest formations (Fig. 9 e2 and f2). The SU_{fuels} estimates were also higher in forest formations (Fig. 9 e2 and f2) than in grasslands (Fig. 9 a2).

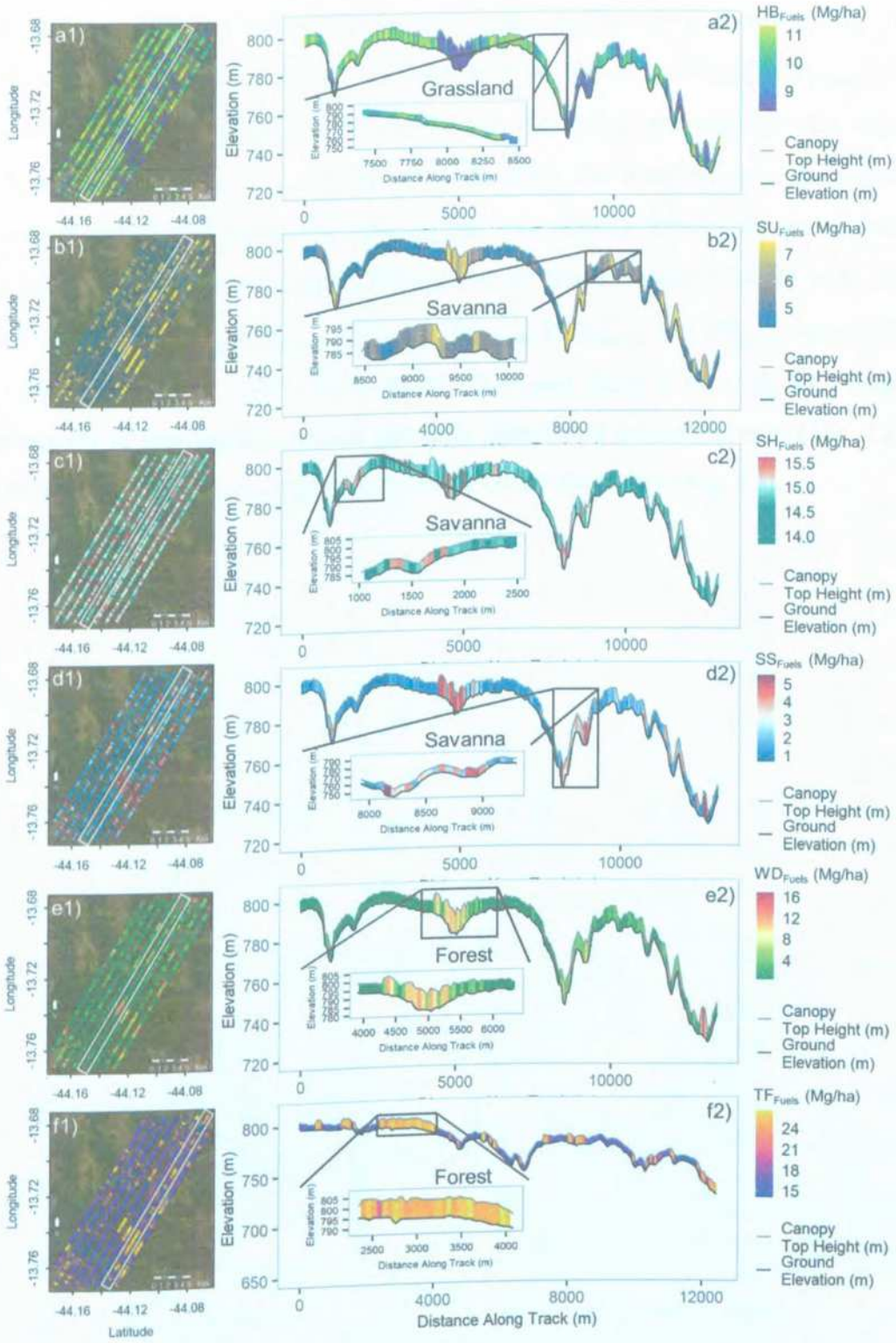

Fig. 9. Depiction of the GEDI footprint level estimates of fuel components showing all the GEDI ground-tracks (a1, b1, c1, d1, e1, f1) and a single-track profile over grassland, savanna, and forest formations (a2, b2, c2, d2, e2, f2). Estimates were done for surface fuels (SU_{fuels}), herbaceous fuels (HB_{fuels}), surface and herbaceous fuels (SH_{fuels}), shrubs and small trees (SS_{fuels}), woody fuels (WD_{fuels}) and total fuel load (TF_{fuels}).

The spatial variation of fuel components estimates in Cerrado is shown in Fig. 10. These maps allowed us to identify regions in Cerrado with higher estimated HB_{fuels} and lower WD_{fuels} in some regions (e.g., ~45°W ~10°S, Fig. 10b and d) and regions with accumulated fuel as in northern Cerrado (e.g., ~45°W ~5°S Fig. 10e). The distribution of the estimates was mostly evenly distributed except for SH_{fuels} that was slightly skewed for higher values, and WD_{fuels} *and* TF_{fuels} that had higher frequencies of lower values (Fig. 11 a-f). The mean estimated values of SU_{fuels}, HB_{fuels}, SH_{fuels}, SS_{fuels}, WD_{fuels}, and TF_{fuels} were 7.63 ± 1.63, 7.87 ± 1.78, 14.74 ± 1.87, 7.58 ± 1.64, 10.29 ± 9.97 and 28.55 ± 11.4 Mg ha^{-1}, respectively. The uncertainty of the predictions was similarly distributed across Cerrado (Fig. 12), with a pattern of lower uncertainty in regions with more GEDI footprints (Fig. 13).

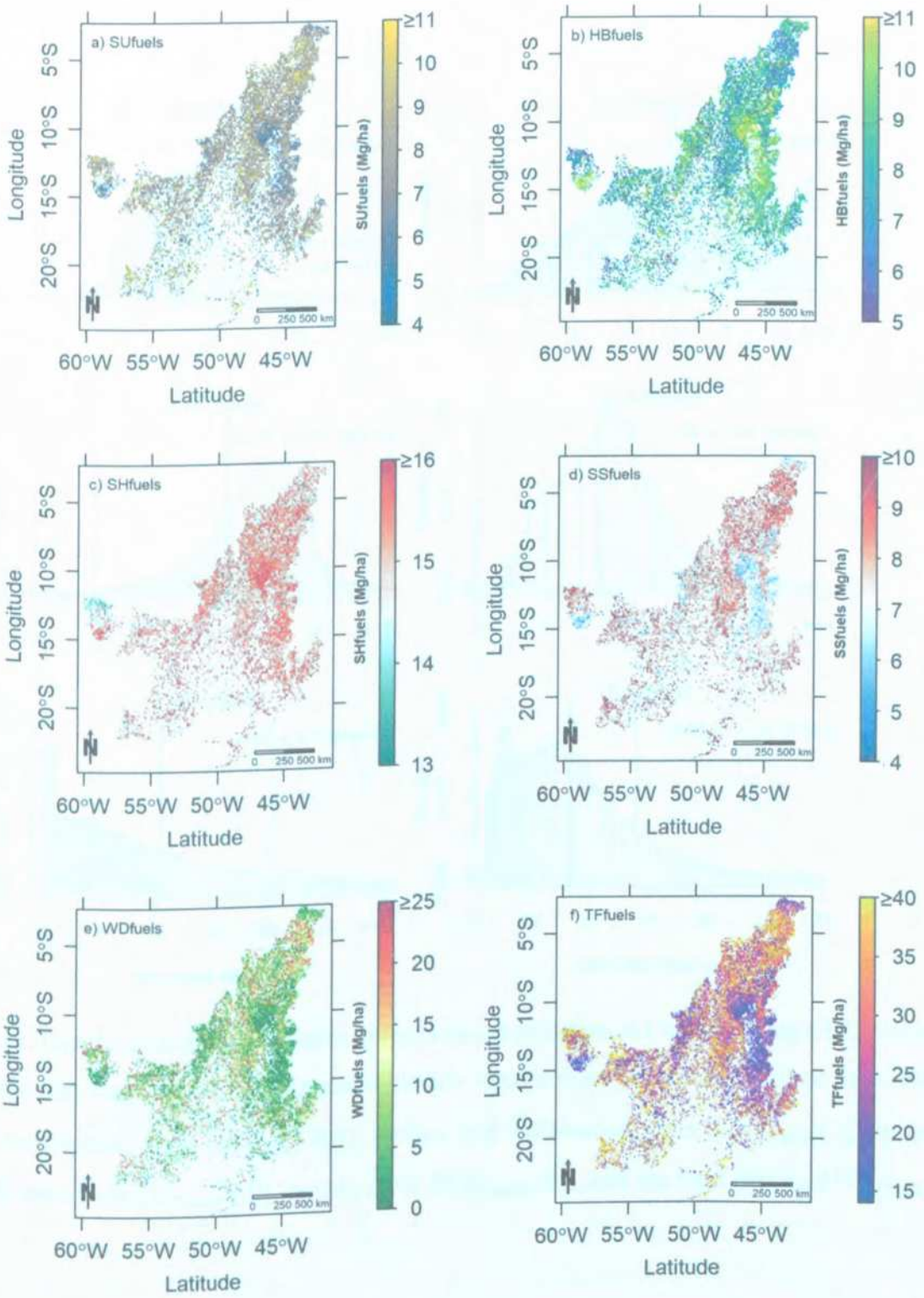

Fig. 10. GEDI-derived large scale fuel load estimates at the 1km grid cell resolution for the entire Cerrado biome. These estimates were aggregated from the footprint-level predictions. Surface fuels (SU_{fuels} (a)), herbaceous fuels (HB_{fuels} (b)), surface and herbaceous fuels (SH_{fuels} (c)), shrubs and small trees fuels (SS_{fuels} (d)), woody fuels (WD_{fuels} (e)), and the total fuel load (TF_{fuels} (f)).

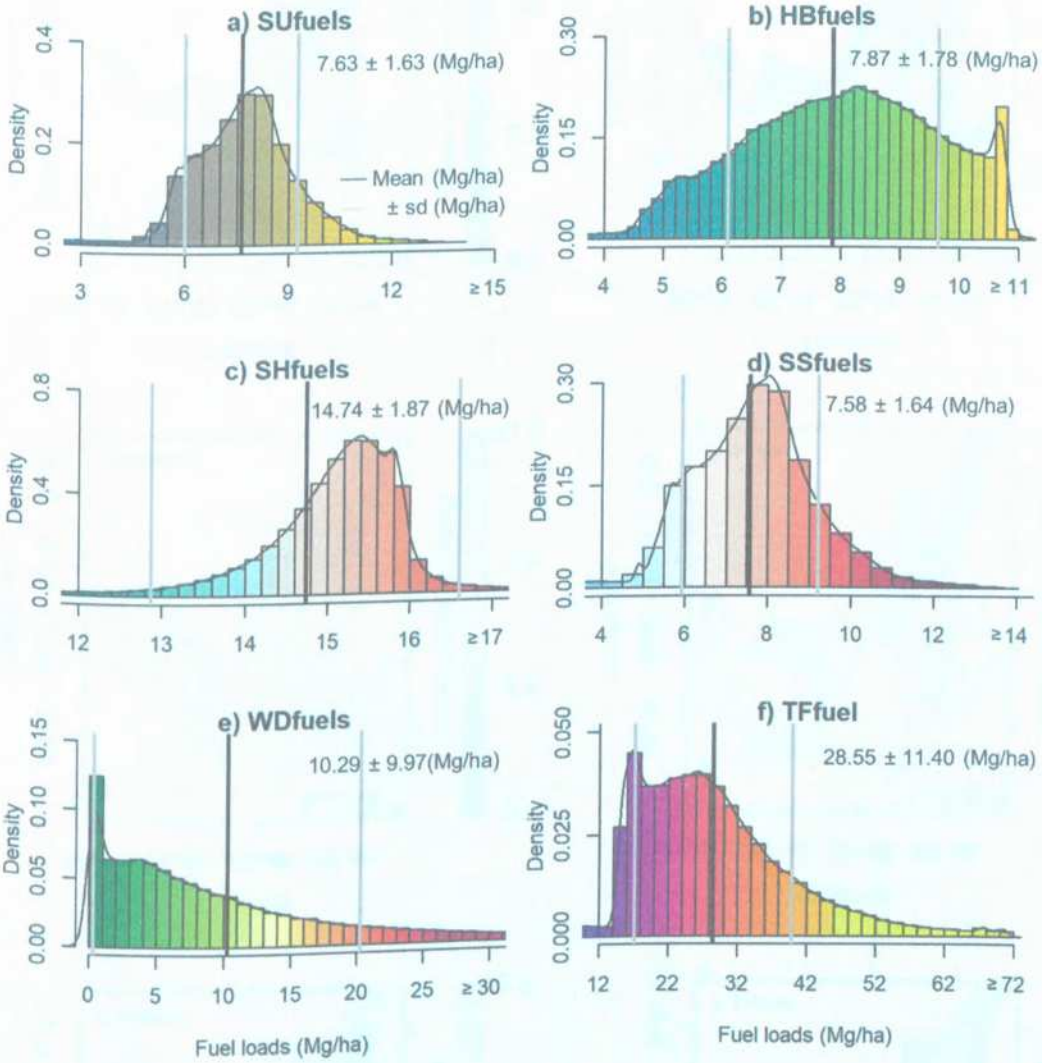

Fig. 11. Distribution of the estimates of fuel load components in Cerrado using GEDI waveform metrics and Random Forest. Separated models were trained to estimate surface fuels (SU_{fuels} (a)), herbaceous fuels (HB_{fuels} (b)), surface and herbaceous fuels (SH_{fuels} (c)), shrubs and small trees fuels (SS_{fuels} (d)), woody fuels (WD_{fuels} (e)), and the total fuel load (TF_{fuels} (f)).

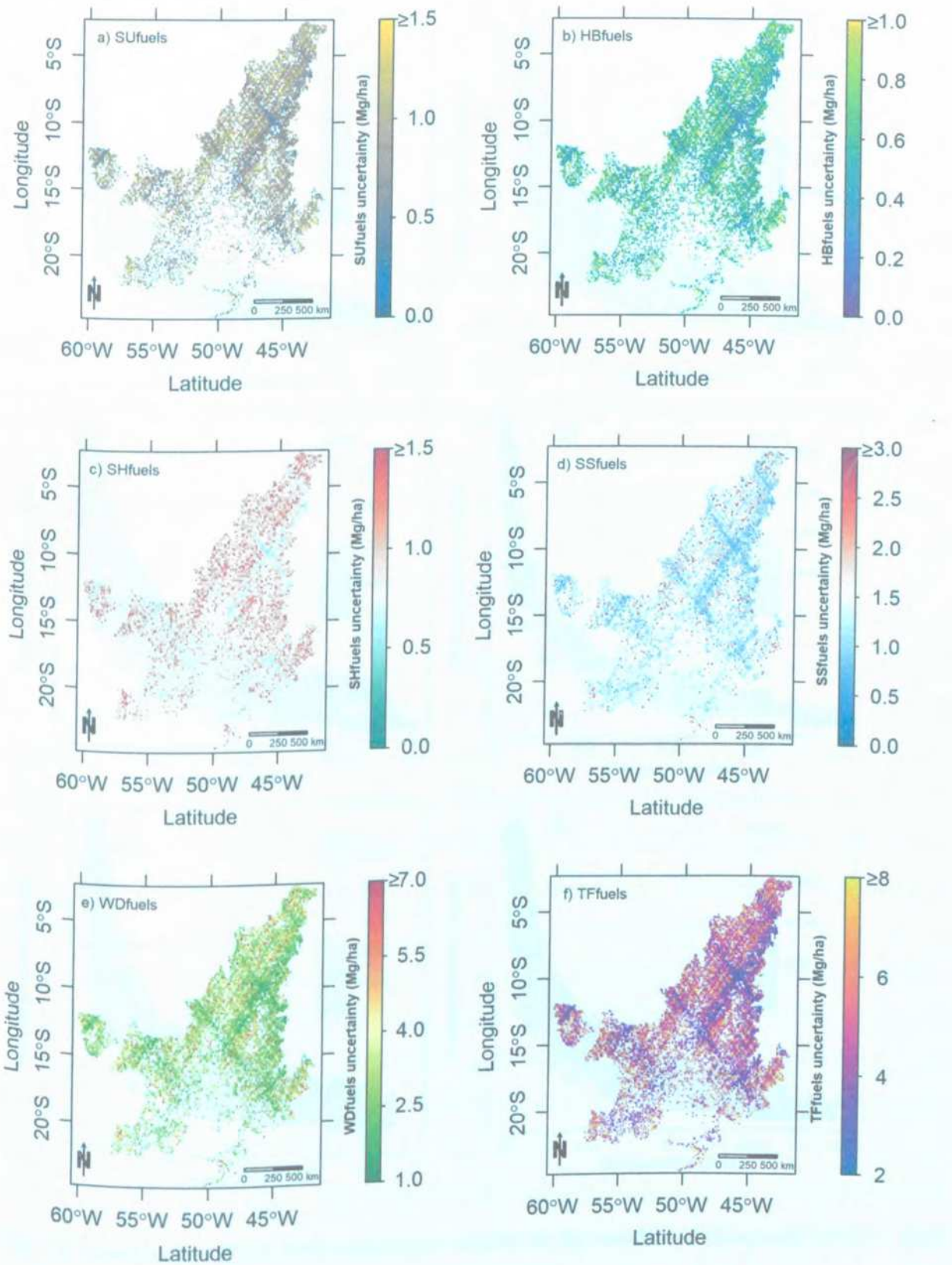

Fig. 12. Uncertainty of fuel load predictions accounting for the footprints' variability within the cell, uncertainty associated with the RF algorithm, and RF lack of fit. Surface fuels (SU_{fuels} (a)), herbaceous fuels (HB_{fuels} (b)), surface and herbaceous fuels (SH_{fuels} (c)), shrubs and small trees fuels (SS_{fuels} (d)), woody fuels (WD_{fuels} (e)), and the total fuel load (TF_{fuels} (f)).

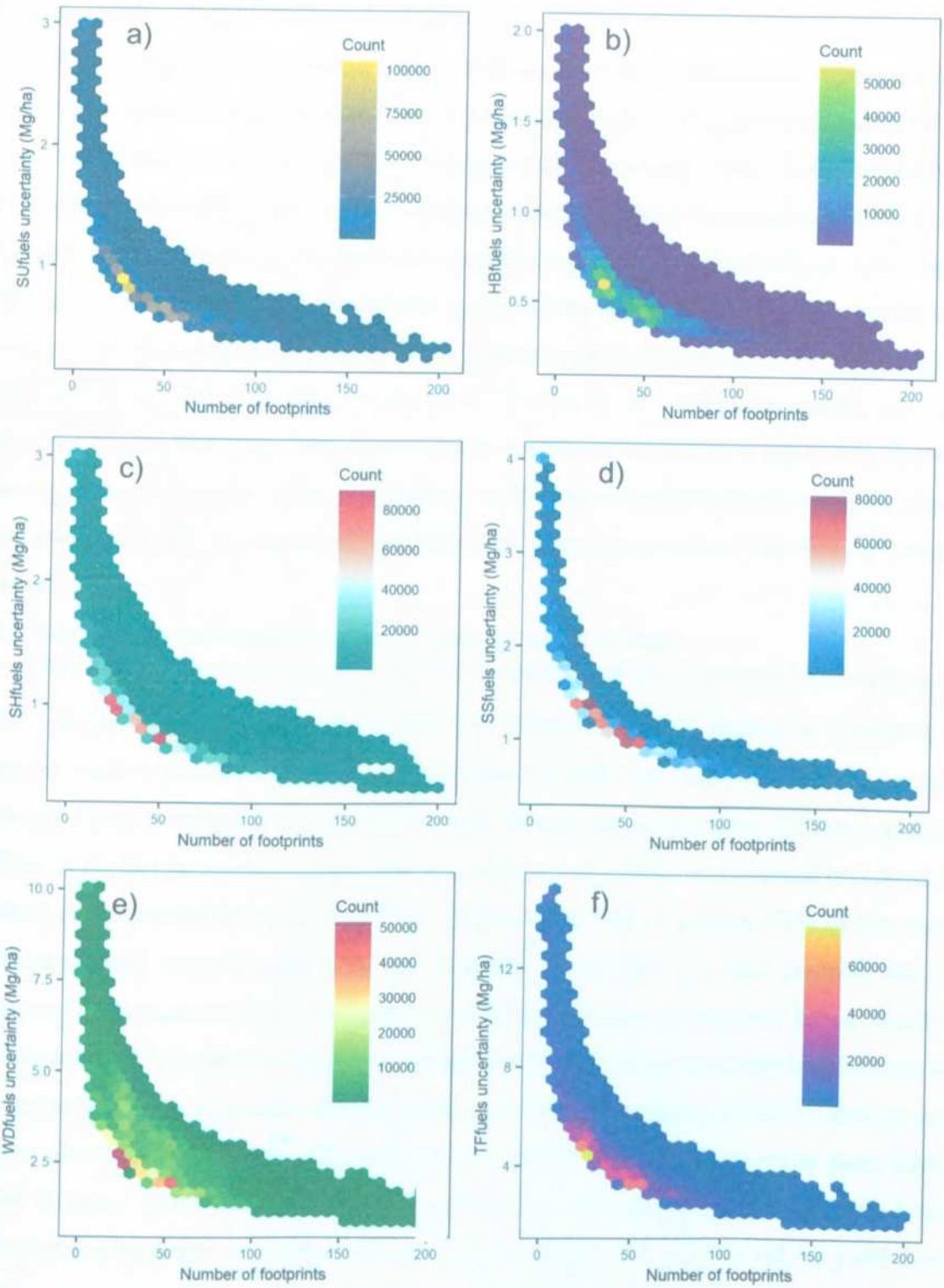

Fig. 13. Uncertainty of fuel load predictions relative to the number of footprints within 1-km2 cells in Cerrado. Count represents the number of cases. Surface fuels (SU_{fuels} (a)), herbaceous fuels (HB_{fuels} (b)), surface and herbaceous fuels (SH_{fuels} (c)), shrubs and small trees fuels (SS_{fuels} (d)), woody fuels (WD_{fuels} (e)), and the total fuel load (TF_{fuels} (f))

4. Discussion

GEDI is capable of providing high resolution 3D canopy structural information of various forest ecosystems (Dubayah et al., 2020a, Schneider et al., 2020) and holds untapped potential for establishing effective forest fire management frameworks. This study demonstrated the potential of using GEDI data to estimate large-scale multi-layer fuels across the whole Brazilian Cerrado by applying both simulated and on-orbit data to model commonly used fuel load layers. The use of spaceborne lidar sensors for fuel mapping has been previously reported mainly to map canopy fuels with GLAS and ICESat-2 sensors (Ashworth et al., 2010, García et al., 2012, Peterson et al., 2013, Gwenzi et al., 2016, Narine et al., 2020). However, this is, to our knowledge, the first study demonstrating the usefulness of GEDI in estimating fuels loads at such a large geographic scale, contributing to the expansion of spaceborne lidar applications for integrated fire management activities and supporting carbon monitoring initiatives in savannas.

4.1. Large scale fuel load estimation using spaceborne lidar

Our results demonstrated a high predictive capacity of GEDI metrics in modelling WD_{fuels} and TF_{fuels} that allows large-scale fuel load estimations. This finding is in agreement with similar studies focused on estimating biomass in different ecosystems using as predictors canopy metrics derived from spaceborne lidar sensors on the satellites ICESat-1 and ICESat-2 (Xiao et al., 2019). A study carried out by Lefsky et al. (2005) in a tropical broadleaf forest in Brazil demonstrated that GLAS-derived heights were able to explain 73% of the variation in field-measured aboveground biomass. Popescu et al. (2011), who mapped aboveground biomass in a temperate forest dominated by pine and oak stands in eastern Texas, found a strong relationship ($R^2 = 0.80$) between GLAS height variables and the reference biomass derived from airborne lidar data. In a more detailed study to test the capabilities of GLAS data in predicting forest aboveground biomass, Chi et al. (2015) estimated R^2 values ranging from 0.64 to 0.90 over different forest zones in China. Nevertheless, it is noteworthy that those studies did not account for important vegetation layers for fire management and that GLAS yield products at a coarser resolution (footprints with diameter of 70 m), despite being a full-waveform lidar as GEDI. Similarly, by using simulated ICESat-2 photon-counting lidar data, Narine et al. (2019) models explained 79% of the variation in AGB in a pine-dominated forest. Gwenzi et al. (2016) described some of the limitations of using ICESat-2 for retrieving vegetation height in structurally complex savannas. They found that canopy height estimation in areas of low-density vegetation cover may have lower precision due to the expected number of signal

photons in these areas. The performance of our models also suggests that GEDI can be more appropriate for this type of vegetation.

Part of the unexplained variance by our SS_{fuels} models may be due to the lower sensitivity of GEDI to herbaceous and low stature shrubs compared to the denser overstory tree canopies the GEDI mission was designed to map. GEDI's utility for mapping short, sparse canopies and understory has yet to be established, and while the accuracies seen here are likely lower than for closed-canopy forests, or canopy fuels, our results suggest that GEDI data are still useful for this more challenging application. The measurement challenge is largely due to convolution of the waveform return from the ground and from short vegetation above the ground, where detecting the vegetation from the waveforms will be more challenging. This issue will be exacerbated over slopes or when vegetation cover is low, which is often the case in the Cerrado. he top portion of small trees and shrub crowns observed in the waveforms may not show enough canopy cover to register as a significant return signal and consequently may not be properly detected using the selected metrics.

Although surface, herbaceous and shrub fuels are a key component in fire behavior and emission models, most previous studies to estimate fuel loads using spaceborne lidar sensors focused on canopy fuels (García et al., 2012, Peterson et al., 2013). Obtaining information on fuels in low stature and sparse vegetation ecosystems, such as savannas and grasslands, is more challenging than in dense vegetation cover (e.g., Popescu et al., 2018). The lower performance for SU_{fuels}, HB_{fuels}, and SH_{fuels} suggests that spaceborne lidar data interacts with this lower stratum less strongly than with tree fuels. In fact, surface components are hardly directly retrieved with lidar measurements (Jakubowski et al., 2013, Hudak et al., 2016b, Price and Gordon 2016, Bright et al., 2017), and it is commonly necessary to rely on their indirect relationship with other variables, such as canopy structure or climate (Hudak et al., 2016a, Mauro et al., 2021). Results in this study demonstrate that the GEDI waveform metrics could also be used as proxies to indirectly explain part of the variability of these fuels in savanna ecosystems and underscore the improvement in modeling HB_{fuels} and SU_{fuels} in separate models rather than a single model (SH_{fuels}). The difference among HB_{fuels} and SU_{fuels} is indicated by their contrasting relationships, such as having greater values of SU_{fuels} in forest formations (e.g., due to litterfall) and having inverse relationships to CCF and HB_{fuels}. Nonetheless, the dynamics of $HB_{fuels}$and SU_{fuels} may be more impacted than WD_{fuels} by plant phenology, seasonality (Costa et al., 2020, Oliveira et al., 2021), and fire events (Gomes et al., 2020b). Roitman et al. (2018) analyzed decades of AGB surveys in Cerrado and also

demonstrated that environmental factors can help to explain part of the AGB variation in Cerrado. As more data become available, future studies could use multitemporal series to exploit the layers' seasonal structural dynamics mainly due to leaf flush and fall, in search for more unexplained variance that might not be obtained otherwise. The complementary use of multispectral and/or hyperspectral images for better distinguishing photosynthetic- from non-photosynthetic vegetation fractions (e.g., Roberts et a. 2003) coupled to GEDI metrics might improve the estimation of some surface fuels (e.g., litter, downed wood) in open-canopy formations and are recommended in future studies.

A multilevel approach by linking field plots, UAV-lidar, and spaceborne lidar data is the backbone of our methodological framework to produce both large scale multi-layer fuel load information in Cerrado. The RF models developed using simulated GEDI full-waveforms from UAV-lidar have the advantage of not being affected by waveform geolocation errors that are inherent with GEDI. Currently, these geolocation errors are around 10-20 m, but are expected to decrease to ~7-8 m after completed mission calibrations (Dubayah et al., 2020a). This error can make it difficult to have coincident – in space and time - field and GEDI data for modeling. Our study is aligned with the simulation approach that has been suitable for GEDI model development and application (Saarela et al., 2018, Hancock et al., 2019, Marselis et al., 2019, Patterson et al., 2019, Qi et al., 2019, Schneider et al., 2020, Dubayah et al., 2020a, Duncanson et al., 2020, Silva et al., 2021). Comprehensive assessments of the accuracy of on-orbit GEDI data in retrieving key structural vegetation parameters by synchronizing field measurements within GEDI footprints may be needed for assessing estimation uncertainty in different scales. Nevertheless, the models developed with simulated GEDI waveforms can be applied to the GEDI footprints covering about the entire globe (~52° N and S) providing a valuable asset for regional to global forest structure analysis as demonstrated for the Cerrado.

4.2. Caveats and source of uncertainty

While it may be straightforward to derive vegetation structural metrics in relatively dense vegetation cover (e.g., Popescu et al., 2018), obtaining such information in low stature and sparse vegetation formations, such as savannas and grasslands, is more challenging (Glen et al., 2016, Gwenzi et al., 2016). One of the current limitations in our findings concerns the uncertainty of estimating surface and low stature vegetation fuels. This issue was also described in different studies using airborne lidar that reported R^2 ranging from ~25 – 45% (Jakubowski et al., 2013, Hudak et al., 2016b, Price and Gordon 2016, Bright et al., 2017). Pesonen et al. (2008) models had a better performance for estimating downed dead wood volume in boreal forests, suggesting a higher predictive capacity for this component. Nonetheless, despite surface

fuels being a key component in fire behavior and emission models, they have received less attention than canopy fuels, particularly using spaceborne sensors (Garcia et al., 2012, Peterson et al., 2013, Bright et al., 2017). Tackling this issue may require inclusion of variables related to fuel dynamics such as time since the last fire (Chen et al., 2017) and precipitation occurrence (Oliveira et al., 2021).

Another consideration is related to GEDI data characteristics. First, the GEDI mission is planned to collect data until 2023, limiting application of models to this time span. Nonetheless, we expect that other missions, such as MOLI (Murooka et al., 2013, Kimura et al., 2017, Asai et al., 2018), will give similar data in the future. The second point is related to the sampling nature of GEDI. We observed here that when aggregating footprints to a 1-km^2 grid cell there were still some areas not yet covered (Fig. 14), which can be due to the GEDI orbit missing the cells, or data loss from cloud cover. Those gaps might be filled with forthcoming dataset updates during the mission; it is expected that most 1 km^2 grid cells will have at least two ground tracks (Patterson et al., 2019) by the end of the GEDI mission lifetime. The number of required footprints to predict fuel load or AGB density in 1-km^2 cells may vary due to the vegetation complexity within the cell, which might need further investigation; nonetheless we observed an exponential decrease in uncertainty with an increase in number of footprints (Fig 13). Finally, the impact of terrain characteristics for detecting ground and retrieving waveform metrics was not covered in this study. When the within footprint terrain slope is high, the interpretation of the signals is more complex causing, for instance, ground and canopy energy at the same height (Harding and Carabajal, 2005, Lefsky et al. 2005). In a study comparing small- and large-footprint lidar sensors, Silva et al. (2018) also observed an effect of terrain slope ($> 20°$) by overestimating ground elevation and RH metrics on large-footprint data, mainly in dense canopies. For instance, an alternative for GLAS waveforms was applying topographic correction using ancillary data (Lefsky et al., 2005, Lefsky et al., 2007). Similar effects of topography in the returned GEDI waveform may need to be investigated and addressed in further studies.

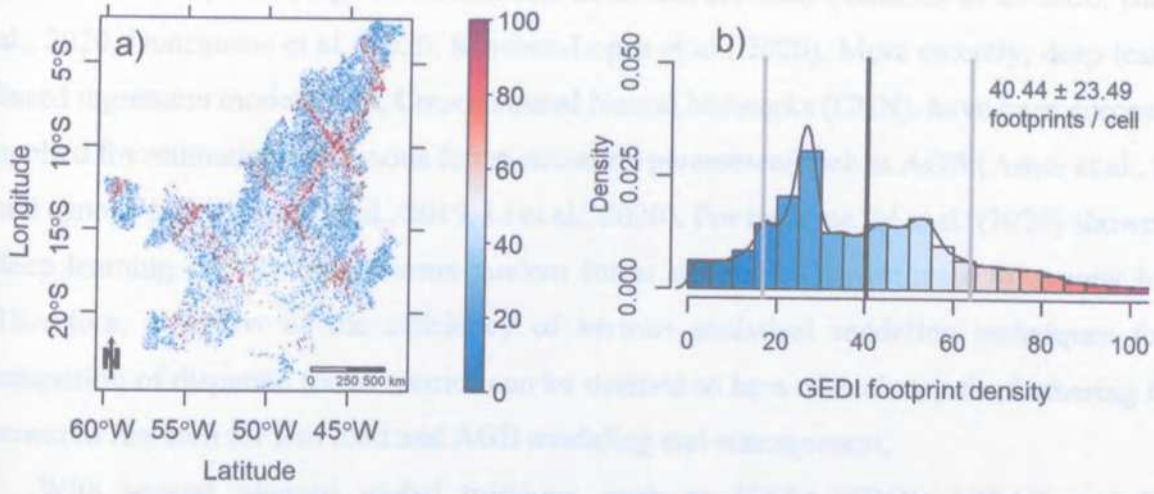

Figure 14. GEDI footprint density map (a) and histogram (b) of data collected between April, 2019 and September, 2020 in the Brazilian tropical savanna, Cerrado.

4.3 Future Applications and Challenges

Previous studies of GEDI have focused on deriving products by using the waveform metrics and its relationships with the vertical structure of the vegetation (Marselis et al., 2019, Schneider et al., 2020, Duncanson et al., 2020). The quality of the metrics relies on the accuracy to detect the ground signal which is expected to vary based on various factors such as canopy cover, GEDI beam energy, weather conditions and topography. However, apart from the environmental characteristics and sensor properties, what determines the ground classification is the algorithm incorporated. Hancock et al. (2019) described and tested Gaussian fitting along with the lowest maximum and inflection point algorithms to detect the ground signal and calculated RH metrics from simulated GEDI waveforms, showing that there might be differences among them. Further research exploring the impact of ground algorithms on GEDI metrics associated with fuel load estimation needs to be conducted, ideally with the study based on individual physiognomies and landscape conditions.

RF was implemented in our study due to its ease of usage, interpretability, versatility in handling missing data, and prior success with respect to fuel load estimation and to GEDI-based studies (Healey et al., 2020, Marshak et al., 2020, Rishmawi et al. 2021). Being an ensemble technique, RF improves the average prediction performance and is robust to outliers. Techniques such as ordinary least square regression, lasso logistic regressions and sensitivity analysis, and combinations of multiple machine learning methods, have also been applied to

GEDI data for quantifying forest traits and structural diversity (Boucher et al. 2020, Burns et al., 2020, Duncanson et al., 2020, Sanchez-Lopez et al., 2020). More recently, deep learning-based regression models, e.g., Convolutional Neural Networks (CNN), have been successfully applied for estimating continuous forest structural parameters such as AGB (Asner et al., 2018) and canopy height (Lang et al., 2019, Li et al., 2020). For instance, Li et al. (2020) showed that deep learning slightly outperforms random forest models in the estimate of canopy height. Therefore, a review of the efficiency of various statistical modeling techniques for the estimation of disparate forest metrics can be deemed to be a critical step for furthering GEDI powered research for fuel load and AGB modeling and management.

With several planned global missions, such as NASA-ISRO's NISAR and ESA's BIOMASS, offering new capabilities, data fusion of GEDI with these distinct sensors can compensate for drawbacks such as influence of clouds, atmospheric haze, multiple scattering, sloped terrain and off-nadir pointing (Pardini et al. 2019, Yang et al., 2011, Quegan et al., 2019, Rosen et al., 2015). We also encourage readers to take full advantage of the Multi-Mission Algorithm and Analysis Platform (MAAP) that hosts a colossal amount of related data, tools, algorithms, and computing capabilities for performing multi-sensor operations (Albinet et al., 2019). During the initial phase of GEDI, several studies had explored the possibility of merging GEDI with synthetic aperture radar (SAR) for improving various forest metrics such as forest height and other structure attribute mapping and characterization (Qi et al., 2019, Qi and Dubayah 2016). Adding to this, a study by Silva et al. (2021) highlighted how integrating NISAR and ICESat-2 with GEDI offer us new opportunities for enhancing AGB mapping in temperate forests with complex terrain. Similarly, data from multispectral sensors also hold potential for improving spatial resolution of GEDI (Potapov et al., 2021). Such multi-sensor data fusion approaches will be important for developing wall-to-wall maps in applications that require higher spatial resolution such as fire behavior models (Benali et al., 2016, Saatchi et al., 2007). Data fusion approaches applicability for estimating large scale forest canopy height, AGB and past forest disturbances assessment has been already demonstrated (Potapov et al., 2021, Saarela et al., 2018, Sanchez-Lopez et al., 2020). Ultimately, data integration from different missions (e.g., NASA's Landsat 8/OLI and NISAR, and ESA's Sentinel 2/MSI and BIOMASS) will be necessary for developing wall-to-wall maps with finer spatial resolutions and for covering regions outside GEDI orbit coverage.

Fuel mapping is one of the most important stages that should be considered in wildfire prevention and planning (Keane and Reeves, 2012, Agee and Skinner, 2005; Franke et al.,

2018). With the proposed framework it is possible to obtain fuel load estimates for large areas, such as the Cerrado biome. This is a key point for advancing on a broad spatial scale understanding of fire effects on ecological processes, ecosystem functioning, carbon emissions, and fuel dynamics (Turner et al., 1995, Bowman et al., 2013, Gomes et al. 2018, Oliveira et al., 2021). Management solutions based on integrated fire management initiatives have taken place in Cerrado conservation areas mainly since 2014 and consider practices of prescribed burning in mosaics to preserve the fire history of a region (Schmidt et al., 2018). The fuel components estimate for large areas as developed here will also be an important resource for this end (Franke et al., 2018, Gomes et al., 2018, Schmidt et al., 2018).

5. Conclusions

In this study we evaluated the capability of GEDI data for estimating large scale multi-layer fuel loads in a tropical savanna ecosystem. We used the random forest algorithm fed by GEDI waveform metrics simulated from high-density UAV-lidar 3D point clouds as our modeling approach. To our knowledge, this is the first attempt to map different fuel components with GEDI waveform metrics. Overall, the models had better performance for predicting woody fuels (e.g., WD_{fuels} and TF_{fuels}). Our results support the expected benefits of using GEDI data for improving models to estimate vegetation traits on structurally-complex ecosystems. Furthermore, we were able to upscale from local to biome-level predictions by applying our models to GEDI data over the entire Cerrado yielding relatively high-resolution fuel load estimates in this region. Therefore, we expect that users can potentially improve large-scale fuel load monitoring using the presented framework and extend the analysis to other fire-prone ecosystems. Following research on data integration of GEDI data with different sensors is expected for meeting spatial and temporal requirements of other fire-related applications - such as assessing fuel load dynamics, modeling fire behavior and calculating carbon emissions - and assist in better understanding the climate-fire interactions across different landscapes.

References

Agee, J. K.; Skinner, C. N. (2005). Basic principles of forest fuel reduction treatments. Forest Ecology and Management, *211*(1-2), 83–96. https://doi.org/10.1016/j.foreco.2005.01.034

Albinet, C., Whitehurst, A. S., Jewell, L. A., Bugbee, K., Laur, H., Murphy, K. J., ... & Duncanson, L. (2019). A joint ESA-NASA multi-mission algorithm and analysis platform (MAAP) for biomass, NISAR, and GEDI. *Surveys in Geophysics*, *40*(4), 1017-1027.

Andela, N., Morton, D.C., Giglio, L., Chen, Y., Van Der Werf, G.R., Kasibhatla, P.S., DeFries, R. S., Collatz, G.J., Hantson, S., Kloster, S., Bachelet, D., Forrest, M., Lasslop, G., Li, F., Mangeon, S., Melton, J. R., Yue, C., Randerson, J. T. (2017). A human-driven decline in global burned area. *Science, 356*(6354), 1356–1362. https://doi.org/10.1126/science.aal4108

Andela, N., Morton, D. C., Chen, Y., Giglio, L., Randerson, J. T. (2018). A Global Fire Atlas of size, duration, and spread from satellite burned area data. In *EGU General Assembly Conference Abstracts* (p. 11269).

Asai, K., Y. Hirata, G. Takao, H. Simoda, Y. Honda, K. Kajiwara, Y. Awaya. (2018). "MOLI (Multi-footprintObservation Lidar and Imager) Mission for Globally Observing Forest Canopy Height and Forest Structural Characteristics from ISS (International Space Station)-JEM (Japanese Experimental Module)." JpGU Meeting: Chiba, Japan. May 20- 24.

Ashworth, A., Evans, D. L., Cooke, W. H., Londo, A., Collins, C., Neuenschwander, A. (2010). Predicting southeastern forest canopy heights and fire fuel models using GLAS data. *Photogrammetric Engineering and Remote Sensing*, *76*(8), 915-922.

Asner, G. P., Brodrick, P. G., Philipson, C., Vaughn, N. R., Martin, R. E., Knapp, D. E., Heckler, J., Evans, L. J., Jucker, T., Goossens, B., Stark, D. J., Reynolds, G., Ong, R., Renneboog, N., Kugan, F., Coomes, D. A. (2018). Mapped aboveground carbon stocks to advance forest conservation and recovery in Malaysian Borneo. *Biological Conservation*, 217, 289–310. https://doi.org/10.1016/j.biocon.2017.10.020

Beck J., Armston J., Hofton M., Luthcke S. (2020), Global Ecosystem Dynamics Investigation (GEDI) Level 02 User Guide, Version 1.0. https://lpdaac.usgs.gov/documents/650/GEDI02_UserGuide_V1.pdf (accessed 13 March 2021)

Benali, A.; Ervilha, A. R.; Sá, A. C. L.; Fernandes, P. M.; Pinto, R. M. S.; Trigo, R. M.; Pereira, J. M. C. (2016). Deciphering the impact of uncertainty on the accuracy of large wildfire spread simulations. *Science of the Total Environment*, 569, 73–85. https://doi.org/10.1016/j.scitotenv.2016.06.112

Blair, J. B., Hofton, M. A. (1999). Modeling laser altimeter return waveforms over complex vegetation using high-resolution elevation data. *Geophysical research letters*, *26*(16), 2509-2512. https://doi.org/10.1029/1999GL010484

Boucher, P. B., Hancock, S., Orwig, D. A., Duncanson, L., Armston, J., Tang, H., ... & Schaaf, C. (2020). Detecting change in forest structure with simulated GEDI lidar waveforms: A case study of the Hemlock Woolly Adelgid (HWA; Adelges tsugae) infestation. *Remote Sensing*, *12*(8), 1304. https://doi.org/10.3390/rs12081304

Bowman, D. M., O'Brien, J. A., & Goldammer, J. G. (2013). Pyrogeography and the global quest for sustainable fire management. *Annual Review of Environment and Resources*, *38*, *57-80*. https://doi.org/10.1146/annurev-environ-082212-134049

Breiman, L., Friedman, J., Stone, C. J., & Olshen, R. A. (1984). *Classification and regression trees*. CRC press.

Breiman, L. (1996). Some properties of splitting criteria. *Machine Learning*, *24*(1), 41-47. https://doi.org/10.1023/A:1018094028462

Bright, B. C., Hudak, A. T., Meddens, A. J., Hawbaker, T. J., Briggs, J. S., Kennedy, R. E. (2017). Prediction of forest canopy and surface fuels from lidar and satellite time series data in a bark beetle-affected forest. *Forests*, *8*(9), 322. https://doi.org/10.3390/f8090322

Broadbent, E. N., Zambrano, AM. A., Omans, G., Adler, A., Alonso, P., Naylor, D., Chenevert, G., Murtha, T., Vogel, J., Almeida, D. R. A., Dalla Corte, A. P., Silva, C. A., Prata, G. A., Merrick, T., D'Oliveira, M. V. N., Detto, M., Ferreira, MP., Wilkinson, B. E., Ferreira, M.E., Muller-Landau, H. C. (2021). In prep. The GatorEye Unmanned Flying Laboratory: sensor fusion for 4D ecological analysis through custom hardware and algorithm integration, accessed Feb 10 2021. Retrieved from http://www.gatoreye.org

Burns, P., Clark, M., Salas, L., Hancock, S., Leland, D., Jantz, P., Goetz, S. J. (2020). Incorporating canopy structure from simulated GEDI lidar into bird species distribution models. Environmental Research Letters, 15(9), 095002. https://doi.org/10.1088/1748-9326/ab80ee

Chave, J., Réjou-Méchain, M., Búrquez, A., Chidumayo, E., Colgan, M. S., Delitti, W. B., ... & Vieilledent, G. (2014). Improved allometric models to estimate the aboveground biomass of tropical trees. *Global change biology*, *20*(10), 3177-3190. https://doi.org/10.1111/gcb.12629

Chen, L., Yang, J., Kong, H. (2017). Lidar-histogram for fast road and obstacle detection. In *2017 IEEE International Conference on Robotics and Automation (ICRA)* (pp. 1343-1348). IEEE. https://doi.org/10.1109/ICRA.2017.7989159

Chi, H., Sun, G., Huang, J., Guo, Z., Ni, W., Fu, A. (2015). National Forest Aboveground Biomass Mapping from ICESat/GLAS Data and MODIS Imagery in China. *Remote Sensing*, *7*(5), 5534-5564. https://doi.org/10.3390/rs70505534

Chuvieco, E., Aguado, I., Salas, J., García, M., Yebra, M., Oliva, P. (2020). Satellite remote sensing contributions to wildland fire science and management. *Current Forestry Reports*, *6*(2), 81-96. https://doi.org/10.1007/s40725-020-00116-5

Chuvieco, E., Aguado, I., Cocero, D., Riano, D. (2003). Design of an empirical index to estimate fuel moisture content from NOAA-AVHRR images in forest fire danger studies.

International Journal of Remote Sensing, *24*(8), 1621-1637. https://doi.org/10.1080/01431160210144660b

Costa, M.B.T. da, Silva, C.A., Broadbent, E.N., Leite, R.V., Mohan, M., Liesenberg, V., Stoddart, J., Amaral, C.H. do, Almeida, D.R.A. de, Silva, A.L. da, Goya, L.R.R.Y., Cordeiro, V.A., Rex, F., Hirsch, A., Marcatti, G.E., Cardil, A., Mendonça, B.A.F. de, Hamamura, C., Dalla Corte, A.P., Matricardi, E.A.T., Hudak, A.T., Zambrano, A.M.A., Valbuena, R., Faria, B.L. de, Junior, C.H.L.S., Aragão, L., Ferreira, M.E., Liang, J., Carvalho, S. de P.C. e, Klauberg, C., (2021). Beyond trees: Mapping total aboveground biomass density in the Brazilian savanna using high-density UAV-lidar data. *Forest Ecology and Management* *491*. https://doi.org/https://doi.org/10.1016/j.foreco.2021.119155

Costa, A.N., Souza, J.R., Alves, K.M., Penna-Oliveira, A., Paula-Silva, G., Becker, I.S., Marinho-Vieira, K., Bonfim, A.L., Bartimachi, A., Vieira-Neto, E.H.M.(2020). Linking the spatiotemporal variation of litterfall to standing vegetation biomass in Brazilian savannas. *Journal of Plant Ecology*. 13, 517–524. https://doi.org/10.1093/jpe/rtaa039

Dubayah, R., Blair, J. B., Goetz, S., Fatoyinbo, L., Hansen, M., Healey, S., Hofton, M., Hurtt, G., Kellner, J., Luthcke, S., Armston, J., Tang, H., Duncanson, L., Hancock, S., Jantz, P., Marselis, S., Patterson, P. L., Qi, W., Silva, C. (2020a). The Global Ecosystem Dynamics Investigation: High-resolution laser ranging of the Earth's forests and topography. *Science of Remote Sensing, 1*, 100002. https://doi.org/10.1016/j.srs.2020.100002

[dataset] Dubayah, R., M. Hofton, J. Blair, J. Armston, H. Tang, S. Luthcke. GEDI L2A Elevation and Height Metrics Data Global Footprint Level V002. 2021, distributed by NASA EOSDIS Land Processes DAAC, https://doi.org/10.5067/GEDI/GEDI02_A.002. Accessed 2021-08-29.

[dataset] Dubayah, R., H. Tang, J. Armston, S. Luthcke, M. Hofton, J. Blair. GEDI L2B Canopy Cover and Vertical Profile Metrics Data Global Footprint Level V002. 2021, distributed by NASA EOSDIS Land Processes DAAC, https://doi.org/10.5067/GEDI/GEDI02_B.002. Accessed 2021-08-29.

Duncanson, L., Neuenschwander, A., Hancock, S., Thomas, N., Fatoyinbo, T., Simard, M., Dubayah, R. (2020). Biomass estimation from simulated GEDI, ICESat-2 and NISAR across environmental gradients in Sonoma County, California. *Remote Sensing of Environment*, *242*, 111779. https://doi.org/10.1016/j.rse.2020.111779

Duncanson, L. I., Niemann, K. O., Wulder, M. A. (2010). Estimating forest canopy height and terrain relief from GLAS waveform metrics. *Remote Sensing of Environment*, *114*(1), 138-154. https://doi.org/10.1016/j.rse.2009.08.018

Durigan, G., Ratter, J. A. (2016). The need for a consistent fire policy for Cerrado conservation. *Journal of Applied Ecology*, *53*(1), 11-15. https://doi.org/10.1111/1365-2664.12559

Durigan, G., Pilon, N. A., Abreu, R. C., Hoffmann, W. A., Martins, M., Fiorillo, B. F., Vasconcelos, H. L. (2020). No net loss of species diversity after prescribed fires in the Brazilian Savanna. *Frontiers in Forests and Global Change*, *3*, 13. https://doi.org/10.3389/ffgc.2020.00013

Erdody, T. L., Moskal, L. M. (2010). Fusion of LiDAR and imagery for estimating forest canopy fuels. *Remote Sensing of Environment*, *114*(4), 725-737. https://doi.org/10.1016/j.rse.2009.11.002

Ferreira, L.G., Urban, T.J., Neuenschawander, A., De Araújo, F.M. (2011). Use of Orbital LIDAR in the Brazilian Cerrado Biome: Potential Applications and Data Availability. *Remote Sensing*, *3*(10), 2187-2206. https://doi.org/10.3390/rs3102187

Franke, J., Barradas, A. C. S., Borges, M. A., Menezes Costa, M., Dias, P. A., Hoffmann, A. A., Orozco Filho, J. C., Melchiori, A. E., Siegert, F. (2018). Fuel load mapping in the Brazilian Cerrado in support of integrated fire management. *Remote Sensing of Environment, 217*, 221–232. https://doi.org/10.1016/j.rse.2018.08.018

Gajardo, J., García, M., & Riaño, D. (2014). Applications of Airborne Laser Scanning in Forest Fuel Assessment and Fire Prevention. In M. Maltamo, E. Næsset, & J. Vauhkonen (Eds.), Forestry Applications of Airborne Laser Scanning: Concepts and Case Studies (pp. 439-462). Dordrecht: Springer Netherlands

García, M., Popescu, S., Riaño, D., Zhao, K., Neuenschwander, A., Agca, M., Chuvieco, E. (2012). Characterization of canopy fuels using ICESat/GLAS data. *Remote Sensing of Environment*, *123*, 81-89. https://doi.org/10.1016/j.rse.2012.03.018

García, M., Saatchi, S., Casas, A., Koltunov, A., Ustin, S.L., Ramirez, C., Balzter, H. (2017). Extrapolating forest canopy fuel properties in the California Rim fire by combining airborne LiDAR and landsat OLI data. *Remote Sensing* 9, 1–18. https://doi.org/10.3390/rs9040394

Glenn, N. F., Neuenschwander, A., Vierling, L. A., Spaete, L., Li, A., Shinneman, D. J., McIlroy, S. K. (2016). Landsat 8 and ICESat-2: Performance and potential synergies for quantifying dryland ecosystem vegetation cover and biomass. *Remote Sensing of Environment, 185*, 233–242. http://dx.doi.org/10.1016/j.rse.2016.02.039

Gomes, L., Miranda, H. S., Silvério, D. V., Bustamante, M. M. C. (2020a). Effects and behaviour of experimental fires in grasslands, savannas, and forests of the Brazilian Cerrado. *Forest Ecology and Management, 458,* 117804,. https://doi.org/10.1016/j.foreco.2019.117804

Gomes, L., Miranda, H.S., Soares-Filho, B., Rodrigues, L., Oliveira, U., Bustamante, M.M.C., (2020b). Responses of Plant Biomass in the Brazilian Savanna to Frequent Fires. Frontiers in Forests and Global Change 3, 1–11. https://doi.org/10.3389/ffgc.2020.507710

Gomes, L., Miranda, H. S., Bustamante, M. M. da C. (2018). How can we advance the knowledge on the behavior and effects of fire in the Cerrado biome?. *Forest Ecology and Management*, *417*, 281–290. https://doi.org/10.1016/j.foreco.2018.02.032

Gwenzi, D., Lefsky, M. A., Suchdeo, V. P., Harding, D. J. (2016). Prospects of the ICESat-2 laser altimetry mission for savanna ecosystem structural studies based on airborne simulation data. *ISPRS Journal of Photogrammetry and Remote Sensing*, *118*, 68-82. https://doi.org/10.1016/j.isprsjprs.2016.04.009

Hall, F. G., Bergen, K., Blair, J. B., Dubayah, R., Houghton, R., Hurtt, G., ... & Wickland, D. (2011). Characterizing 3D vegetation structure from space: Mission requirements. *Remote Sensing of Environment*, *115*(11), 2753-2775.

Hancock, S., Armston, J., Hofton, M., Sun, X., Tang, H., Duncanson, L. I., Dubayah, R. (2019). The GEDI simulator: A large-footprint waveform lidar simulator for calibration and validation of spaceborne missions. *Earth and Space Science*, *6*(2), 294-310. https://doi.org/10.1029/2018EA000506

Hantson, S., Pueyo, S., Chuvieco, E. (2015). Global fire size distribution is driven by human impact and climate. *Global Ecology and Biogeography*, *24*(1), 77-86. https://doi.org/10.1111/geb.12246

Harding, D. J., Carabajal, C. C. (2005). ICESat waveform measurements of within-footprint topographic relief and vegetation vertical structure. *Geophysical research letters*, *32*(21), 4. https://doi.org/10.1029/2005GL023471

Healey, S. P., Yang, Z., Gorelick, N., Ilyushchenko, S. (2020). Highly Local Model Calibration with a New GEDI LiDAR Asset on Google Earth Engine Reduces Landsat Forest Height Signal Saturation. *Remote Sensing, 12*(17), 2840. https://doi.org/10.3390/rs12172840

Hermosilla, T., Coops, N. C., Ruiz, L. A., Moskal, L. M. (2014). Deriving pseudo-vertical waveforms from small-footprint full-waveform LiDAR data. *Remote sensing letters*, *5*(4), 332-341. https://doi.org/10.1080/2150704X.2014.903350

Hoffmann, W. A., Jaconis, S. Y., McKinley, K. L., Geiger, E. L., Gotsch, S. G., & Franco, A. C. (2012). Fuels or microclimate? Understanding the drivers of fire feedbacks at savanna–forest boundaries. *Austral Ecology*, *37*(6), 634-643. https://doi.org/10.1111/j.1442-9993.2011.02324.x

Hofton M., and Blair J.B. (2019) Algorithm Theoretical Basis Document (ATBD) for GEDI Transmit and Receive Waveform Processing for L1 and L2 Products. https://lpdaac.usgs.gov/documents/581/GEDI_WF_ATBD_v1.0.pdf. (accessed 13 March 2021)

Hu, T., Ma, Q., Su, Y., Battles, J.J., Collins, B. M., Stephens, S. L., Kelly, M., Guo, Q. (2019). A simple and integrated approach for fire severity assessment using bi-temporal airborne

LiDAR data. *International Journal of Applied Earth Observation and Geoinformation,* 78, 25–38. https://doi.org/10.1016/j.jag.2019.01.007

Hudak, A. T., Bright, B. C., Pokswinski, S. M., Loudermilk, E. L., O'Brien, J. J., Hornsby, B. S., Silva, C. A. (2016a). Mapping forest structure and composition from low-density LiDAR for informed forest, fuel, and fire management at Eglin Air Force Base, Florida, USA. *Canadian Journal of Remote Sensing*, *42*(5), 411-427. https://doi.org/10.1080/07038992.2016.1217482

Hudak, A. T., Dickinson, M. B., Bright, B. C., Kremens, R. L., Loudermilk, E. L., O'Brien, J. J., Ottmar, R. D. (2016b). Measurements relating fire radiative energy density and surface fuel consumption–RxCADRE 2011 and 2012. *International Journal of Wildland Fire*, *25*(1), 25-37. https://doi.org/10.1080/07038992.2016.1217482

Jakubowksi, M. K., Guo, K., Collins, B., Stephens, S., Kelly, M. (2013). Predicting Surface Fuel Models and Fuel Metrics Using Lidar and CIR Imagery in a Dense, Mountainous Forest. *Photogrammetric Engineering & Remote Sensing*, *79*(1), 37–49. https://doi.org/10.14358/PERS.79.1.37

Keane, R. E., Herynk, J. M., Toney, C., Urbanski, S. P., Lutes, D. C., Ottmar, R. D. (2013). Evaluating the performance and mapping of three fuel classification systems using Forest Inventory and Analysis surface fuel measurements. *Forest Ecology and Management, 305*, 248–263. https://doi.org/10.1016/j.foreco.2013.06.001

Keane, R. E., Reeves, M. (2012). Use of Expert Knowledge to Develop Fuel Maps for Wildland Fire Management. A. H. Perera et al. (eds.), Expert Knowledge and Its Application in Landscape Ecology. Springer. (pp 211-228). https://doi.org/10.1007/978-1-4614-1034-8_11.

Kimura, T., Imai, T., Sakaizawa, D., Murooka, J., Mitsuhashi, R. (2017). The overview and status of vegetation Lidar mission, MOLI. In *2017 IEEE International Geoscience and Remote Sensing Symposium (IGARSS)* (pp. 4228-4230). IEEE. https://doi.org/10.1109/IGARSS.2017.8127935

Klauberg, C., Hudak, A. T., Silva, C. A., Lewis, S. A., Robichaud, P. R., Jain, T. B. (2019). Characterizing fire effects on conifers at tree level from airborne laser scanning and high-resolution, multispectral satellite data. *Ecological Modelling*, *412*, 108820. https://doi.org/10.1016/j.ecolmodel.2019.108820

Kuhn, M., Wing, J., Weston, S., Williams, A., Keefer, C., Engelhardt, A., Benesty, M. (2020). Package 'caret'. *The R Journal*, 223.

Lang, N., Schindler, K., Wegner, J. D. (2019). Country-Wide High-Resolution Vegetation Height Mapping with Sentinel-2. *Remote Sensing of Environment*, 233, 111347. http://doi.org/10.1016/j.rse.2019.111347

Lê, S., Josse, J., Husson, F. (2008). FactoMineR: an R package for multivariate analysis. *Journal of statistical software*, *25*(1), 1-18.

Lefsky, M. A., Keller, M., Pang, Y., De Camargo, P. B., Hunter, M. O. (2007). Revised method for forest canopy height estimation from Geoscience Laser Altimeter System waveforms. *Journal of Applied Remote Sensing*, *1*(1), 013537. https://doi.org/10.1117/1.2795724

Lefsky, M. A., Harding, D. J., Keller, M., Cohen, W. B., Carabajal, C. C., Espirito-Santo, F. D., ... & de Camargo, P. B. (2006). Correction to "Estimates of forest canopy height and aboveground biomass using ICESat". *Geophysical Research Letters*, *32*(5), L05501. https://doi.org/10.1029/2005GL025518.

Lefsky, M. A., Harding, D. J., Keller, M., Cohen, W. B., Carabajal, C. C., Espirito-Santo, F. D., (2005). Estimates of forest canopy height and aboveground biomass using ICESat. *Geophysical research letters*, *32*(22). https://doi.org/10.1029/2005GL023971

Lehmann, C.E.R., Anderson, T.M., Sankaran, M., Higgins, S.I., Archibald, S., Hoffmann, W.A., Hanan, N.P., Williams, R.J., Fensham, R.J., Felfili, J., Hutley, L.B., Ratnam, J., San Jose, J., Montes, R., Franklin, D., Russell-Smith, J., Ryan, C.M., Durigan, G., Hiernaux, P., Haidar, R., Bowman, D.M.J.S., Bond, W.J., (2014). Savanna vegetation-fire-climate relationships differ among continents. *Science* 343, 548–552. https://doi.org/10.1126/science.1247355

Li,W., Niu, Z., Shang, R., Qin, Y., Wang, L., Chen, H. (2020). High-Resolution Mapping of Forest Canopy Height Using Machine Learning by Coupling ICESat-2 LiDAR with Sentinel-1, Sentinel-2 and Landsat-8 Data. *International Journal of Applied Earth Observation and Geoinformation*, *92*, 102163. https://doi.org/10.1016/j.jag.2020.102163

MacArthur, R. H., & Horn, H. S. (1969). Foliage profile by vertical measurements. *Ecology*, *50*(5), 802-804. https://doi.org/10.2307/1933693

Marselis, S. M., Tang, H., Armston, J., Abernethy, K., Alonso, A., Barbier, N., ... & Dubayah, R. (2019). Exploring the relation between remotely sensed vertical canopy structure and tree species diversity in Gabon. *Environmental Research Letters*, *14*(9), 094013.

Marselis, S. M., Tang, H., Armston, J. D., Calders, K., Labrière, N., Dubayah, R. (2018). Distinguishing vegetation types with airborne waveform lidar data in a tropical forest-savanna mosaic: A case study in Lopé National Park, Gabon. *Remote sensing of environment*, *216*, 626-634.

Marshak, C., Simard, M., Duncanson, L., Silva, C. A., Denbina, M., Liao, T. H., ... & Armston, J. (2020). Regional Tropical Aboveground Biomass Mapping with L-Band Repeat-Pass Interferometric Radar, Sparse Lidar, and Multiscale Superpixels. Remote Sensing, 12(12), 2048. https://doi.org/10.3390/rs12122048

Mauro, F., Hudak, A. T., Fekety, P. A., Frank, B., Temesgen, H., Bell, D. M., ... & McCarley, T. R. (2021). Regional Modeling of Forest Fuels and Structural Attributes Using Airborne Laser Scanning Data in Oregon. Remote Sensing, 13(2), 261. https://doi.org/10.3390/rs13020261

Murooka, J., Kobayashi, T., Imai, T., Suzuki, K., Sakaizawa, D., Yamakawa, S., ... & Asai, K. (2013). Overview of Japan's spaceborne vegetation lidar mission. In *Lidar Technologies, Techniques, and Measurements for Atmospheric Remote Sensing IX* (Vol. 8894, p. 88940B). International Society for Optics and Photonics.

Myers, N., Mittermeier, R. A., Mittermeier, C. G., Da Fonseca, G. A., & Kent, J. (2000). Biodiversity hotspots for conservation priorities. *Nature*, *403*(6772), 853-858. https://doi.org/10.1117/12.2029119

Narine, L. L., Popescu, S. C., & Malambo, L. (2020). Using ICESat-2 to estimate and map forest aboveground biomass: A first example. *Remote Sensing*, *12*(11), 1824.

Narine, L. L., Popescu, S., Neuenschwander, A., Zhou, T., Srinivasan, S., Harbeck, K. (2019). Estimating aboveground biomass and forest canopy cover with simulated ICESat-2 data. *Remote Sensing of Environment, 224*, 1–11. https://doi.org/10.1016/j.rse.2019.01.037

Ogle, S. M., Kurz, W. A., Green, C., Brandon, A., Baldock, J., Domke, G., Herold, M., Bernoux, M., … & Waterworth, R. M. (2019). Chapter 2: Generic Methodologies Applicable To Multiple Land-Use Categories. 2019 Refinement to the 2006 IPCC Guidelines for National Greenhouse Gas Inventories 1–59.

Oliveira, U., Soares-Filho, B., de Souza Costa, W.L., Gomes, L., Bustamante, M., Miranda, H., (2021). Modeling fuel loads dynamics and fire spread probability in the Brazilian Cerrado. Forest Ecology and Management 482. https://doi.org/10.1016/j.foreco.2020.118889

Pardini, M., Armston, J., Qi, W., Lee, S. K., Tello, M., Bes, V. C., ... & Fatoyinbo, L. E. (2019). Early lessons on combining lidar and multi-baseline SAR measurements for forest structure characterization. *Surveys in Geophysics*, *40*(4), 803-837. https://doi.org/10.1007/s10712-019-09553-9

Patterson, P. L., Healey, S. P., Ståhl, G., Saarela, S., Holm, S., Andersen, H. E., ... & Yang, Z. (2019). Statistical properties of hybrid estimators proposed for GEDI—NASA's global ecosystem dynamics investigation. *Environmental Research Letters*, *14*(6), 065007. https://doi.org/10.1088/1748-9326/ab18df

Pesonen, A., Maltamo, M., Eerikäinen, K., Packalèn, P. (2008). Airborne laser scanning-based prediction of coarse woody debris volumes in a conservation area. *Forest Ecology and Management*, *255*(8-9), 3288-3296. https://doi.org/10.1016/j.foreco.2008.02.017

Peterson, B., Nelson, K., & Wylie, B. (2013). Towards integration of GLAS into a national fuel mapping program. *Photogrammetric Engineering & Remote Sensing*, *79*(2), 175-183. https://doi.org/10.14358/PERS.79.2.175

Popescu, S. C.; Zhou, T.; Nelson, R.; Neuenschwander, A.; Sheridan, R.; Narine, L.; Walsh, K. M. (2018). Photon counting LiDAR: An adaptive ground and canopy height retrieval algorithm for ICESat-2 data. *Remote Sensing of Environment, 208*, 154–170. https://doi.org/10.1016/j.rse.2018.02.019

Popescu, S. C., Zhao, K., Neuenschwander, A., Lin, C. (2011). Satellite lidar vs. small footprint airborne lidar: Comparing the accuracy of aboveground biomass estimates and forest structure metrics at footprint level. *Remote Sensing of Environment, 115*(11), 2786–2797. https://doi.org/10.1016/j.rse.2011.01.026

Potapov, P., Li, X., Hernandez-Serna, A., Tyukavina, A., Hansen, M. C., Kommareddy, A., ... & Hofton, M. (2021). Mapping global forest canopy height through integration of GEDI and Landsat data. *Remote Sensing of Environment*, *253*, 112165. https://doi.org/10.1016/j.rse.2020.1121

Price, O. F., Gordon, C. E. (2016). The potential for LiDAR technology to map fire fuel hazard over large areas of Australian forest. *Journal of Environmental Management, 181*, 663-673. http://dx.doi.org/10.1016/j.jenvman.2016.08.042

Qi, W., Dubayah, R. O. (2016). Combining Tandem-X InSAR and simulated GEDI lidar observations for forest structure mapping. Remote Sensing of Environment, 187, 253-266. https://doi.org/10.1016/j.rse.2016.10.018

Qi, W., Lee, S. K., Hancock, S., Luthcke, S., Tang, H., Armston, J., Dubayah, R. (2019). Improved forest height estimation by fusion of simulated GEDI Lidar data and TanDEM-X InSAR data. *Remote sensing of environment*, *221*, 621-634. https://doi.org/10.1016/j.rse.2018.11.035

Quegan, S., Le Toan, T., Chave, J., Dall, J., Exbrayat, J. F., Minh, D. H. T., ... & Williams, M. (2019). The European Space Agency BIOMASS mission: Measuring forest above-ground biomass from space. *Remote Sensing of Environment*, *227*, 44-60. https://doi.org/10.1016/j.rse.2019.03.032

R Core Team. (2020). R: A Language and Environment for Statistical Computing. R Foundation for Statistical Computing. Vienna, Austria. https://www.R-project.org/. (accessed 13 March 2021)

Rishmawi, K., Huang, C., & Zhan, X. (2021). Monitoring Key Forest Structure Attributes across the Conterminous United States by Integrating GEDI LiDAR Measurements and VIIRS Data. *Remote Sensing*, *13*(3), 442. https://doi.org/10.3390/rs13030442

Roberts, D.A., Dennison, P.E., Gardner, M.E., Hetzel, Y., Ustin, S.L., Lee, C.T. (2003). Evaluation of the potential of Hyperion for fire danger assessment by comparison to the airborne visible/infrared imaging spectrometer. IEEE Transactions on Geoscience and Remote Sensing 41, 1297–1310. https://doi.org/10.1109/TGRS.2003.812904

Roitman, I., Bustamante, M.M.C., Haidar, R.F., Shimbo, J.Z., Abdala, G.C., Eiten, G., Fagg, C.W., Felfili, M.C., Felfili, J.M., Jacobson, T.K.B., Lindoso, G.S., Keller, M., Lenza, E., Miranda, S.C., Pinto, J.R.R., Rodrigues, A.A., Delitti, W.B.C., Roitman, P., Sampaio, J.M., 2018. Optimizing biomass estimates of savanna woodland at different spatial scales in the Brazilian Cerrado: Re-evaluating allometric equations and environmental influences. PLoS ONE 13, 1–21. https://doi.org/10.1371/journal.pone.0196742

Rosan, T. M., Aragão, L. E., Oliveras, I., Phillips, O. L., Malhi, Y., Gloor, E., & Wagner, F. H. (2019). Extensive 21st-century woody encroachment in South America's savanna. *Geophysical Research Letters*, 46(12), 6594-6603.

Rosen, P. A., Hensley, S., Shaffer, S., Veilleux, L., Chakraborty, M., Misra, T., ... & Satish, R. (2015, May). The NASA-ISRO SAR mission-An international space partnership for science and societal benefit. In *2015 IEEE Radar Conference (RadarCon)* (pp. 1610-1613). IEEE.

Saarela, S., Holm, S., Healey, S. P., Andersen, H. E., Petersson, H., Prentius, W., ... & Ståhl, G. (2018). Generalized hierarchical model-based estimation for aboveground biomass assessment using GEDI and Landsat data. *Remote Sensing*, *10*(11) 1832. https://doi.org/10.3390/rs10111832

Saatchi, S.; Halligan, K.; Despain, D. G.; Crabtree, R. L. Estimation of forest fuel load from radar remote sensing (2007). *IEEE Transactions on Geoscience and Remote Sensing, 45*(6), 1726–1740. https://10.1109/TGRS.2006.887002.

Sanchez-Lopez, N., Boschetti, L., Hudak, A. T., Hancock, S., Duncanson, L. I. (2020). Estimating Time Since the Last Stand-Replacing Disturbance (TSD) from Spaceborne Simulated GEDI Data: A Feasibility Study. *Remote Sensing*, *12*(21), 3506. https://doi.org/10.3390/rs12213506

Sandberg, D. V., Ottmar, R. D., & Cushon, G. H. (2001). Characterizing fuels in the 21st century. *International Journal of Wildland Fire*, *10*(4), 381-387. https://doi.org/10.1071/WF01036

Schmidt, I. B., Moura, L. C., Ferreira, M. C., Eloy, L., Sampaio, A. B., Dias, P. A., & Berlinck, C. N. (2018). Fire management in the Brazilian savanna: First steps and the way forward. Journal of applied ecology, 55(5), 2094-2101. https://doi.org/10.1111/1365-2664.13118

Schneider, F. D., Ferraz, A., Hancock, S., Duncanson, L. I., Dubayah, R. O., Pavlick, R. P., Schimel, D. S. (2020). Towards mapping the diversity of canopy structure from space with GEDI. *Environmental Research Letters*, *15*(11), 115006. https://doi.org/10.5068/D16T06

Silva, C.A., Duncanson, L., Hancock, S., Neuenschwander, A., Thomas, N., Hofton, M., Fatoyinbo, L., Simard, M., Marshak, C.Z., Armston, J., Lutchke, S., Dubayah, R., (2021). Fusing simulated GEDI, ICESat-2 and NISAR data for regional aboveground biomass mapping. *Remote Sensing of Environment* 253. https://doi.org/10.1016/j.rse.2020.112234

Silva, C. A., Hamamura,C., Valbuena, R., Hancock, S., Cardil, A., Broadbent, E. N., Almeida, D. R. A., Silva Junior, C. H. L., Klauberg, C. (2020). rGEDI: NASA's Global Ecosystem Dynamics Investigation (GEDI) Data Visualization and Processing. version 0.1.8, accessed on October. 22 2020, available at: https://CRAN.R-project.org/package=rGEDI

Silva, C. A., Saatchi, S., Garcia, M., Labriere, N., Klauberg, C., Ferraz, A., ... & Hudak, A. T. (2018). Comparison of small-and large-footprint lidar characterization of tropical forest aboveground structure and biomass: A case study from central gabon. *IEEE Journal of Selected Topics in Applied Earth Observations and Remote Sensing*, *11*(10), 3512-3526. https://doi.org/10.1109/JSTARS.2018.2816962

Simon, M.F.; Grether, R.; Queiroz, L.P.; Skema, C.; Pennington, R.T. Hughes, C. E. (2009). Recent assembly of the Cerrado, a Neotropical plant diversity hotspot, by in situ evolution of adaptations to fire. Proceedings of the National Academy of Science USA, *106*(48): 20359-20364. https://doi.org/10.1073/pnas.0903410106

Souza, C.M., Shimbo, J.Z., Rosa, M.R., Parente, L.L., Alencar, A.A., Rudorff, B.F.T., Hasenack, H., Matsumoto, M., Ferreira, L.G., Souza-Filho, P.W.M., de Oliveira, S.W., Rocha, W.F., Fonseca, A. V., Marques, C.B., Diniz, C.G., Costa, D., Monteiro, D., Rosa, E.R., Vélez-Martin, E., Weber, E.J., Lenti, F.E.B., Paternost, F.F., Pareyn, F.G.C., Siqueira, J. V., Viera, J.L., Neto, L.C.F., Saraiva, M.M., Sales, M.H., Salgado, M.P.G., Vasconcelos, R., Galano, S., Mesquita, V. V., Azevedo, T. (2020). Reconstructing three decades of land use and land cover changes in brazilian biomes with landsat archive and earth engine. Remote Sensing 12. https://doi.org/10.3390/RS12172735

Stavros, E. N., Coen, J., Peterson, B., Singh, H., Kennedy, K., Ramirez, C., Schimel, D. (2018). Use of imaging spectroscopy and LIDAR to characterize fuels for fire behavior prediction. *Remote Sensing Applications: Society and Environment*, *11*, 41–50. https://doi.org/10.1016/j.rsase.2018.04.010

Stefanidou, A., Gitas, I. Z., Korhonen, L., Stavrakoudis, D., & Georgopoulos, N. (2020). LiDAR-based estimates of canopy base height for a dense uneven-aged structured forest. *Remote Sensing*, *12*(10), 1565. https://doi.org/10.3390/rs12101565

Strassburg, B. B., Brooks, T., Feltran-Barbieri, R., Iribarrem, A., Crouzeilles, R., Loyola, R., ... & Balmford, A. (2017). Moment of truth for the Cerrado hotspot. *Nature Ecology & Evolution*, *1*(4), 1-3. https://doi.org/10.1038/s41559-017-0099

Szpakowski, D. M., Jensen, J. L. (2019). A review of the applications of remote sensing in fire ecology. *Remote Sensing*, *11*(22), 2638. https://doi.org/10.3390/rs11222638

Tang, H., Armston, J. (2019). Algorithm Theoretical Basis Document (ATBD) for GEDI L2B Footprint Canopy Cover and Vertical Profile Metrics. https://lpdaac.usgs.gov/documents/588/GEDI_FCCVPM_ATBD_v1.0.pdf. (accessed 13 March 2021)

Turner, M. G., Gardner, R. H., & O'neill, R. V. (1995). Ecological dynamics at broad scales. *BioScience*, *45*, S29-S35.

Wulder, M.A., White, J.C., Nelson, R.F., Næsset, E., Ørka, H.O., Coops, N.C., Hilker, T., Bater, C.W., Gobakken, T. (2012). Lidar sampling for large-area forest characterization: A review. *Remote Sensing of Environment*. 121, 196–209. https://doi.org/10.1016/j.rse.2012.02.001

Xiao, J., Chevallier, F., Gomez, C., Guanter, L., Hicke, J.A., Huete, A.R., Ichii, K., Ni, W., Pang, Y., Rahman, A.F., Sun, G., Yuan, W., Zhang, L., Zhang, X. (2019) Remote sensing of the terrestrial carbon cycle: A review of advances over 50 years. *Remote Sensing of Environment*, 233, 111383. https://doi.org/10.1016/j.rse.2019.111383.

Yang, W., Ni-Meister, W., & Lee, S. (2011). Assessment of the impacts of surface topography, off-nadir pointing and vegetation structure on vegetation lidar waveforms using an extended geometric optical and radiative transfer model. *Remote Sensing of Environment*, *115*(11), 2810-2822. https://doi.org/10.1016/j.rse.2010.02.021

Zanne, A., Lopez-Gonzalez, G Coomes, D., Ilic, J., Jansen, S., Lewis, S., Miller, R., Swenson, N., Wiemann, M., & Chave, J. 2009. Data from: Towards a worldwide wood economics spectrum. Dryad Digital Repository https://doi.org/10.5061/dryad.234.

Zwally, H. J., Schutz, B., Abdalati, W., Abshire, J., Bentley, C., Brenner, A., ... & Thomas, R. (2002). ICESat's laser measurements of polar ice, atmosphere, ocean, and land. *Journal of Geodynamics*, *34*(3-4), 405-445. https://doi.org/10.1016/S0264-3707(02)00042-X

Chapter 3: Using the new generation of Earth observation systems to improve wildfire management

ABSTRACT

LEITE, Rodrigo Vieira, Universidade Federal de Viçosa, December, 2022. **Using the new generation of Earth observation systems to improve wildfire management.** Adviser: Cibele Hummel do Amaral.

Managing vegetation fuels is necessary to preserve fire regimes and the functionality of ecosystems across the world. Data from remote sensors make large-area assessment possible especially when coupled in satellite systems. Even though there are over 50 years of available space-based Earth observations data, the new generation of passive and active sensors can bring new insights and opportunities for characterizing vegetation fuels. In this paper, the applications of these sensors were assessed based on their potential to fill knowledge gaps for improving fuel characterization in large areas. Here we segment the available sensors to those that deliver freely available data, with spatial resolution of at least 70 m to enable upscaling from field plots and that were launched in the last 6 years (2017-2022)

1. Introduction

Most recent IPCC's report showed there is a trend in increasing fires weathers (i.e., hot, dry, and windy events) as consequence of global warming (Seneviratne et al. 2021). Such conditions favor the occurrences of extremely rare wildfires wherein large forest areas (hundreds of hectares) are severely burnt (Gill and Allan, 2008; Tedim et al., 2018). Not occasionally, extreme wildfire events have been increasing in the last two decades (e.g., Fidelis et al. 2019, Lizundia-Loiola et al. 2019, Adams et al. 2020, Turco et al., 2019). Understanding vegetation-fire interactions and developing fire management strategies on global scale is therefore urging to prevent socioenvironmental losses in the context of climate change (Bowman et al. 2020).

Wildfires need to be managed due to the long-term effects of human changes in landscape characteristics (Bowman et al. 2013, Kelly et al. 2020). Many practices focus on managing fuels since other parameters related to fire are harder or not possible to directly control (e.g., ignition source, weather, wind, topography). The fuel load, structure, and physical and chemical properties affect fire ignition probability, spreading rate, fire emissions and the potential fire severity and extent (Chuvieco et al. 2020, Stavros et al. 2018; Figure 1). With the information of fuel amount, type, condition and distribution, it is possible to prescribe low-severity burns, model fire behavior and predict fire risk (Gale et al. 2021).

Earth observation satellite systems come into play to help managers in the task of managing fuels in large areas. Field analysis can be upscaled from local to continental/global regions and improve the understanding of the fire-vegetation interactions (Yebra et al. 2019, Gale et al. 2021, Zhu et al. 2021). This is achieved by relating fuel measures to remote-sensing products.

There are now over 50 years of consistent space-based Earth observations (see Wulder et al., 2022) and freely available data from more than 48 sensors that can be used for mapping fuels and managing `fire (Ustin et al. 2021). We might, nevertheless, be entering on a new phase of co-occurrence of Earth observation in finer spatial, spectral and temporal scales thanks to the advances on space technology and sensors. It is expected that many theoretical and technical issues related to fuel mapping can benefit from the different characteristics of these spaceborne sensors.

Here we assess the importance and challenges of fuel load mapping in large scales and present a set of the new generation of spaceborne sensors that can help in this task. The focus

was given to sensors with freely available data launched in the last 6 years (2017 – 2022) and spatial resolution of at least 70 m to enable upscaling from field plots.

2. Challenges in large-scale fuel mapping

Extensive field campaigns for fuel characterization are conducted to quantify fuel characteristics and help fire managers. Important characteristics to account for are the fuel load (section 2.1.), fuel moisture content (2.2.), live-dead fuel ratio (2.3.), continuity (2.4.), and diversity (2.5.) (**Table 1**).

Part of the role of remote sensors are reducing the amount of fuel field reconnaissance and upscaling the analysis to large extents,potentially, at continental or global levels with spaceborne sensors. This is possible as spaceborne sensors measurements and products can be related to different vegetation traits (Skidmore et al. 2021) and, thus, can be used to characterize fuels (**Table 1**). Different types of sensors have been used for this end but there are still limitations and cavities to improve the outputs of fuel measurements from space.

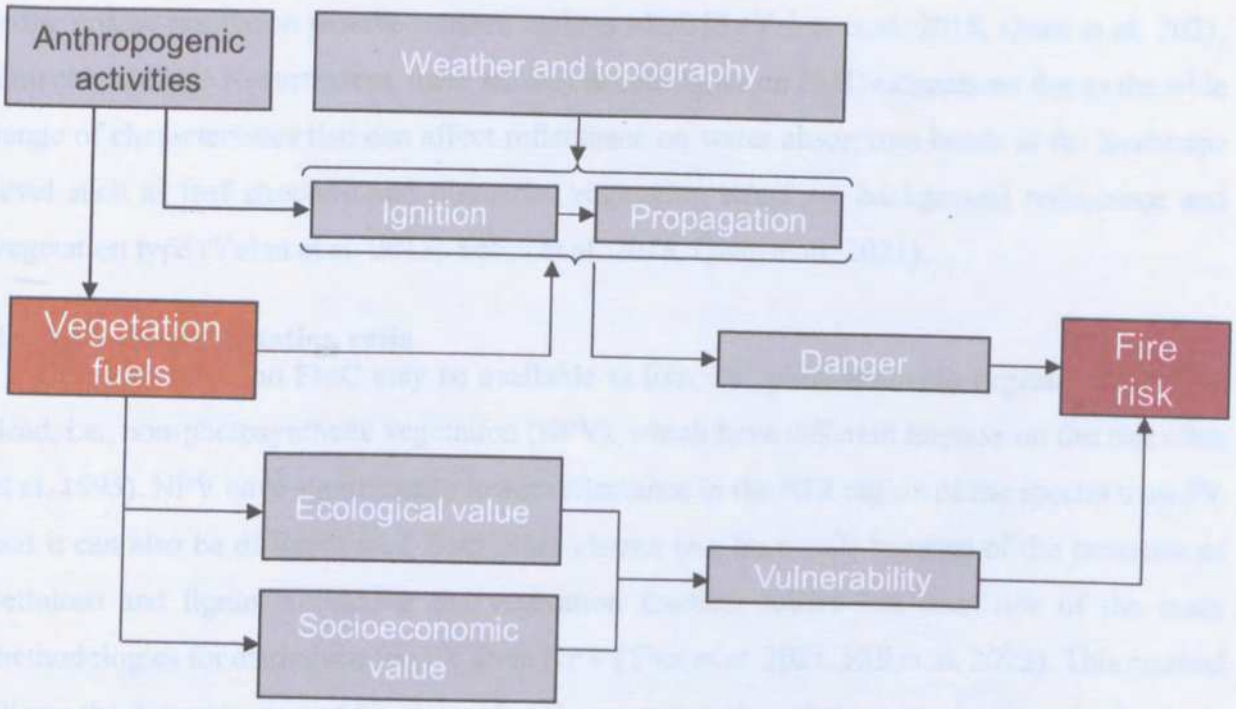

Figure 1. Fire risk framework adapted from Chuvieco et al. 2014

2.1. Fuel load

The amount of vegetation biomass available for burning – defined in wildfire science as fuel loads – is one of the main variables related to fire risk as it is directly related to how much energy can be released from a wildfire (van Wagtendok 2006). It is also an important variable for calculating the potential carbon emissions derived from vegetation burning. Reducing the amount of fuel is a common practice to avoid wildfires with high severity. One of the current most challenging issues in quantifying fuels through remote sensing is measuring sub-canopy and surface fuels such as understory, grasses, litter, woody debris and duff (Gale et al. 2021). Measuring ladder fuels that occur between ground and tree canopy is also challenging for large scales that may requires sensors with high penetration capacity through the canopy.

2.2. Fuel moisture content

Fuels availability to fire is dependent on the fuel moisture content (FMC). This variable is usually separated into live (LFMC) and dead fuel moisture content (DFMC). While DFMC are more related to weather conditions, LFMC is also affected by plant physiology and water availability in the soil. The use of passive sensors is justified by the water absorption features in the NIR and SWIR spectral regions generally centered at about 970, 1200, 1450, and 1940 nm (Knipling 1970, Yebra 2013) and by the variations in surface temperature. There are currently large-scale LFMC products developed for constant monitoring of LFMC dynamics using coarse resolution passive sensors such as MODIS (Yebra et al. 2018, Quan et al. 2021, Zhu et al. 2021). Nevertheless, there are still uncertainties on FMC estimations due to the wide range of characteristics that can affect reflectance on water absorption bands at the landscape level such as leaf structure and pigments, vegetation structure, background reflectance and vegetation type (Yebra et al. 2013, Yebra et al. 2018, Quan et al. 2021).

2.3. Live-dead vegetation ratio

Both fuel load and FMC may be available as live, i.e., photosynthetic vegetation (PV), or dead, i.e., non-photosynthetic vegetation (NPV), which have different impacts on fire risk (Sun et al. 1995). NPV have significantly lower reflectance in the NIR region of the spectra than PV and it can also be differentiated from other classes (e.g bare soil) because of the presence of cellulose and lignin. Unmixing the vegetation fraction covers has been one of the main methodologies for distinguishing PV from NPV (Tian et al. 2021, Hill et al. 2022). This method allows the determination of fractions of each vegetation class that are present in a single pixel.

2.4. Fuel distribution

Fire spread, final fire extent and severity is highly dependent on how those fuels are distributed in the landscape (Reszka et al. 2020). Fuels can be horizontally (e.g., through ground, surface vegetation and thick vegetation) or vertically connected (e.g. through ladder fuels). Both active and passive sensors are used for mapping fuel distribution on the landscape. The vertical distribution can only be thoroughly assessed with sensors with penetration capabilities to describe vertical structure, such as lidar and radar. Nevertheless, vegetation types and other land cover classes can be characterized by using passive sensors, active sensors, or their fusion.

2.5. Fire-related species diversity traits

In a broad perspective, continuously distributed accumulated fuel load with low levels of FMC can potentially yield high-intensity fire events. Nonetheless, other specific vegetation diversity traits may also increase or diminish wildfire risk since species physical-chemical traits affects vegetation flammability (Anderson 1970, Martin et al. 1994, White et al. 2010) – defined as a combination of vegetation ignitability (how easy is to ignite the fuel), combustibility (how intense is the combustion), consumability (how much was entirely combusted) and sustainability (how long the fuel burns). Flammability depends on several vegetation characteristics. For instance, woody or grass species with thicker leaves or with lower surface-area-to-volume ratio might be harder to ignite. In addition, after a fire starts, the presence of chemical constituents may hasten or slow fire combustion. The impacts of leaf traits may be even more apparent for deciduous tree species where most of the canopy will become surface fuels in a given season. The leaf decay and decomposition may also differ due to species phenology and constituents, especially C:N and C:P relationships (Simpson et al. 2016). Many other traits can characterize species traits and its ecosystem function such as leaf shape, canopy structure, bark thickness, resin concentration. Nevertheless, efficiently scaling up trait diversity from local to global levels is an important growing study topic (Carmona et al. 2016, Jetz et al. 2016). Leaf pigments (e.g. Chl_a, Chl_b, carotenoids) and chemical constituents (e.g., N, P) has been mapped using imaging spectroscopy. On the other hand, structural traits (e.g. canopy height, density and structure) are directly retrieved with active sensors, especially lidar.

3. Characteristics of novel Earth observation systems to help fuel mapping

Space technology has been developed in many countries around the world and many have developed and launched Earth observation sensors to space (Ustin et al. 2021). The endeavors come from governmental agencies, private companies or partnerships between both. Here we

segment the available sensors to those that have freely available data, have a spatial resolution of at least 70 m (corresponding to what can be used for a "field plot-level" analysis) and were launched in the last 6 years (2017-2022).

3.1. Passive sensors

3.1.1. Multispectral and thermal sensors

Part of the electromagnetic radiation that comes from the sun is reflected by objects in the Earth's surface and can be captured by a spaceborne sensor orbiting the Earth. This energy is captured on specific wavelengths - usually from 400 to 1,000 (VNIR) or to 2,500 nm (VSWIR) - depending on sensors' design. Broad-band remote sensors with full width at half maximum (FWHM) of about 100 nm (a.k.a. multispectral sensors) represent most of the available spaceborne sensors in orbit today. Those sensors are characterized by capturing a wider range of wavelengths in a band. The benefits come from capturing more energy per band and making more feasible sensors with higher spatial resolution for a defined spectra region. Many of those sensors are also able to capture thermal information from Earth's objects, since all objects with temperature greater than 0 K (-273.15 °C) emit thermal radiation in a range of the spectrum called thermal infrared (TIR, ~3,000 to 14,000 nanometers) (Neinavaz et al. 2021), such as sensors of the Landsat mission.

The ECOsystem Spaceborne Thermal Radiometer Experiment on Space Station (ECOSTRESS) – launched in 2017 – was developed to monitor vegetation evapotranspiration around the terrestrial globe. ECOSTRESS combination of non-sun-synchronous orbit and Thermal Infrared Sensor (TIR) bands provides a capacity for understanding plant dynamics on a relatively fine scale at different times of the day (Fisher et al. 2020, Xiao et al. 2021). ECOSTRESS have 5 spectral bands covering the spectral range from 8,000 to 12,500 nm, and have an additional band centered at 1,600 nm for geolocation and cloud detection (Figure 2). The spatial resolution is ~38 x 69 m that is resampled to 70-m cells. Revisit time is dependent on the International Space Station – ISS - orbit but it is expected to be about 1-5 days. ECOSTRESS main high-level products to be used in fuel characterization are the land surface temperature (L2), Evapotranspiration (L3), Water use Efficiency (L4), and Evaporative Stress Index (L4). In addition, there is a preliminary fire detection product under development (ECOSTRESS, 2021). ECOSTRESS may be used to understand variations in plant water content due to vegetation diurnal cycles that may also affect FMC, especially under drought or stress conditions (Xiao et al. 2021, Poulos et al. 2021).

Important achievements were also done in multispectral remote sensing of the visible and near infrared regions of the spectrum, especially related to the increase of sensors' temporal resolution. In 2021, the Amazonia-1 was launched with the objective of reducing revisit time of multispectral remote sensors and track deforestation, especially in the Amazon rainforest (Coronel et al. 2020, Moutinho 2021). The satellite is composed by 3 wide-range cameras with 4 bands [blue, green, red and near-infrared (NIR)] and a spatial resolution of ~60 m. Amazonia-1 has a sun-synchronous orbit and a revisit time of 5 days, which is planned to be used jointly with other spaceborne sensors (e.g. Landsat, Sentinel and CBERS) to have images from an area every 1-2 days.

Another great development in 2021 was the launch of Landsat-9 (L9) (Masek et al. 2020). The Landsat program is the longest Earth observation satellite program having data available for almost 50 years. L9 sensors (OLI-2 and TIRS-2) has similar characteristics to Landsat 8 (L8) sensors (OLI-1 and TIRS-1) with bands in the visible and near-infrared (VNIR), short-wave infrared (SWIR) and thermal ranges of the spectrum. For instance, the spatial resolution of panchromatic, VNIR/SWIR and TIR bands are 15 m, 30 m and 100 m, respectively. Nonetheless, L9 has an improved version of the L8 thermal sensors, e.g., correcting for the stray light problems and increasing lifetime. L9 also have an improved 14-bit image (it was 12-bit in L8) and an orbit that is 8-day out of phase from L8; which means that it is possible to have images every 8 days while L8 and L9 are in orbit together. It is expected that United States Geological Survey (USGS) will distribute operational Level-2 (Surface reflectance and surface temperature) data products that will be assembled into a collection that can be directly used for science and several applications (Masek et al. 2020).

3.1.2. Imaging spectroscopy

Narrow-band imaging sensors (referred to as imaging spectroscopy or hyperspectral sensors) captures such energy in bands of about 10 nm of resolution, which may result in hundreds of bands, and can give detailed information on vegetation chemical and physical constituents. In 2018 in a joint effort of the German Aerospace Center (DLR) the DLR Earth Sensing Imaging Spectrometer (DESIS) was launched. DESIS has 235 spectral channels from 400 to 1000 nm with a spectral sampling interval of 2.5 nm and full-width-half-maximum (FWHM) of 3.5 nm (Figure 2). This sensor image the Earth in a 30 km swath with revisit time varying according to position on Earth due to the non-sun synchronous ISS orbit (Alonso et al. 2019, Krutz et al. 2019). The Italian Space Agency also funded a hyperspectral satellite mission named PRecursore IperSpecttrale della Missione Applicativa (PRISMA) (Cogliati et al. 2021).

PRISMA provide high spatial and spectral resolution images of the land surface – from about 70° N-S, and 180° W-E. It provides 241 narrow bands with the unique combination of two sensors covering from 400 to 2,500 nm (30 m spatial resolution) with a panchromatic sensor (5 m spatial resolution) (Figure 2). PRISMA also generates scenes of 30 x 30 km similar to DESIS. Also in 2019, in an effort by the Japanese Ministry of Economy, trade and Industry, the Hyperspectral imager suite (HISUI) was launched. HISUI offers 185 bands covering from 400 to 2,500 nm of the electromagnetic spectrum (Matsunaga et al. 2020). The spatial resolution in HISUI images are 30 m along track and 20 m cross track and it covers a swath of 20 km. The EnMAP sensor (Guanter et al. 2015) launched in 2022 samples the electromagnetic spectra in 242 bands. The system's orbit yields a revisit time of 27 days near nadir (~5 °) and up to 4 days off-nadir (~30°).

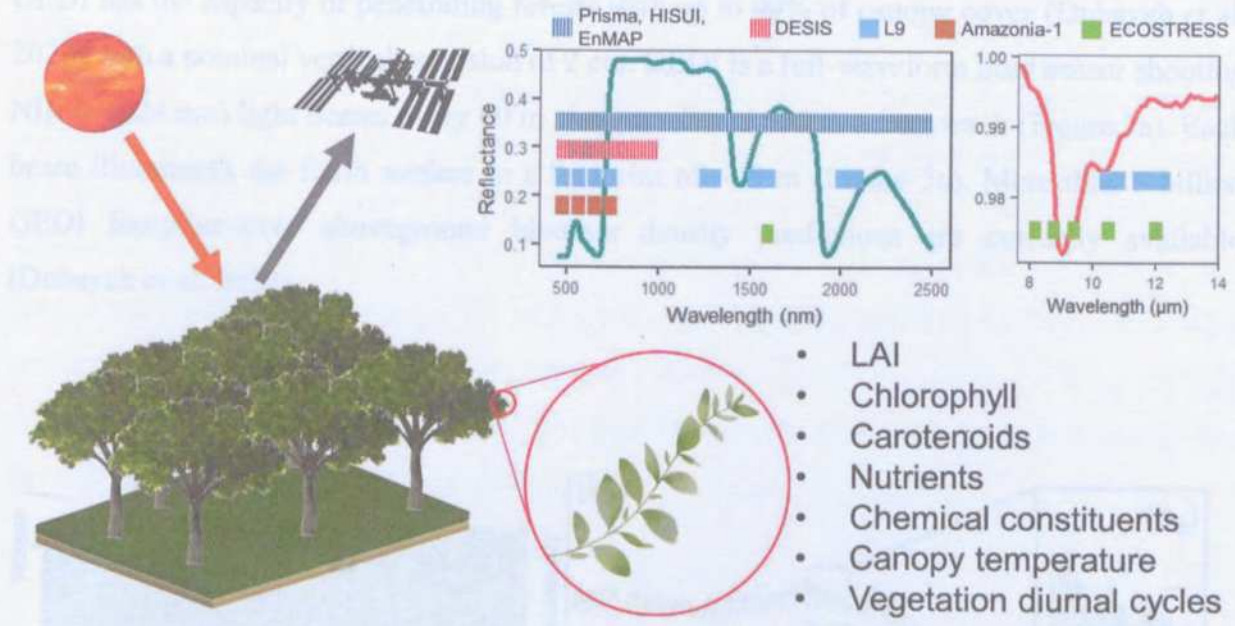

Figure 3. New generation of spaceborne passive sensors sampling characteristics featuring PRISMA, HISUI, DESIS, Landsat-9 (L9), Amazonia-1 and ECOSTRESS. List of leaf and canopy characteristics depict potential variables to be mapped using visible to thermal infrared data from these sensors. *LAI - leaf area index.

3.2. Active sensors

Active remote sensors can penetrate through forest canopies delivering 3D information of the vegetation. Light Detection and Ranging (lidar) has been the main sensor type for obtaining such data due its high penetration capabilities. In 2018, the spaceborne lidar mission Ice, Cloud and Land Elevation Satellite-2 (IceSat-2) was launched to collect data over the globe with the main objective of measuring and monitoring ice sheets changes and their related applications (Neumann et al. 2019). However, its characteristics and global coverage allowed other applications such as mapping vegetation biomass (Narine et al. 2020). The ATLAS sensor on board of IceSat-2 is a photon-counting lidar shooting 6 laser beams of green light (at 532 nm) to the Earth surface. The beams are organized in 3 pairs about 3 km apart and with a distance between paired beams of ~90 m (Figure 3a). Each beam illuminates an area of 13 m on Earth's surface (footprint) with a vertical precision of about 3 cm (Markus et al. 2017). Later in 2018, the first spaceborne lidar sensor designed to map Earth's vegetation, namely GEDI (Global Ecosystem Dynamics Investigation), was launched to the International Space Station (ISS). GEDI has the capacity of penetrating forests with up to 99% of canopy cover (Dubayah et al. 2020) with a nominal vertical precision of 2 cm. GEDI is a full-waveform lidar sensor shooting NIR (~1024 nm) light beams every 60 m along track and 600 m across track (Figure 3a). Each beam illuminates the Earth surface in a footprint of ~25 m (Figure 3c). More than 5 billion GEDI footprint-level aboveground biomass density predictions are currently available (Dubayah et al. 2022)

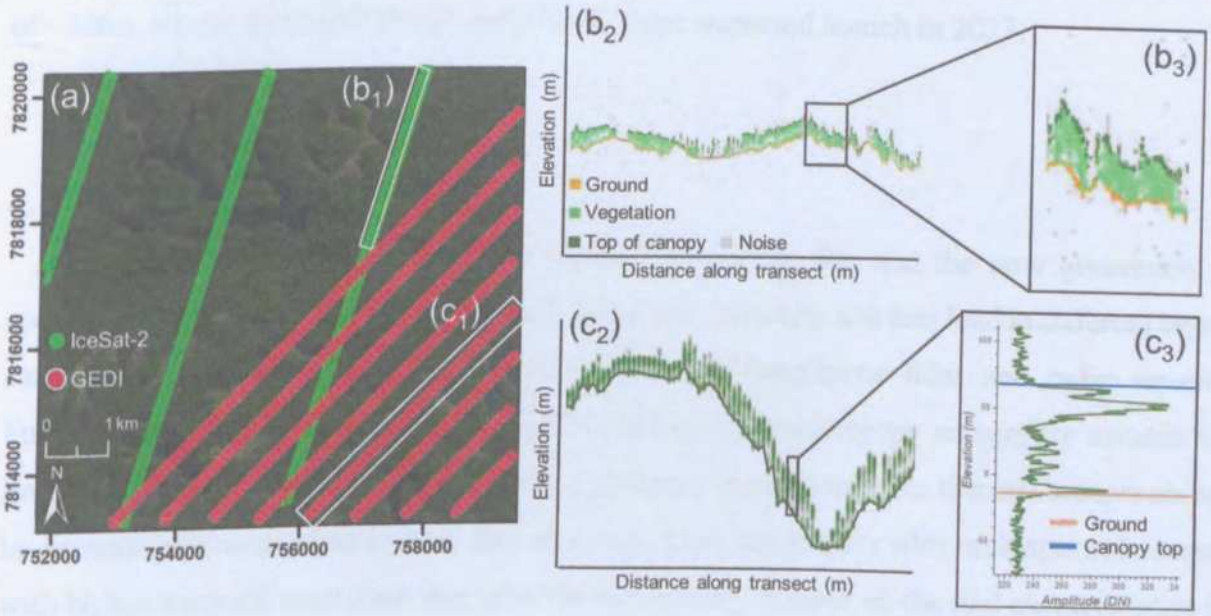

Figure 3. IceSat-2 and GEDI footprints sampling pattern (a) and example profiles (b_2 and c_2) from an orbit subset (b_1 and b_2). Canopy and ground returns are identified in GEDI full-waveforms (c_3) and on IceSat-2 point cloud classification (b_2 and b_3). Profiles were adapted from Narine et al. 2020 and GEDI L2A processing tutorial (available at: https://lpdaac.usgs.gov/resources/e-learning/getting-started-gedi-l2a-data-python/)

3.3. Looking forward

Although not yet launched, it is worth mentioning about radar sensors under development that should be available in the next two years. Radar works by emitting radio waves, i.e., with wavelengths of about 0.75 to 100 cm tracking the strength and time delay of the returned signal that may vary depending on the target characteristics. Radar sensors are usually antennas built to work using synthetic aperture techniques – referred to as synthetic aperture radar (SAR) – that allows the generation of images with finer spatial resolution (Meyer, 2019). The spaceborne SAR sensor BIOMASS was developed by the European Space Agency (ESA) with the objective of mapping Earth's aboveground biomass (Quegan et al. 2019). It is the first sensor built to emit P-band (435 MHz) wavelengths, which have high penetration capability in dense canopies and sensitivity to aboveground biomass. In addition, its operating characteristics will allow the application of SAR tomography techniques from space for the first time. It is expected that aboveground biomass, forest height and forest disturbance products to be delivered a spatial resolution of ~200 x 200 m for the first two products and ~50 x 50 m for third. Furthermore, a spaceborne SAR sensor using L (~24 cm) and S (~10 cm) radar bands named NISAR is being developed through a collaboration between NASA and ISRO (Kellog et al. 2020). Aboveground biomass and disturbance products will also be delivered with a spatial resolution of ~100 x 100 m. Both BIOMASS and NISAR have expected launch in 2023.

4. Final considerations

Fuel characterization is essential to efficiently manage fire and the new generation of spaceborne sensors can be used for this task. Structural variables and fuel load in different layers can be obtained due to the penetration capacity of spaceborne lidar and radar sensors. Furthermore, the narrow-band characteristics of imaging spectroscopy sensors are suitable for improving moisture and diversity traits measurements, in addition to the thermal sensors ability to estimate plot-to-ecosystem level fuel moisture. Data integration with multispectral sensors with higher temporal resolution may give the opportunity to scale up the fuel characteristics in

space and time and understand their variation due to subtle climatic, anthropogenic changes. Ultimately, sensor's integration is key for efficiently characterizing fuels (Table 1). It is noteworthy that several global-scale missions are planned for the next decade such as ESA's BIOMASS (radar) and CHIME (hyperspectral), NASA's NISAR (radar) and SBG (hyperspectral) providing a new set of active and passive sensor's data with similar spatial resolution and high temporal resolution. Together, they can boost fuel mapping and monitoring applications in the next decades constituting the basis for a new era of fuel monitoring from space.

Table 1. Key fuel characteristics that can be retrieved using Earth observation sensors and common used remote sensing products to map vegetation that can be used to characterize fuels(RS-EBVs products - Skidmore et al. 2021)

Fuel characteristic	Definition	Implications for fire risk management	References	Sensors	Potential RSE-EBVs
Load	Amount of combustible material including live and dead vegetation biomass	Increasing fuel load can increase the potential energy release from a fire and fire severity. It can also affect fire spread rate depending on particle size, density, moisture and ratio between live and dead vegetation.	van Wagtendok 2006; McLauchlan et al. 2020; Gale et al. 2021	GEDI, IceSat-2	aboveground biomass; land cover (vegetation type); fraction of vegetation cover; habitat structure
Moisture content	Ratio between vegetation's water and total dry mass	Affects fuel ignition probability and spread rate. Drier vegetation ignite more easily and makes fire spread faster since water works as a heat sink. Dead fuel moisture is usually related to weather but live vegetation moisture is also affected by plant phenology, adaptative traits and soil water availability	Yebra et al. 2013; Pettinari and Chuvieco et al. 2020	DESIS, HISUI, PRISMA, EnMAP, Landsat-9, Amazonia-1, ECOSTRESS	leaef dry matter content; green-up (start of season); senescence (end of season); ecosystem soil moisture; evapotranspiration
Live-dead ratio	The ratio between photosynthetic and non-photosynthetic active vegetation	There are differences in ingnitability and spread rate between photosynthetic and non-photosynthetic vegetation. Fire usualy easier to ignite and spread faster on non-photosynthetic vegetation	Sun et al. 1995; Rezka et al. 2020	DESIS, HISUI, PRISMA, EnMAP, Landsat-9, Amazonia-1, ECOSTRESS	senescence (end of season); deadwood habitat; fraction of vegetation cover
Continuity	Degree or extent of continuous or uninterrupted distribution of fuel particles in a fuel bed.	It can be determinant to whether fire spread or not over the landscape and from ground to top of trees affecting, therefore, fire severity.	NWCG 2018; Dury 2020	GEDI, IceSat-2, DESIS, HISUI, PRISMA, EnMAP, Landsat-9, Amazonia-1, ECOSTRESS	Plant area index profile (canopy cover); leaf area index; habitat structure

Species diversity traits	Morphological, physiological or phenological features measurable at the individual level	Vegetation traits affect vegetation flammability characterized by the combination of ignitability, combustibility and sustainability.	Violle et al. 2007; Anderson 1970; Grootmaat et al. 2015; Simpson et al. 2016	GEDI, IceSat-2, DESIS, HISUI, PRISMA, EnMAP, Landsat-9, Amazonia-1, ECOSTRESS	chlorophyl content; foliar NPK content; polyphenols; lignin; cellulose; non-structural carbohydrates; functional diversity

References

Adams, M.A., Shadmanroodposhti, M., Neumann, M., 2020. Causes and consequences of Eastern Australia's 2019–20 season of mega-fires: A broader perspective. Global Change Biology 26, 3756–3758. https://doi.org/10.1111/gcb.15125

Alonso, K., Bachmann, M., Burch, K., Carmona, E., Cerra, D., de los Reyes, R., Dietrich, D., Heiden, U., Hölderlin, A., Ickes, J., Knodt, U., Krutz, D., Lester, H., Müller, R., Pagnutti, M., Reinartz, P., Richter, R., Ryan, R., Sebastian, I., Tegler, M., 2019. Data products, quality and validation of the DLR earth sensing imaging spectrometer (DESIS). Sensors (Switzerland) 19, 1–44. https://doi.org/10.3390/s19204471

Anderson, H.E., 1970. Forest fuel ignitibility. Fire Technology, 6, 312–319.

Ashworth, A., Evans, D.L., Cooke, W.H., Londo, A., Collins, C., Neuenschwander, A., 2010. Predicting southeastern forest canopy heights and fire fuel models using GLAS data. Photogrammetric Engineering and Remote Sensing 76, 915–922. https://doi.org/10.14358/PERS.76.8.915

Bowman, D.M.J.S., Kolden, C.A., Abatzoglou, J.T., Johnston, F.H., van der Werf, G.R., Flannigan, M., 2020. Vegetation fires in the Anthropocene. Nature Reviews Earth and Environment 1, 500–515. https://doi.org/10.1038/s43017-020-0085-3

Bowman, D.M.J.S., O'Brien, J.A., Goldammer, J.G., 2013. Pyrogeography and the global quest for sustainable fire management. Annual Review of Environment and Resources 38, 57–80. https://doi.org/10.1146/annurev-environ-082212-134049

Carmona, C.P., de Bello, F., Mason, N.W.H., Lepš, J., 2016. Traits Without Borders: Integrating Functional Diversity Across Scales. Trends in Ecology and Evolution 31, 382–394. https://doi.org/10.1016/j.tree.2016.02.003

Chuvieco, E., Aguado, I., Jurdao, S., Pettinari, M.L., Yebra, M., Salas, J., Hantson, S., De La Riva, J., Ibarra, P., Rodrigues, M., Echeverría, M., Azqueta, D., Román, M. V., Bastarrika, A., Martínez, S., Recondo, C., Zapico, E., Martínez-Vega, F.J., 2014. Integrating geospatial information into fire risk assessment. International Journal of Wildland Fire 23, 606–619. https://doi.org/10.1071/WF12052

Chuvieco, E., Aguado, I., Salas, J., García, M., Yebra, M., Oliva, P., 2020. Satellite Remote Sensing Contributions to Wildland Fire Science and Management. Current Forestry Reports 6, 81–96. https://doi.org/10.1007/s40725-020-00116-5

Cogliati, S., Sarti, F., Chiarantini, L., Cosi, M., Lorusso, R., Lopinto, E., Miglietta, F., Genesio, L., Guanter, L., Damm, A., Pérez-López, S., Scheffler, D., Tagliabue, G., Panigada, C., Rascher, U., Dowling, T.P.F., Giardino, C., Colombo, R., 2021. The PRISMA imaging spectroscopy mission: overview and first performance analysis. Remote Sensing of Environment 262. https://doi.org/10.1016/j.rse.2021.112499

Coronel, G.G., Marques, F.L., Venticinque, G. Loureiro, G., 2020. Assembly, Integration and Test (AIT) Campaign of the Amazonia-1 satellite In: Annals of the 71st International Astronautical Congress (IAC). Retrieved from: https://iafastro.directory/iac/paper/id/59962/summary/. Accessed on November 07, 2021.

Drury, S., 2020. Fuel Continuity, in: Encyclopedia of Wildfires and Wildland-Urban Interface (WUI) Fires. Springer International Publishing, Cham, pp. 1–3. https://doi.org/10.1007/978-3-319-51727-8_239-1

Dubayah, R. et al. GEDI launches a new era of biomass inference from space. Environ. Res. Lett. 17, 095001 (2022).

Dubayah, R., Blair, J.B., Goetz, S., Fatoyinbo, L., Hansen, M., Healey, S., Hofton, M., Hurtt, G., Kellner, J., Luthcke, S., Armston, J., Tang, H., Duncanson, L., Hancock, S., Jantz, P., Marselis, S., Patterson, P.L., Qi, W., Silva, C., 2020. The Global Ecosystem Dynamics Investigation: High-resolution laser ranging of the Earth's forests and topography. Science of Remote Sensing 1, 100002. https://doi.org/10.1016/j.srs.2020.100002

ECOSTRESS, 2021 – Preliminary Fire Product – Retrieved from: https://ecostress.jpl.nasa.gov/fire. Accessed on November 13,2021

Fidelis, A., Alvarado, S., Barradas, A., Pivello, V., 2018. The Year 2017: Megafires and Management in the Cerrado. Fire 1, 49. https://doi.org/10.3390/fire1030049

Fisher, J.B., Lee, B., Purdy, A.J., Halverson, G.H., Dohlen, M.B., Cawse-Nicholson, K., Wang, A., Anderson, R.G., Aragon, B., Arain, M.A., Baldocchi, D.D., Baker, J.M., Barral, H., Bernacchi, C.J., Bernhofer, C., Biraud, S.C., Bohrer, G., Brunsell, N., Cappelaere, B., Castro-Contreras, S., Chun, J., Conrad, B.J., Cremonese, E., Demarty, J., Desai, A.R., De Ligne, A., Foltýnová, L., Goulden, M.L., Griffis, T.J., Grünwald, T., Johnson, M.S., Kang, M., Kelbe, D., Kowalska, N., Lim, J.H., Maïnassara, I., McCabe, M.F., Missik, J.E.C., Mohanty, B.P., Moore, C.E., Morillas, L., Morrison, R., Munger, J.W., Posse, G., Richardson, A.D., Russell, E.S., Ryu, Y., Sanchez-Azofeifa, A., Schmidt, M., Schwartz, E., Sharp, I., Šigut, L., Tang, Y., Hulley, G., Anderson, M., Hain, C., French, A., Wood, E., Hook, S., 2020. ECOSTRESS: NASA's Next Generation Mission to Measure Evapotranspiration From the International Space Station. Water Resources Research 56, 1–20. https://doi.org/10.1029/2019WR026058

Gale, M.G., Cary, G.J., Van Dijk, A.I.J.M., Yebra, M., 2021. Forest fire fuel through the lens of remote sensing: Review of approaches, challenges and future directions in the remote sensing of biotic determinants of fire behaviour. Remote Sensing of Environment 255. https://doi.org/10.1016/j.rse.2020.112282

Grootemaat, S., Wright, I.J., van Bodegom, P.M., Cornelissen, J.H.C., Cornwell, W.K., 2015. Burn or rot: Leaf traits explain why flammability and decomposability are decoupled across species. Functional Ecology 29, 1486–1497. https://doi.org/10.1111/1365-2435.12449

He, B., Lai, G., Liu, X., 2021. International Journal of Applied Earth Observations and Geoinformation Global fuel moisture content mapping from MODIS 101.

Hill, M.J., Guerschman, J.P., 2022. Global trends in vegetation fractional cover: Hotspots for change in bare soil and non-photosynthetic vegetation. Agriculture, Ecosystems & Environment 324, 107719. https://doi.org/10.1016/j.agee.2021.107719

Jetz, W., Cavender-Bares, J., Pavlick, R., Schimel, D., Davis, F.W., Asner, G.P., Guralnick, R., Kattge, J., Latimer, A.M., Moorcroft, P., Schaepman, M.E., Schildhauer, M.P., Schneider,

F.D., Schrodt, F., Stahl, U., Ustin, S.L., 2016. Monitoring plant functional diversity from space. Nature Plants 2, 1–5. https://doi.org/10.1038/NPLANTS.2016.24

Kellogg, K. et al. NASA-ISRO Synthetic Aperture Radar (NISAR) Mission. in 2020 IEEE Aerospace Conference 1–21 (IEEE, 2020). doi:10.1109/AERO47225.2020.9172638.

Kelly, L.T., Giljohann, K.M., Duane, A., Aquilué, N., Archibald, S., Batllori, E., Bennett, A.F., Buckland, S.T., Canelles, Q., Clarke, M.F., Fortin, M.J., Hermoso, V., Herrando, S., Keane, R.E., Lake, F.K., McCarthy, M.A., Morán-Ordóñez, A., Parr, C.L., Pausas, J.G., Penman, T.D., Regos, A., Rumpff, L., Santos, J.L., Smith, A.L., Syphard, A.D., Tingley, M.W., Brotons, L., 2020. Fire and biodiversity in the Anthropocene. Science 370. https://doi.org/10.1126/science.abb0355

Knipling, E.B., 1970. Physical and physiological basis for the reflectance of visible and near-infrared radiation from vegetation. Remote Sensing of Environment 1, 155–159. https://doi.org/10.1016/S0034-4257(70)80021-9

Krutz, D., Müller, R., Knodt, U., Günther, B., Walter, I., Sebastian, I., Säuberlich, T., Reulke, R., Carmona, E., Eckardt, A., Venus, H., Fischer, C., Zender, B., Arloth, S., Lieder, M., Neidhardt, M., Grote, U., Schrandt, F., Gelmi, S., Wojtkowiak, A., 2019. The instrument design of the DLR earth sensing imaging spectrometer (DESIS). Sensors (Switzerland) 19, 1–16. https://doi.org/10.3390/s19071622

Leite, R.V., Silva, C.A., Broadbent, E.N., Amaral, C.H. do, Liesenberg, V., Almeida, D.R.A. de, Mohan, M., Godinho, S., Cardil, A., Hamamura, C., Faria, B.L. de, Brancalion, P.H.S., Hirsch, A., Marcatti, G.E., Dalla Corte, A.P., Zambrano, A.M.A., Costa, M.B.T. da, Matricardi, E.A.T., Silva, A.L. da, Goya, L.R.R.Y., Valbuena, R., Mendonça, B.A.F. de, Silva Junior, C.H.L., Aragão, L.E.O.C., García, M., Liang, J., Merrick, T., Hudak, A.T., Xiao, J., Hancock, S., Duncason, L., Ferreira, M.P., Valle, D., Saatchi, S., Klauberg, C., 2022. Large scale multi-layer fuel load characterization in tropical savanna using GEDI spaceborne lidar data. Remote Sensing of Environment 268, 112764. https://doi.org/10.1016/j.rse.2021.112764

Lizundia-Loiola, J., Pettinari, M.L., Chuvieco, E., 2020. Temporal anomalies in burned area trends: Satellite estimations of the amazonian 2019 fire crisis. Remote Sensing 12. https://doi.org/10.3390/RS12010151

Markus, T., Neumann, T., Martino, A., Abdalati, W., Brunt, K., Csatho, B., Farrell, S., Fricker, H., Gardner, A., Harding, D., Jasinski, M., Kwok, R., Magruder, L., Lubin, D., Luthcke, S., Morison, J., Nelson, R., Neuenschwander, A., Palm, S., Popescu, S., Shum, C.K., Schutz, B.E., Smith, B., Yang, Y., Zwally, J., 2017. The Ice, Cloud, and land Elevation Satellite-2 (ICESat-2): Science requirements, concept, and implementation. Remote Sensing of Environment 190, 260–273. https://doi.org/10.1016/j.rse.2016.12.029

Martin R.E., Gordon D.A., Gutierrez M.E., Lee D.S., Molina D.M., Schroeder R.A., Sapsis D.B., Stephens S.L., Chambers M., 1994. Assessing the flammability of domestic and wildland vegetation. In 'Proceedings of the 12th conference on fire and forest meteorology', 26–28 October 1993, Jekyll Island, GA. pp. 130–137. (Society of American Foresters: Bethesda, MD)

Masek, J. G. et al. Landsat 9: Empowering open science and applications through continuity. Remote Sensing of Environment 248, 111968 (2020).

Masek, J.G., Wulder, M.A., Markham, B., McCorkel, J., Crawford, C.J., Storey, J., Jenstrom, D.T., 2020. Landsat 9: Empowering open science and applications through continuity. Remote Sensing of Environment 248. https://doi.org/10.1016/j.rse.2020.111968

McLauchlan, K.K., Higuera, P.E., Miesel, J., Rogers, B.M., Schweitzer, J., Shuman, J.K., Tepley, A.J., Varner, J.M., Veblen, T.T., Adalsteinsson, S.A., Balch, J.K., Baker, P., Batllori, E., Bigio, E., Brando, P., Cattau, M., Chipman, M.L., Coen, J., Crandall, R., Daniels, L., Enright, N., Gross, W.S., Harvey, B.J., Hatten, J.A., Hermann, S., Hewitt, R.E., Kobziar, L.N., Landesmann, J.B., Loranty, M.M., Maezumi, S.Y., Mearns, L., Moritz, M., Myers, J.A., Pausas, J.G., Pellegrini, A.F.A., Platt, W.J., Roozeboom, J., Safford, H., Santos, F., Scheller, R.M., Sherriff, R.L., Smith, K.G., Smith, M.D., Watts, A.C., 2020. Fire as a fundamental ecological process: Research advances and frontiers. Journal of Ecology 108, 2047–2069. https://doi.org/10.1111/1365-2745.13403

Meyer, Franz. "Spaceborne Synthetic Aperture Radar – Principles, Data Access, and Basic Processing Techniques." SAR Handbook: Comprehensive Methodologies for Forest Monitoring and Biomass Estimation. Eds. Flores, A., Herndon, K., Thapa, R., Cherrington, E. NASA. 2019. DOI: 10.25966/ez4f-mg98

Moutinho, S., 2021. First Brazilian-made satellite watches the Amazon. Science 371, 975. https://doi.org/10.1126/science.371.6533.975

Narine, L.L., Popescu, S.C., Malambo, L., 2020. Using ICESat-2 to estimate and map forest aboveground biomass: A first example. Remote Sensing 12, 1–16. https://doi.org/10.3390/rs12111824

National Wildfire Coordinating Group (NWCG), NWCG Glossary of Wildland Fire, PMS 205, 2018. Retrieved from: https://www.nwcg.gov/glossary/a-z. Acessed on November 07, 2021.

Neinavaz, E., Schlerf, M., Darvishzadeh, R., Gerhards, M., Skidmore, A.K., 2021. Thermal infrared remote sensing of vegetation: Current status and perspectives. International Journal of Applied Earth Observation and Geoinformation 102, 102415. https://doi.org/10.1016/j.jag.2021.102415

Neumann, T.A., Martino, A.J., Markus, T., Bae, S., Bock, M.R., Brenner, A.C., Brunt, K.M., Cavanaugh, J., Fernandes, S.T., Hancock, D.W., Harbeck, K., Lee, J., Kurtz, N.T., Luers, P.J., Luthcke, S.B., Magruder, L., Pennington, T.A., Ramos-Izquierdo, L., Rebold, T., Skoog, J., Thomas, T.C., 2019. The Ice, Cloud, and Land Elevation Satellite – 2 mission: A global geolocated photon product derived from the Aadvanced Ttopographic Llaser Aaltimeter Ssystem. Remote Sensing of Environment 233, 111325. https://doi.org/10.1016/j.rse.2019.111325

Obata, K., Tsuchida, S., Nagatani, I., Yamamoto, H., Kouyama, T., Yamada, Y., Yamaguchi, Y., Ishii, J., 2016. An overview of ISS HISUI hyperspectral imager radiometric calibration. International Geoscience and Remote Sensing Symposium (IGARSS) 2016-November, 1924–1927. https://doi.org/10.1109/IGARSS.2016.7729495

Pettinari, M.L., Chuvieco, E., 2020. Fire Danger Observed from Space. Surveys in Geophysics 41, 1437–1459. https://doi.org/10.1007/s10712-020-09610-8

Poulos, H.M., Barton, A.M., Koch, G.W., Kolb, T.E., Thode, A.E., 2021. Wildfire severity and vegetation recovery drive post-fire evapotranspiration in a southwestern pine-oak forest, Arizona, USA. Remote Sensing in Ecology and Conservation 1–13. https://doi.org/10.1002/rse2.210

Quegan, S. et al. The European Space Agency BIOMASS mission: Measuring forest above-ground biomass from space. Remote Sensing of Environment 227, 44–60 (2019).

Reszka, P., Cruz, J.J., Valdivia, J., González, F., Rivera, J., Carvajal, C., Fuentes, A., 2020. Ignition delay times of live and dead pinus radiata needles. Fire Safety Journal 112. https://doi.org/10.1016/j.firesaf.2020.102948

Sanchez-Lopez, N., Boschetti, L., Hudak, A.T., Hancock, S., Duncanson, L.I., 2020. Estimating time since the last stand-replacing disturbance (TSD) from spaceborne simulated GEDI data: A feasibility study. Remote Sensing 12, 1–25. https://doi.org/10.3390/rs12213506

Simpson, K.J., Ripley, B.S., Christin, P.A., Belcher, C.M., Lehmann, C.E.R., Thomas, G.H., Osborne, C.P., 2016. Determinants of flammability in savanna grass species. Journal of Ecology 104, 138–148. https://doi.org/10.1111/1365-2745.12503

Skidmore, A.K., Coops, N.C., Neinavaz, E., Ali, A., Schaepman, M.E., Paganini, M., Kissling, W.D., Vihervaara, P., Darvishzadeh, R., Feilhauer, H., Fernandez, M., Fernández, N., Gorelick, N., Geijzendorffer, I., Heiden, U., Heurich, M., Hobern, D., Holzwarth, S., Muller-Karger, F.E., Van De Kerchove, R., Lausch, A., Leitão, P.J., Lock, M.C., Mücher, C.A., O'Connor, B., Rocchini, D., Turner, W., Vis, J.K., Wang, T., Wegmann, M., Wingate, V., 2021. Priority list of biodiversity metrics to observe from space. Nature Ecology and Evolution 5, 896–906. https://doi.org/10.1038/s41559-021-01451-x

Stavros, E.N., Coen, J., Peterson, B., Singh, H., Kennedy, K., Ramirez, C., Schimel, D., 2018. Use of imaging spectroscopy and LIDAR to characterize fuels for fire behavior prediction. Remote Sensing Applications: Society and Environment 11, 41–50. https://doi.org/10.1016/j.rsase.2018.04.010

Sun, L., Zhou, X., Mahalingam, S., Weise, D.R., 2006. Comparison of burning characteristics of live and dead chaparral fuels. Combustion and Flame 144, 349–359. https://doi.org/10.1016/j.combustflame.2005.08.008

Tatem, A.J., Goetz, S.J., Hay, S.I., 2009. UKPMC Funders Group Fifty Years of Earth Observation Satellites : Earth 96, 1–7. https://doi.org/10.1511/2008.74.390.Fifty

Tian, J., Su, S., Tian, Q., Zhan, W., Xi, Y., Wang, N., 2021. A novel spectral index for estimating fractional cover of non-photosynthetic vegetation using near-infrared bands of Sentinel satellite. International Journal of Applied Earth Observation and Geoinformation 101, 102361. https://doi.org/10.1016/j.jag.2021.102361

Ustin, S.L., Middleton, E.M., 2021. Current and near-term advances in Earth observation for ecological applications. Ecological Processes 10, 1–57. https://doi.org/10.1186/s13717-020-00255-4

Van Wagtendonk, J. W., 2006. Fire as a physical process. Fire in California's ecosystems, 38-57.

Violle, C., Navas, M.-L., Vile, D., Kazakou, E., Fortunel, C., Hummel, I., Garnier, E., 2007. Let the concept of trait be functional! Oikos 116, 882–892. https://doi.org/10.1111/j.2007.0030-1299.15559.x

White, R.H., Zipperer, W.C., 2010. Testing and classification of individual plants for fire behaviour: Plant selection for the wildlandurban interface. International Journal of Wildland Fire 19, 213–227. https://doi.org/10.1071/WF07128

Xiao, J., Fisher, J.B., Hashimoto, H., Ichii, K., Parazoo, N.C., 2021. Emerging satellite observations for diurnal cycling of ecosystem processes. Nature Plants 7, 877–887. https://doi.org/10.1038/s41477-021-00952-8

Yebra, M., Quan, X., Riaño, D., Rozas Larraondo, P., van Dijk, A.I.J.M., Cary, G.J., 2018. A fuel moisture content and flammability monitoring methodology for continental Australia based on optical remote sensing. Remote Sensing of Environment 212, 260–272. https://doi.org/10.1016/j.rse.2018.04.053

Yebra, M., Scortechini, G., Badi, A., Beget, M.E., Boer, M.M., Bradstock, R., Chuvieco, E., Danson, F.M., Dennison, P., Resco de Dios, V., Di Bella, C.M., Forsyth, G., Frost, P., Garcia, M., Hamdi, A., He, B., Jolly, M., Kraaij, T., Martín, M.P., Mouillot, F., Newnham, G., Nolan, R.H., Pellizzaro, G., Qi, Y., Quan, X., Riaño, D., Roberts, D., Sow, M., Ustin, S., 2019. Globe-LFMC, a global plant water status database for vegetation ecophysiology and wildfire applications. Scientific Data 6, 1–8. https://doi.org/10.1038/s41597-019-0164-9

Zhu, L., Webb, G.I., Yebra, M., Scortechini, G., Miller, L., Petitjean, F., 2021. Live fuel moisture content estimation from MODIS: A deep learning approach. ISPRS Journal of Photogrammetry and Remote Sensing 179, 81–91. https://doi.org/10.1016/j.isprsjprs.2021.07.010

Final remarks

Cerrado is the most biodiverse tropical savanna in the world and evolved in the presence of fire. However, anthropic activities have changed landscape and fire regimes which can threaten the stability of this biome. Characterizing vegetation fuels is one of the main tasks to develop efficient integrated fire management approaches necessary to preserve fire regimes and the functionality of Cerrado and other fire-prone ecosystems across the world. This dissertation supports the use of remote sensors as a way to characterize fuels. This is boosted by the recent launch of spaceborne remote sensors with unprecedented characteristics that allows large-scale fuel characterization.

The potential of spectroscopy to obtain biochemical characteristics was used to retrieve fuel moisture content (FMC). The differences observed in the spectral response of the range of fuel moisture classes were summarized into vegetation indices that are a straightforward dimensionality reduction method and less influenced by sensor-specific noise. Furthermore, the results supported the importance of FMC prediction using variables related to several plant traits other than water as for i) the close opposite relationship between FMC and leaf dry matter, ii) effects of water reduction in plant physiology and in biochemical constituents. Species-specific models could potentially improve models' performance as specific leaf structure, morphology and biochemistry could also impact leaf spectral response.

In addition, the potential of obtaining fuel load for several vegetation layers was demonstrated using spaceborne full-waveform lidar data from GEDI. This includes surface layers that are often kept aside for spaceborne-based fuel load characterization. The results support the use of lidar data for obtaining structural-related vegetation characteristics. Lower stratum components - such as herbaceous and litter layers – were harder to retrieve. Nonetheless, indirectly relationships with the waveform metrics helped to explain part of the variability of these fuels in the different Cerrado vegetation formations. This is important

mainly because those are crucial fuel components that are often put aside in fuel models using spaceborne data.

The results are encouraging for large-scale fuel characterization in Cerrado or other fire-prone ecosystems. The models and frameworks developed here can help on the upscaling of fuel characteristics to support fire management. Ultimately, data integration from different missions will be necessary for both i) developing wall-to-wall maps with finer spatial resolutions, ii) balancing sensors' specific limitations, iii) deriving multiple fuel load properties that are important to fire risk. Incorporating the developed frameworks with the opportunities arising from the new generation of spaceborne remote sensors can become assets for fire managers to prevent fire negative effects on vegetation ecosystems and society especially by preserving sites-specific natural fire regimes.